REPORT DOCUMENTATION PAGE

Form Approved
OMB No. 0704-0188

1. REPORT DATE *(DD-MM-YYYY)*: 06-01-2012

2. REPORT TYPE: Final Technical Report

3. DATES COVERED *(From - To)*: Mar 2010 to Jun 2012

4. TITLE AND SUBTITLE
Tunable Artificial Receptor as a Chemical Sensor for V- and G-agents

5a. CONTRACT NUMBER: HDTRA1-10-C-0010

5b. GRANT NUMBER: N/A

5c. PROGRAM ELEMENT NUMBER: N/A

6. AUTHOR(S)
Donald W. Zehnder II. Ph.D., John R. Shaw, Ph.D.

5d. PROJECT NUMBER: N/A

5e. TASK NUMBER: N/A

5f. WORK UNIT NUMBER: N/A

7. PERFORMING ORGANIZATION NAME(S) AND ADDRESS(ES)
Battelle Memorial Institute
505 King Ave.
Columbus, OH 43201

8. PERFORMING ORGANIZATION REPORT NUMBER: N/A

9. SPONSORING/MONITORING AGENCY NAME(S) AND ADDRESS(ES)
Defense Threat Reduction Agency
8725 John J. Kingman Rd.
Fort Belvoir, VA 22060-6201

10. SPONSOR/MONITOR'S ACRONYM(S): DTRA

11. SPONSOR/MONITOR'S REPORT NUMBER(S): N/A

12. DISTRIBUTION/AVAILABILITY STATEMENT
DISTRIBUTION STATEMENT A. Approved for public release; distribution is unlimited

13. SUPPLEMENTARY NOTES
N/A

14. ABSTRACT
Battelle investigated the development of a tunable artificial receptor designed with a sliding ring (e.g., Host-[2]rotaxane) that detects the presence of V- and G- nerve agents. The ultimate purpose for this work is to develop a tunable hazard mitigation system capable of capturing, detecting, and destroying chemical agents. Agent capture occurs by the receptor's use of two cooperative non-covalent interactions: hydrophobic binding and salt-bridging. Agent capture efficiency was evaluated using Soman (GD). GD was effectively bound in water at 10-5 M demonstrating the potential ability to sequester GD for subsequent decontamination. Computational studies were performed by modeling docking interactions using EPP, GA, and GD to understand the nature of the binding motifs. Two binding motifs are suggested for the EPP complex, a "phenyl-in" and an "ethyl-in" mode. The phenyl group inside the cyclophane is significantly more strongly bound than the EPP complex with the ethyl group inside the cyclophane. Both binding motifs show stable binding energies ranging from 0 – 5 kcal/mol which is expected for hydrophobic interactions. This finding supports the cross-over use of cyclophanes as design elements for capturing chemical agents in artificial receptor systems.

15. SUBJECT TERMS
Rotaxane, Shuttling, Tunable, Chemical Sensor, G-and V-Chemical Agents, Colorimetric Sensor, Fluorescence, Binding Efficiency

16. SECURITY CLASSIFICATION OF: a. REPORT	b. ABSTRACT	c. THIS PAGE	17. LIMITATION OF ABSTRACT	18. NUMBER OF PAGES	19a. NAME OF RESPONSIBLE PERSON
UNCLASS	UNCLASS	UNCLASS	UNCLASS	128	Donald W. Zehnder II
					19b. TELEPHONE NUMBER *(Include area code)* 614-424-3046

Contract No: HDTRA1-10-C-0010

FINAL TECHNICAL REPORT
(1 JUNE 2012)

on

Tunable Artificial Receptor as a Chemical Sensor for V- and G-agents

to

Charles Bass, Ph.D.
Senior Science and Technology Manager
Hazard Mitigation DTRA-CBT
8725 John J. Kingman Rd
Fort Belvoir, VA 22060-6201
703-767-3311
charles.bass@dtra.mil

by

Donald W. Zehnder II, Ph.D.
614-424-3046
John R. Shaw, Ph.D.
614-424-4113

Battelle
1425 St. Rte 142
West Jefferson, OH 43162

EXECUTIVE SUMMARY

Battelle investigated the development of a tunable artificial receptor designed with a sliding ring (e.g., Host-[2]rotaxane) that detects the presence of V- and G- nerve agents. The ultimate purpose for this work is to develop a tunable hazard mitigation system capable of capturing, detecting, and destroying chemical agents. This research has established ground work towards the development of a durable artificial catalytic system that efficiently destroys chemical agents. Critical to the full development of this system is mastering the underlying chemistry of 1) selective molecular recognition of chemical agents 2) controlled shuttling of the ring between two points along the axle and 3) catalysis which uses environmentally available water to render chemical agent inert.

Evaluation of artificial receptor **1** with GD and GA indicates that this artificial receptor will bind GD effectively in water at 10^{-5} M. Artificial receptor **1** has demonstrated, in these initial studies, the ability to sequester GD for subsequent removal or decontamination. The artificial receptor system captures GD through use of two cooperative non-covalent interactions: hydrophobic binding and a salt bridging interaction. Figure E1 depicts this binding motif.

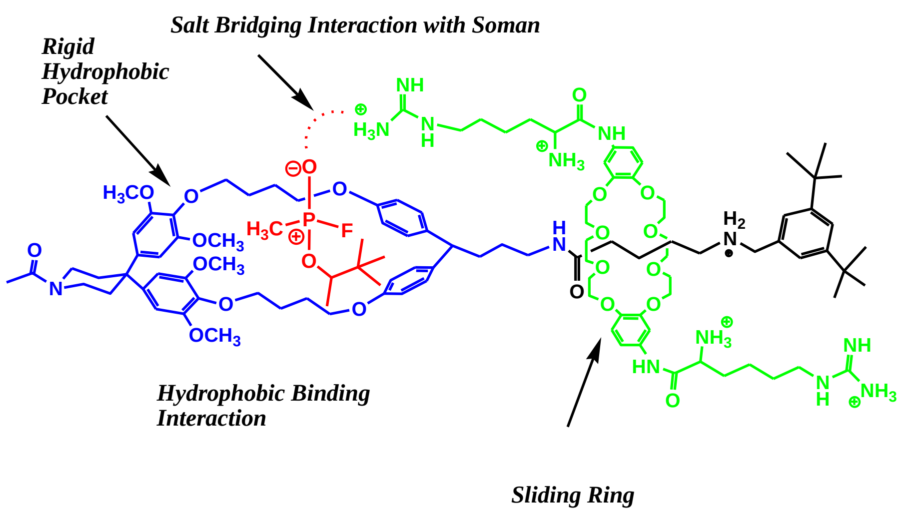

Figure E1. Structure of Artificial Receptor 1 Depicting Binding of Soman (GD)

Table E1. Design Elements of Host-[2]Rotaxane for Detection of CWAs

Rotaxane Molecular Component	Color	Function
Cyclophane pocket	Blue	Binding analytes of interest
Sliding ring	Green	Activation from non-binding to bound state, via a salt-bridge interaction, triggering a response
Tether	Black	Provides an axle template for the sliding ring and attachment for the pocket and potential signaling indicators
Soman (GD)	Red	Example analyte for binding pocket

The binding capability of cyclophane pocket (Blue) was initially investigated by nuclear magnetic resonance (NMR) spectroscopy using a simulant, ethyl phenylphosphinate (EPP). EPP was chosen because its key physical properties, size, shape and functionality, are similar to the G-series chemical agents. Results indicated the operational solvent range for effective binding of the cyclophane pocket is between 5 and 15 percent water in DMSO. Overall the hydrophobic interaction is a weak interaction and the measured binding constants (between 220 and 470 M^{-1}) were consistent with other hydrophobic cyclophanes reported in the literature.

A computational study was performed to understand the binding motifs of EPP, GA, and GD with the cyclophane pocket. Two binding motifs are suggested for the EPP complex, a "phenyl-in" and an "ethyl-in" mode. The phenyl group inside the cyclophane is significantly more strongly bound than the EPP complex with the ethyl group inside the cyclophane. Both binding motifs show stable binding, and the binding energies are 0 – 5 kcal/mol which is expected for mainly hydrophobic interactions. This result is consistent with the binding constants observed experimentally during the studies of the cyclophane pocket with EPP.

The agent binding performance of artificial receptor **1** was assessed by challenging the receptor with chemical agents GD and GA at three concentration ranges: 10^{-5} M, 10^{-6} M and 10^{-7} M. Agent binding performance was determined by extraction of solutions containing increasing concentrations of artificial receptor **1** and a constant concentration of agent (GA and GD). GC-MS analysis was used to quantify the amount of extracted or "unbound" agent. All unrecovered agent was assumed to be "bound" by artificial receptor **1**. The data acquired at 10^{-5} M was analyzed using a Scatchard plot (Figure E2). Analysis showed that multiple binding events occurred during the experiment. This observation is consistent with the computational modeling study results indicating the possibility of multiple binding configurations.

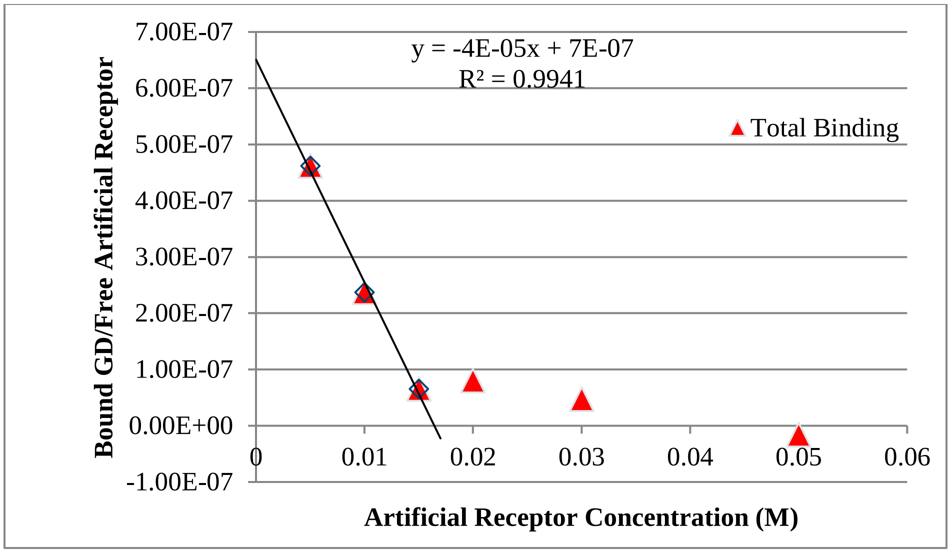

Figure E2. Scatchard Plot of Bound GD/Free Artificial Receptor vs. Artificial Receptor Concentration, Highlighting the Linear Region.

The slope from the linear region in Figure E2 indicates a dissociation binding constant (K_D) for GD and artificial receptor **1** on the order of 4 x 10^{-5} M. Based on the inverse relationship of K_D to the association binding constant (K_a), the binding constant of GD to artificial receptor **1** is estimated to be 25,000 M^{-1}. This is two orders of magnitude stronger than the hydrophobic interaction observed with the cyclophane pocket alone. This implies assistance in binding the analyte, possibly due to salt-bridge interactions with the sliding ring guanidine groups. Because the binding was evaluated using an indirect method for analyte concentration, the receptor binding mechanism can only be speculated upon for GD. To further evaluate binding performance, direct spectral evidence is required: (e.g. NMR or fluorescence).

Artificial receptor **1** did not effectively bind GA at 10^{-5} M. There was no observed difference in the amount of extracted GA from the positive control and the GA test solutions. While the available data does not provide a full understanding of this result, it is possible the cyanide functionality within GA is reducing or negating salt bridging effects. Binding performance studies were not feasible at low concentration (10^{-6} and 10^{-7} M) with GD and GA due to method detection limits.

Evaluation of artificial receptor **1** with GD and GA indicates that this artificial receptor will bind GD effectively in water at 10^{-5} M for subsequent removal or decontamination. Furthermore, the data suggests the initial binding interaction induced movement of the sliding ring. This result is an important step in the development of a hazard mitigation strategy using rotaxanes as catalytic molecular machines for agent decontamination.

Table of Contents

Table of Figures

Table of Tables

This Page Intentionally Left Blank

LIST OF ABBREVIATIONS

AcOH	acetic acid
BChE	butyrylcholinesterase
$(Boc)_2O$ / BOC	di-tert-butyl dicarbonate
CCl_4	carbon tetrachloride
CH_2Cl_2	methylene chloride
CH_3CN	acetonitrile
CH_3OH	methanol
Cl^-	chloride ion
CWA	chemical warfare agent
δ	chemical shift in NMR spectroscopy
d	days
DB24C8	dibenzo-24-crown-8-ether
DCC	dicyclohexylcarbodimide
DCM	dichloromethane
DCU	dicyclohexylurea
DMF	*N*,*N*-dimethylformamide
DMMP	Dimethyl methylphosphonate
DMSO	dimethyl sulfoxide
EPP	Ethyl phenylphosphinate
Et_2O	diethyl ether
ESI MS	electrospray mass spectroscopy
g	gram
GA	Tabun
GD	Soman
h	hours
HCl	hydrochloric acid
H_2	hydrogen
HPLC	high pressure liquid chromatography
HNO_3	nitric acid
H_2SO_4	sulfuric acid
Hz	hertz
J	coupling constant (NMR)
K_D	dissociation constant
K_a	association constant
K_2CO_3	potasium carbonate
KOH	potassium hydroxide
L	liter
m	meta
m	multiplet (NMR)
mg	milligram

mL	milliliter
min	minutes
mmol	millimole
$MgSO_4$	magnesium sulfate
N	Normal
$NaBH_4$	sodium borohydride
NaH	sodium hydride
NaOH	sodium hydroxide
NaN_3	sodium azide
Na_2CO_3	sodium carbonate
Na_2SO_4	sodium sulfate
NH_4PF_6	ammonium hexafluorophosphate
NMR	nuclear magnetic resonance
ND	not detected
NR	no reaction
p	para
Pd/C	10% palladium on carbon
PF_6^-	hexafluorophosphate ion
TEA	triethylamine
TFA	trifluoroacetic acid
THF	tetrahydrofuran
μL	microliter

This Page Intentionally Left Blank

1.0 Introduction

The technology described herein was performed for the Chemical and Biological Technologies Directorate of the Defense Threat Reduction Agency (DTRA) Research & Development (R&D) Enterprise in its mission to seek new and innovative ideas for experimental and theoretical development of technologies (specifically, a “smart” hazard mitigation system) to fill US Department of Defense (DoD) requirements for chemical and biological defense.

2.0 Scope

Battelle investigated the development of a tunable artificial receptor designed with a sliding ring (e.g., Host-[2]rotaxane) that detects the presence of V- and G- nerve agents using fluorescence. This receptor system incorporates a hydrophobic binding pocket, a salt-bridge interaction, and a fluorescent signaling indicator. Signaling occurs through a 2-stage process, depicted with Soman (GD) as an example in Figures 2-1 and 2-2. In stage 1, a hydrophobic binding interaction occurs between the chemical warfare agent (CWA) and the pocket site. In stage 2, the charged guanidine functionality on the sliding ring forms a salt-bridge interaction with the bound agent. This interaction causes the ring to slide away from the fluorescent sensor. As a result, the indicator is no longer quenched, thus free to emit light. This signaling alerts personnel to the presence of CWAs in real time.

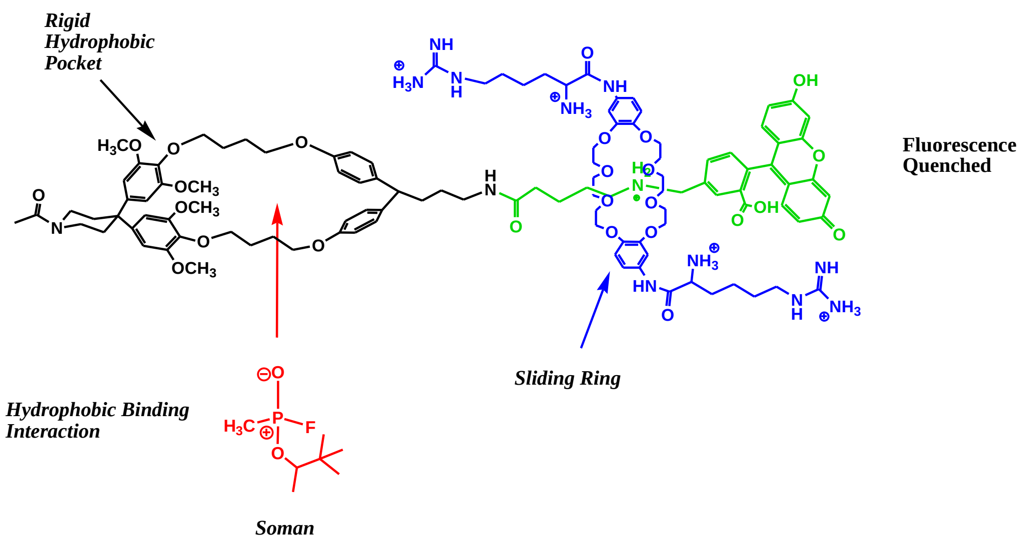

Figure 2-1. Stage 1 Hydrophobic Binding

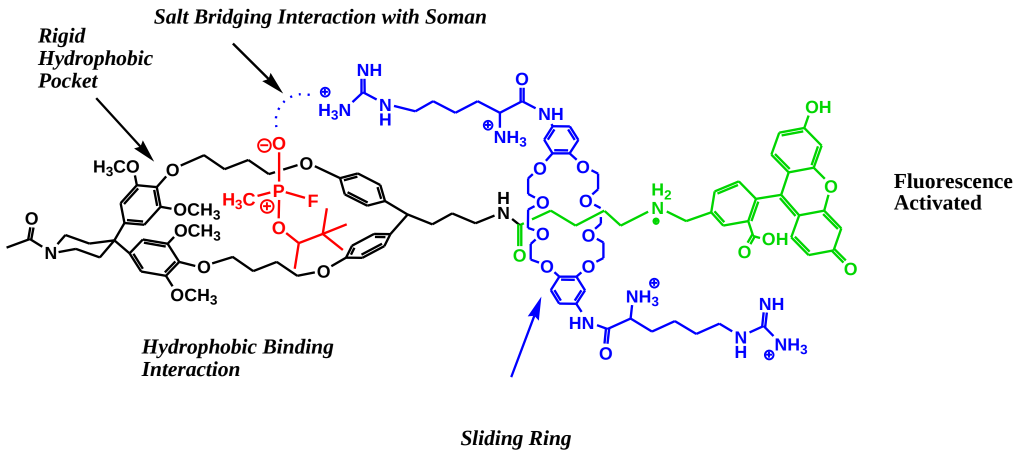

Figure 2-2. Stage 2 Salt Bridging and Signal Activation (Shown as Fluorescence)

3.0 Background

The major goals for designing and producing chemical warfare agents (CWAs) sensors include selectivity, rapid signal transduction, and minimization of false positive or negative responses. Molecular recognition of a specific analyte in a matrix arises from host species having the right size, shape, flexibility, and unique placement of functionality within the scaffold.

In an effort to develop more selective sensors, chemists have studied enzymes for their ability to selectively recognize, transform, and then catalytically produce various biomolecules with high turn-over rates under very low concentration conditions (Diederich, 1991). From these ongoing efforts, chemists have made advances in understanding the cooperative, non-covalent interactions that drive these host-guest processes. Rotaxane molecules have potential use as logic molecular switching elements and molecular shuttles (Clemente-Léon, et al., 2006). These molecular "machines" are usually based on the movement of a cyclophane on a straight chain axle, terminated at each end with a large molecule (stopper/terminus). The cyclophane can rotate, like a wheel and axle, or it can slide along its axis from one site to another. Controlling the position of the cyclophane allows the rotaxane to function as molecular switch, with each possible location of the cyclophane corresponding to a different state. Rotaxanes can be manipulated both by chemical and photochemical inputs.

In combining host-guest chemistry and rotaxane-based molecular machines, host-[2]rotaxanes have been studied as mimics for protein binding and cellular transport. Such transport agents need to be soluble in different environments and need to strongly bind a guest molecule. Dvornikovs, et al. (2003) has demonstrated that a host-[2]rotaxane containing a derivatized dibenzo-24-crown-8 (DB24C8) ring and a calix[4]arene can bind a variety of guests in water, dimethyl sulfoxide (DMSO), and mixed solvent systems. In addition, transportability of the rotaxane into cellular membranes was observed using a fluorescent tagged inhibitor.

The chemistry of macrocyclic recognition is akin to having a toolkit of multiple components and a strategy of using them to form artificial receptors designed to bind and detect specific compounds. Precedence for organophosphate binding has been demonstrated using imprinted polymers, yet this approach does not offer the flexibility needed for multi-application use. Having similar design principles for binding, host-[2]rotaxanes can be incorporated into different media, depending on the application, and can have the advantage of flexible built-in detection probes that avoid the need for secondary analysis. The binding, transport, and signal generating properties of host-[2]rotaxanes offer a compelling structure for organophosphate chemical sensor design.

3.1 Synthesis Background

A key aspect of a rotaxane design strategy is the ring's mobility along the axle. A means to study this mobility is to incorporate a signaling moiety (e.g., a fluorescent indicator) as the stopper within the rotaxane structure. The movement of the ring can either induce or quench the signal. From this action, the kinetics of mobility can be quantified. During the first year of this effort, work was focused on the synthesis of the artificial receptor that included a fluorescent signaling element. The following sections summarize the synthetic approaches taken, and discuss the difficulties encountered with this approach.

3.1.1 Attachment of Fluorescein

Rotaxane molecules are non-covalently linked interlocking bimolecular systems. Rotaxanes are consistently prepared in good yields through the use of template directed synthesis techniques also known as self-assembly. For artificial receptor **1**, the rotaxane is prepared by taking advantage of the collective partial negative charges on a crown ether ring (dibenzyl-24-crown-8-ether). The collective partial charge is able to displace a soft counterion such as hexafluorophosphate ($^{-}PF_6$). A threaded state maximizes the charge interactions; thus, creating a threaded state Figure 3-1. Once threaded, the rotaxane is easily attached to any molecule large enough to keep the ring from sliding off.

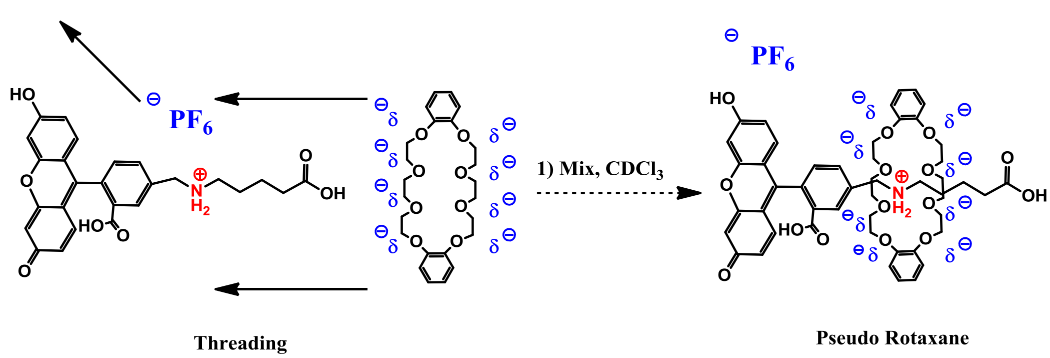

Figure 3-1. Template-directed Assembly Mechanism

For this system, two strategies were employed in the attempts to add a fluorescent indicator to the tail of the rotaxane molecule. The first effort was to build a "tether" to fluorescein. Figure 3-2 shows the design concept for a fluorescent tether. The highly electrophilic nature of fluorescein required the used of carefully selected protecting groups to prevent side reactions as the tether components were installed. Ultimately, the reagents required for completing the tether were incompatible with all feasible protections for fluorescein (Appendix C). The complete description of the efforts to prepare a fluorescent tether is described in the first year report.[1] Data pertaining to the synthesis products for this route are contained in Appendix D of this report.

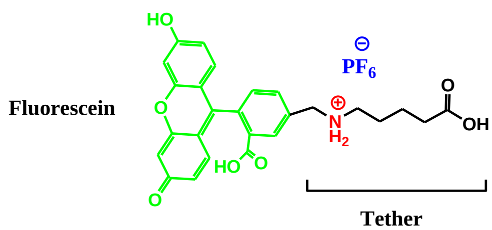

Figure 3-2. Fluorescent Tether Concept

The second strategy placed a functional group on the end of the tether to act as a handle from which an indicator can be added Figure 3-3. This design has two significant advantages: 1) the sensitive fluorescent indicator can be added late the preparation of **1** and 2) the handle allows for the addition of several different types of indicators.

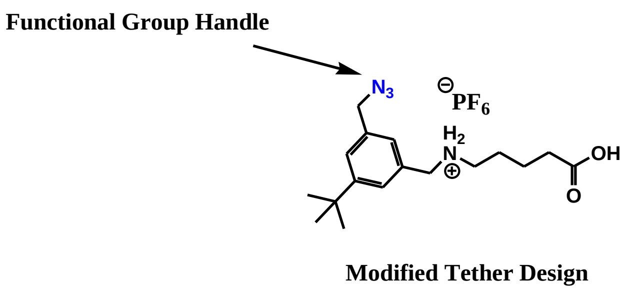

Figure 3-3. Modified Tether Concept

The synthesis route of this modified tether was longer as a result of the asymmetric induction. Despite the longer route, the tether was prepared and tested for rotaxane forming ability. This

[1] Battelle, "Tunable Artificial Receptor as a Chemical Sensor for V- and G-agents", FY10 Year Technical report (31 March 2011) for Contract HDTRA1-10-C-0010.

tether can be threaded by the crown ether; however, it was quickly discovered that the handle was unable to keep the crown ether on the tether (see Figure 3-4). As a result, the ring slipped off the back during the attempt to couple it to the receptor body. The complete description of the efforts to prepare a fluorescent tether is described in the first year report.[1] Data pertaining to the synthesis products of this approach is contained in Appendix D.

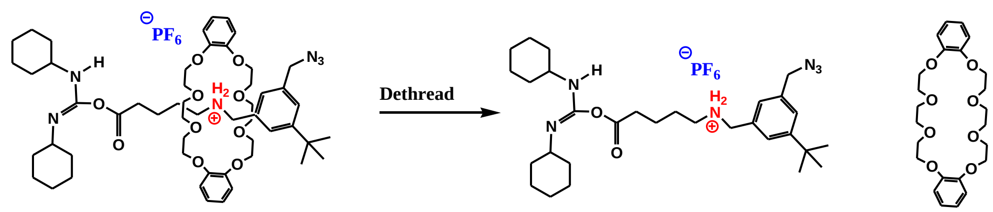

Figure 3-4. De-threading of Modified Tether

These two synthetic strategies focused on alterations to the tether's stopper. In both cases these changes have unexpectedly compromised the non-covalent threading mechanism. This result suggests that any alterations to the aromatic functionally in the tether are not compatible with high yielding rotaxane formation. Future design modifications need to retain both of the t-butyl groups and the aromatic ring in its current electronic state.

One other potential design concept was considered. This design involves adding a short tail in-between the two t-butyl functionalities as shown in Figure 3-5. This modification moves the indicator away from the ring while maintaining both the t-butyl and the electronic state of aromatic ring. This design was not perused for two reasons. First, it is uncertain if a quenching interaction between the crown ether ring and the fluorescein would take place. Second, increased synthetic difficulty renders the concept unattractive for large scale production.

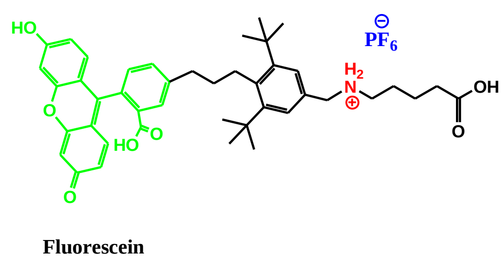

Figure 3-5. Tether Concept with Extended Axle Tail

There are other areas within the receptor system where signaling can be introduced. Signaling could be introduced by attaching fluorescein to the crownether. The overall sliding concept of the receptor is retained; however, the triggering role is transferred from the tail to the ring. The signaling mechanism is similar in that the t-butyl functionality on the tether quenches fluorescence in the crownether at the unbound state. As the receptor binds agent, the ring moves and fluorescent signaling occurs. Alternatively, a signaling plate could be installed across the

bottom of the cyclophane creating a bowl shape pocket. As agent is captured, signaling is actuated as result of the interaction between the agent and cavity's bowl. A significant advantage to this design concept it that the signaling mechanism does not require any changes to the existing rotaxane forming methodology.

After attempting three different approaches to attach the indicator to the tether, a simplified tether (tether **33**), (Dvornikovs, et al. 2003) without an attached indicator, was used to synthesize artificial receptor 1 (Mitigation plan C outlined in Appendix C).

3.2 Synthesis of Artificial Receptor 1

The synthetic strategy for preparing the artificial receptor **1** follows a convergent synthesis of the main sections of the molecule. This reduced the overall risk by compartmentalizing the synthesis of each moiety so that subsequent successful completion of one was not dependent on the initial successful completion of another. The cyclophane pocket, a modified crown ether and tether are all prepared independently of one another. These components are then assembled into one large molecular system using proven template directed synthesis techniques. Once the molecule is assembled, the amino-acid, arginine, is installed on the crown ether. Figure 3-6 shows receptor **1** with its main components accentuated by different colors.

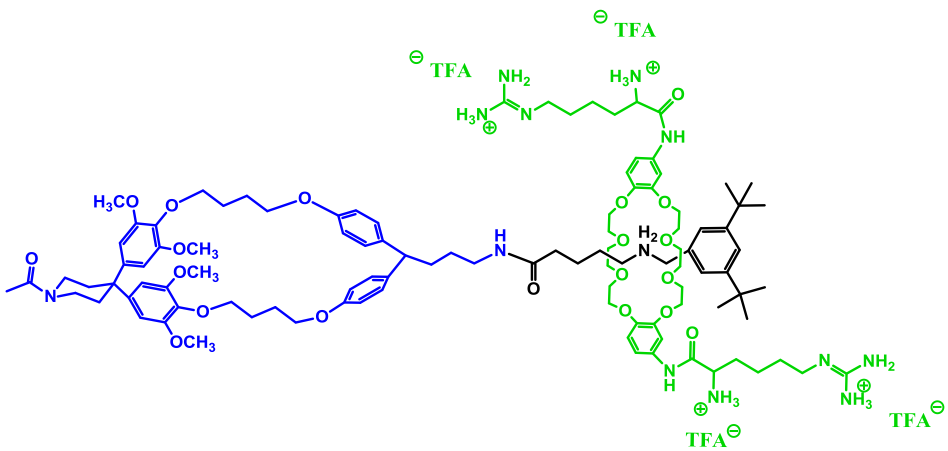

1

Figure 3-6. Artificial Receptor 1: Cyclophane Pocket (Blue), Tether (Black), and Modified Crown Ether (Green)

3.2.1 Synthesis of the Cyclophane Pocket

A convergent synthesis strategy was used to synthesize the cyclophane pocket. Two components (referred to as left and right half) were prepared in good yield and independently following literature procedures (Dvornikovs, et al. 2003). Figure 3-7 provides the structure for each half.

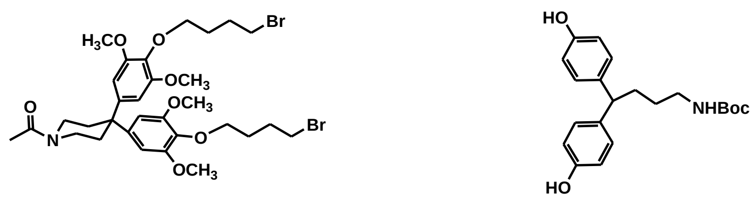

Left Half

Right Half

Figure 3-7. Structures of the Left and Right Halves of the Cyclophane Pocket

3.2.1.1 Synthesis of the Left Half

Construction of the left half of the cyclophane was completed following the route shown in Figure 3-8. Cleft component **21** was synthesized in 81% yield by mixing *N*-acetylpiperidinone with 2,6-dimethoxyphenol in the presence of concentrated sulfuric acid. The cleft material was then mixed with excess 1,4-dibromobutane in the presence of cesium carbonate to give the target molecule in 98% yield after purification by column chromatography.

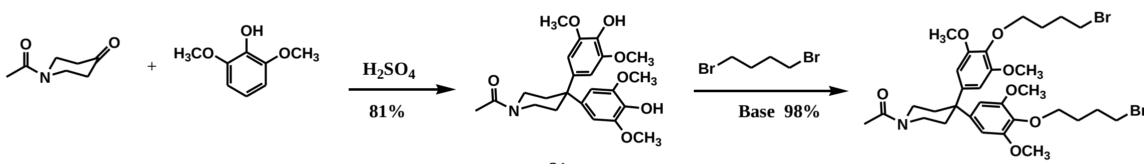

Figure 3-8. Synthetic Route for Left Half of Cyclophane

3.2.1.2 Synthesis of the Right Half

Construction of the right half of the cyclophane was completed as illustrated in Figure 3-9.

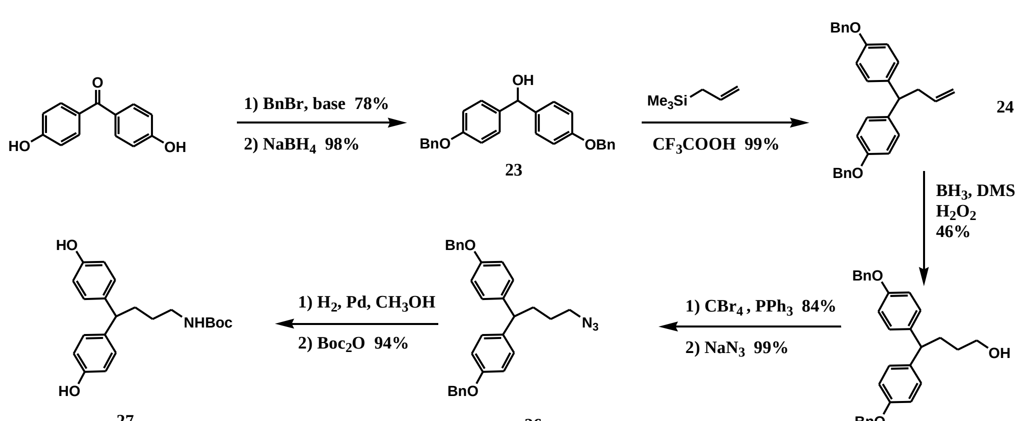

Figure 3-9. Synthetic Route for the Right Half of the Cyclophane

Alcohol **23** was prepared by mixing benzyl bromide with 4,4'dihydroxybenzophenone in the presence of cesium carbonate. This material was reduced with sodium borohydride under reflux conditions to give **23** in a high 76% yield for the 2 steps. Alcohol **23** was treated with trimethylallylsilane in the presence of trifluoroacetic acid which provided **24** in near quantative yield. Olefin **24** was treated with borane dimethylsulfide followed by oxidation with peroxide. These conditions achieved the desired product **25a**; however, yields for this reaction were low. Purification by column chromatography afforded a thick clear resin of alcohol **25a** in a 46% yield. Alcohol **25a** was converted into bromide **25** in an 84% yield through the reaction with carbon tetrabromide and triphenylphosphine. Conversion of the bromide to azide **26** using sodium azide was quantitative. The right half was completed in good yield by treating **26** with palladium black under a 55 psi hydrogen atmosphere for up to 5 days followed by $(Boc)_2O$ to mask the amine.

3.2.1.3 Assembly of the Cyclophane Pocket

The two halves of the cyclophane were combined under dilute basic conditions in DMF and stirred for 2 weeks. The BOC protecting group was then removed by stirring cyclophane **34** in chloroform containing 5% TFA for 16 hours to yield cyclophane **35**. The ^1H NMR of **35** is shown in Figure 3-10. Some of this material was retained for use in binding studies with selected simulants (Section 4.1).

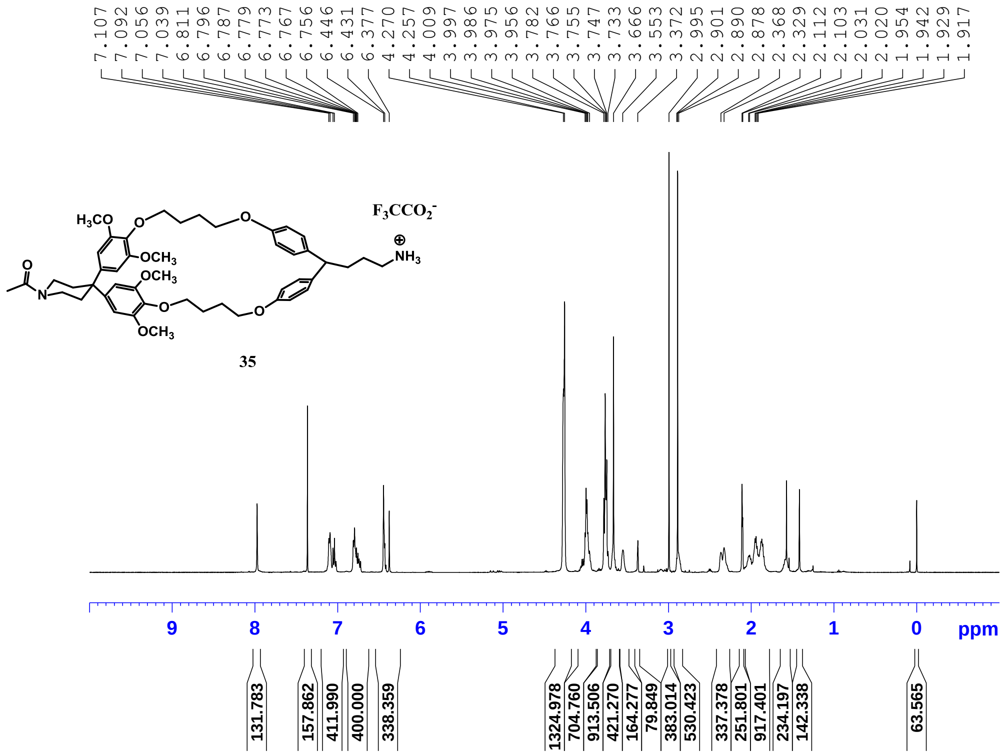

Figure 3-10. ^{1}H NMR of Cyclophane 35 (TFA salt)

3.2.2 Synthesis of the Crown Ether

Dibenzyl-24-crown-8-ether (DB24C8) was nitrated in high yield by reaction with concentrated nitric acid in acetic acid. The nitrated ring was reduced and protected *in situ* with $(Boc)_2O$ under standard hydrogenation conditions using 10% palladium on carbon in a hydrogen atmosphere.

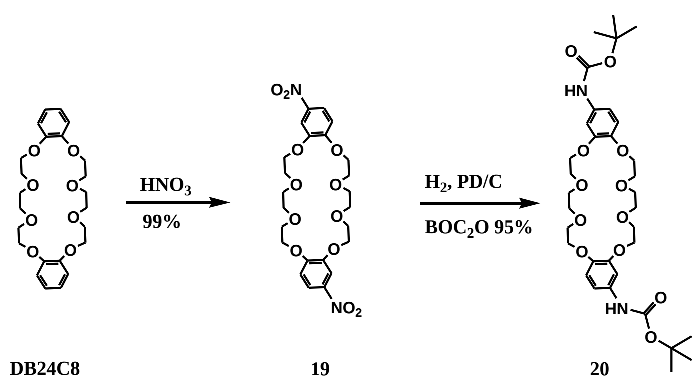

Figure 3-11. Synthesis of Modified DB24C8

3.2.3 Synthesis of the Tether

The tether was prepared from 3,5-di-*tert*-butyltoluene in high yields and high quality following the route outlined in Figure 3-12. (Zehnder and Smithrud, 2001)

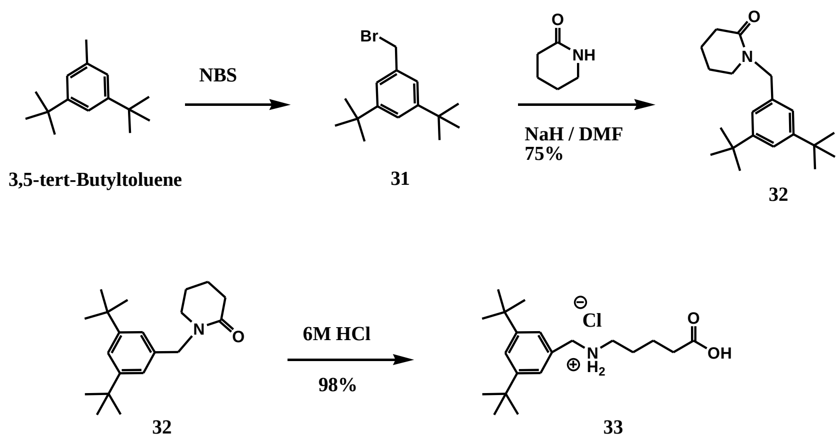

Figure 3-12. Synthesis of the "Simplified" Tether

Bromide **31** was prepared in good yields from commercially available 3,5-di-*tert*-butyltoluene by mixing with NBS and benzoyl peroxide in carbon tetrachloride. After filtration and concentration by removal of the solvent, this material was used without further purification. Intermediate **32** was prepared in good yield by mixing **31** with sodium δ-valerolactate in DMF at 0 °C. It is important to consume all of the δ-valerolactam otherwise purification becomes difficult. Hydrolysis of **32** was performed by heating to 125 °C in 6N HCl for 48 hours. Tether **33** was collected by filtration and dried under vacuum to give a 90% yield.

3.2.4 Synthesis of Host-[2]Rotaxane

Cyclophane **35** was neutralized with 2N sodium hydroxide then mixed with DCC-[2]rotaxane reagent following the scheme in Figure 3-13 below.

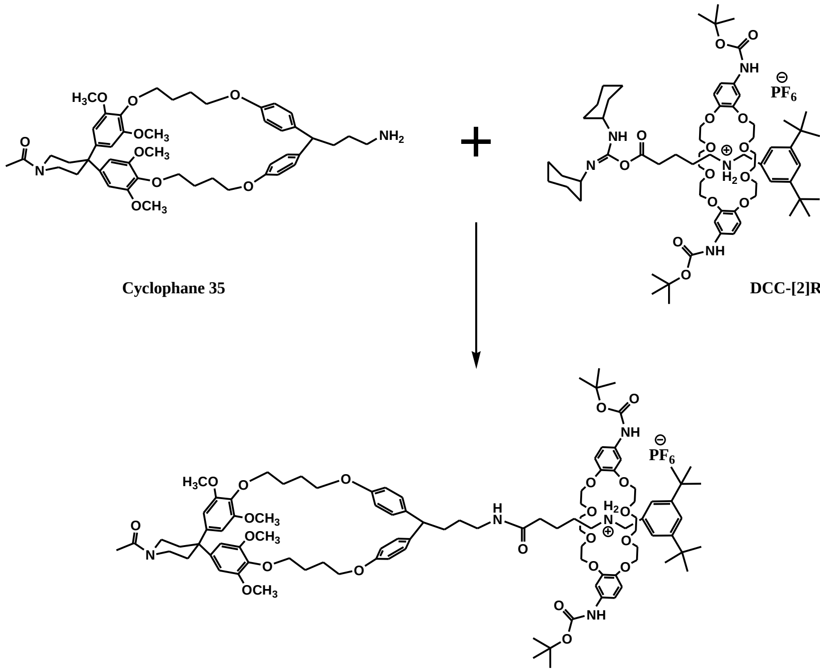

Cyclophane 35

DCC-[2]Rotaxane Reagent

Host-[2]Rotaxane 36

Figure 3-13. Synthetic Scheme for Preparing the Host-[2]Rotaxane

The mixture was stirred for three days at room temperature to facilitate complete conversion. A small amount of white precipitate (dicyclohexylurea, DCU) had formed, indicating the coupling reaction had occurred. DCU was completely removed by changing solvents to acetonitrile and then filtering the solution. After purification by column chromatography, three compounds were recovered: cyclophane **35**, DCC-[2]rotaxane reagent and the host-[2]rotaxane **36**. No other by-products were found. The un-reacted cyclophane **35** was estimated at 83% based on the amount of host-[2]rotaxane recovered. The isolated yield of host-[2]rotaxane was (1.0 g, 17%); ^{1}H NMR of host-[2]rotaxane **36** is shown in Figure 3-14.

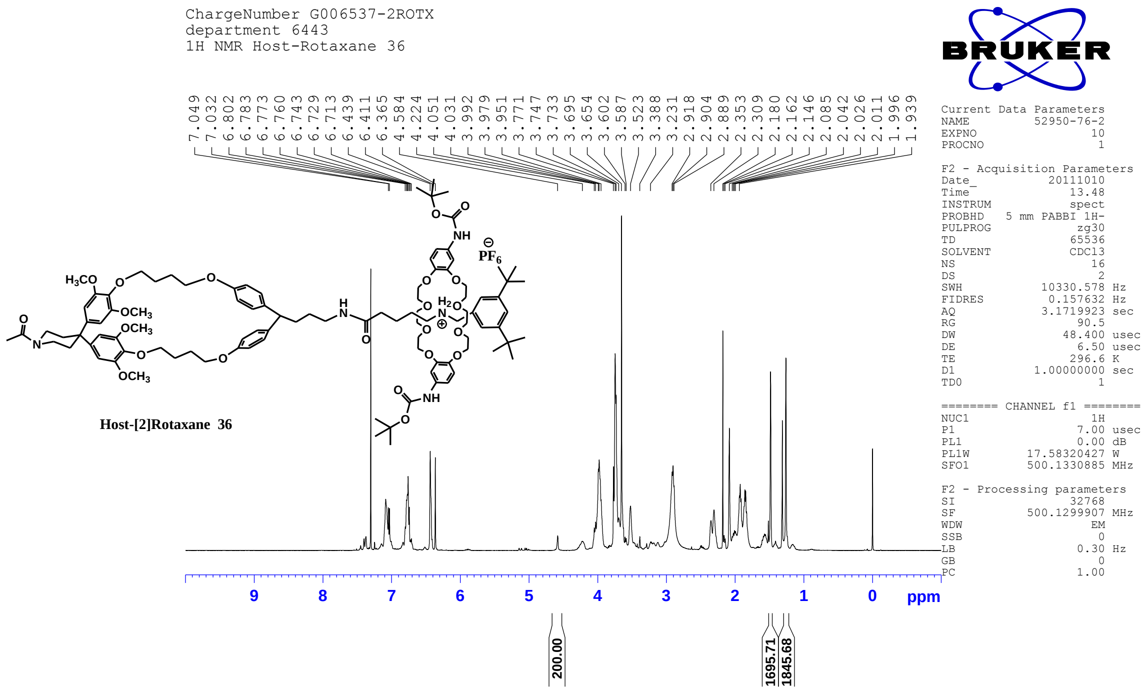

Figure 3-14. [1]H NMR of Host-[2]Rotaxane 36

The low conversion rate is not yet fully understood. Based on literature precedent, the expected yield for this reaction was between 60 and 70% (Dvornikovs, et al. 2003). Optimizing reaction conditions such as time, temperature and solvent should improve yields. There is some evidence which suggests that cyclophane **35** may be changing its configuration through folding and / or twisting of the pocket. This conformational change would inhibit access to the primary amine on the cyclophane. The synthesis of the host-[2]rotaxane was repeated following the same procedure; however, the ammonium ion on the cyclophane was neutralized with triethylamine. After purification by column chromatography the reaction generated a higher yield of host-[2]rotaxane **36** (2 g, 26% yield). While the yields did improve, the conversion is still lower than expected. Both batches of host-[2]rotaxane were combined for the completion of the artificial receptor following the scheme in Figure 3-15.

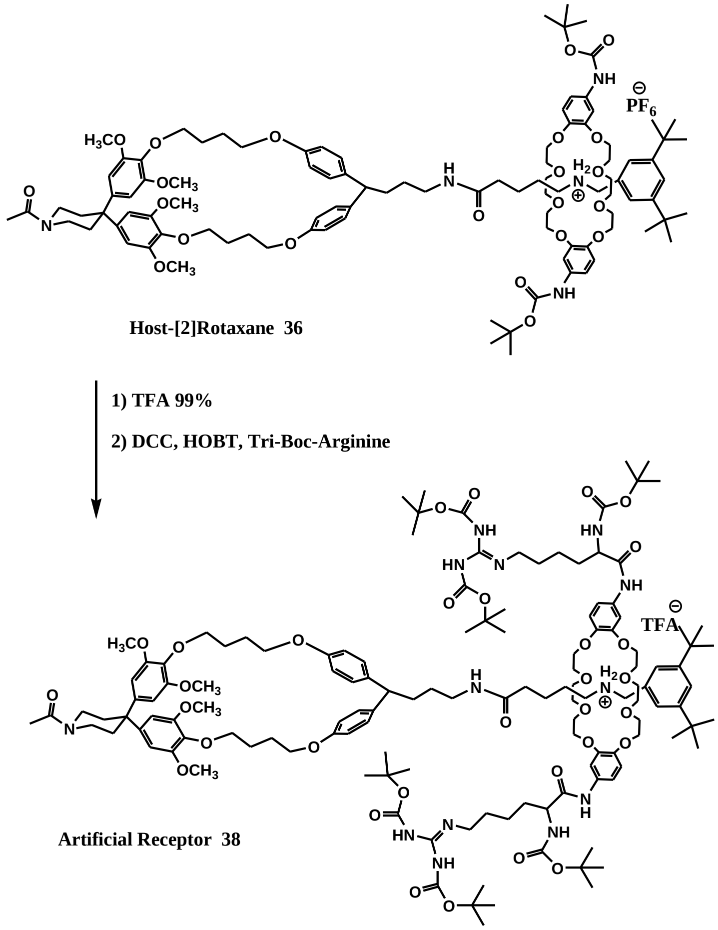

Figure 3-15. Final Stage Synthesis Scheme for the Artificial Receptor

The BOC protecting groups on the host-[2]rotaxane were quantitatively removed at room temperature by stirring with 5% TFA in chloroform for 3 hours. Tri-BOC-arginine was installed on the host-[2]rotaxane using DCC and a catalytic amount of 1-hydroxybenzotriazole hydrate. The DCU byproduct was removed and then the compound was purified by column chromatography to afford **38** in 70% yield. The ^{1}H NMR spectrum is shown in Figure 3-16. Note the presence of the multiple BOC t-butyl groups on the arginine at δ 1.5.

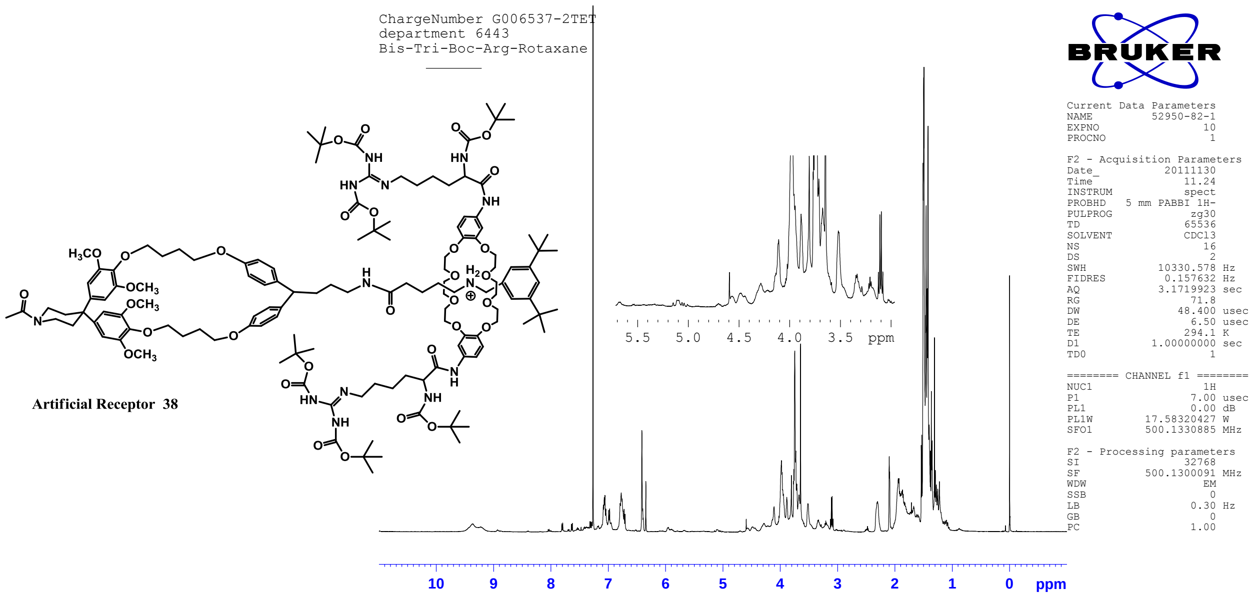

Figure 3-16. [1]H NMR of Bis-Tri-Boc-Arg-Host-[2]Rotaxane 38

The final step, removal of the BOC-protecting groups, was achieved by mixing rotaxane **38** in DCM with 50% TFA in acetic acid. After removing the volatiles, the material was solvated with DMSO, and then precipitated with hexane to give target molecule **1** as an amorphous glass Figure 3-17. The [1]H NMR spectrum of the product is shown in Figure 3-18. Note the δ 4.6 for the retained methylene group between the primary amine and the benzylic "stopper" confirming presence of the rotaxane configuration. In addition, there is an absence of BOC groups in region of δ 1.5, corresponding with the deprotection of the pendant amine functionalities. Mass spectral confirmation of the material was hampered by the multiple charges on the molecule. Samples were sent to the Ohio State University's high resolution mass spectrometry facility. Similar difficulties for interpretation of the spectrum occurred.

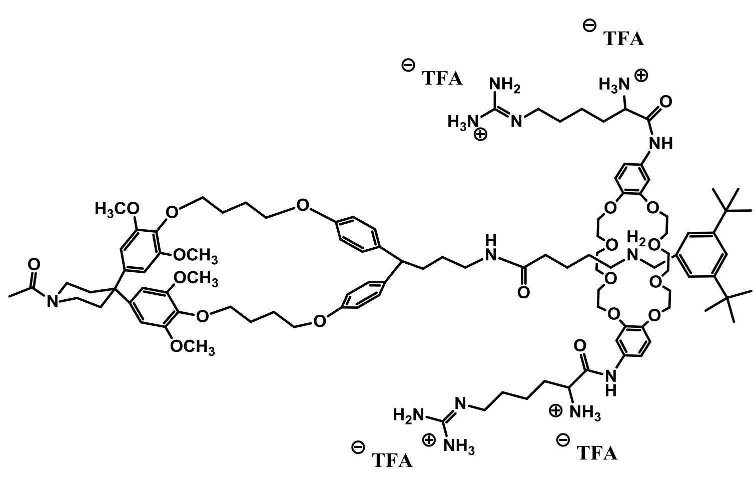

Figure 3-17. Structure of Bis-Tri-Arg-Host-[2]Rotaxane 1

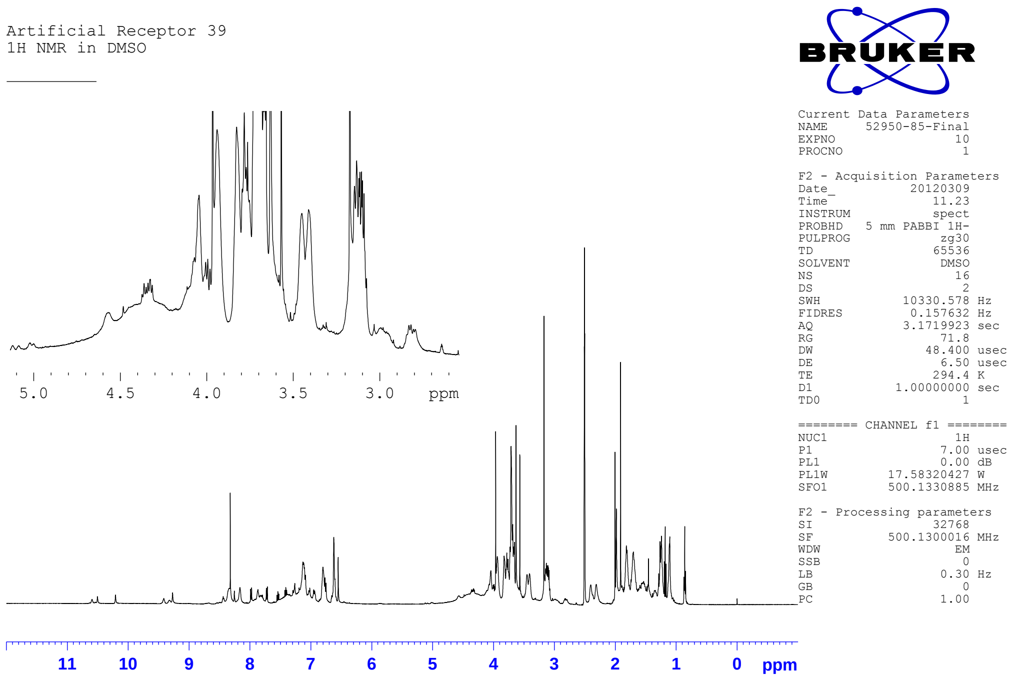

Figure 3-18. ^{1}H NMR of Target Compound: Bis-Tri-Arg-Host-[2]Rotaxane 1

The receptor **1** was readily solvated in a mixture of 95% water 5% DMSO to maximize the performance of the hydrophobic pocket within the receptor.

3.3 Synthesis Lessons Learned

The incorporation of fluorescein into the rotaxane structure was not successful due to the inability to adequately "protect" the indicator during key reaction steps. While it may be possible to incorporate other indicators in a similar manner, it will be important to consider the reaction conditions subsequent to the attachment of the indicator. This will allow the synthetic steps to proceed without interference or unwanted decomposition. Complete descriptions of the synthetic paths to the artificial receptor, including potential designs incorporating a signaling indicator are given in Appendices A and D.

The rotaxane formation reaction was a low yielding reaction. Reasons for this may include low accessibility of primary amine on the cyclophane tail. The large pocket size allows the tail to "tuck" into the pocket, preventing reaction with the rotaxane forming reagent. The pocket structure can be strengthened by using more rigid arms instead of alkyl chains. Optimizing reaction conditions could be performed to thermodynamically favor the unfolded pocked configuration.

4.0 Binding Studies

To fully evaluate the ability of the artificial receptor to capture the intended targets (CWAs), a series of binding studies were performed. These studies included evaluation of the cyclophane pocket **35** with simulants, using nuclear magnetic resonance (NMR) spectroscopy to gage the magnitude of the hydrophobic interactions. Modeling of the cyclophane-analyte interactions was also performed to estimate the binding energies of the complex. Finally, a series of binding studies were performed using GC-MS to determine the amount of binding between the artificial receptor **1** and chemical agents GD and GA.

4.1 Binding Studies on Cyclophane 35

The binding capability of cyclophane **35** was investigated using simulants. Size and shape are key physical properties the simulant need to have in common with the agents. A list of simulant candidates with similar structure and molecular volume to GA and GD was assembled in Table 4-1. From this list, ethyl phenylphosphinate (EPP), malathion and pinacolyl methylphosphonate were selected for study. EPP was bound by cyclophane **35**. The ensuing binding study provided binding performance as well as aqueous environment tolerance information on cyclophane **35**. Malathion and pinacolyl methylphosphonate suffered from NMR signal overlap issues with cyclophane **35**; therefore, definitive evidence of binding could not be observed.

Table 4-1. Potential Simulant Compounds for Study

Name	CAS #	Structure	Mol. Weight (g/mol)	Mol. Volume (cm^3/mol)
Ethyl phenyl phosphinate (EPP)	2511-09-3	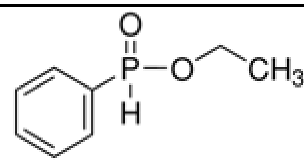	170.15	150.7
Malathion	**121-75-5**	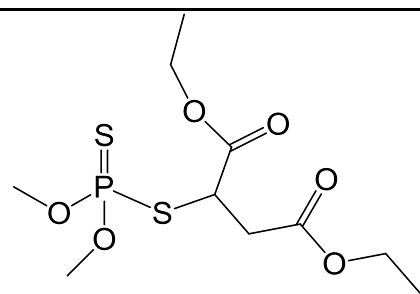	330.36	259.653
Dimethyl methylphosphonate (DMMP)	756-79-6	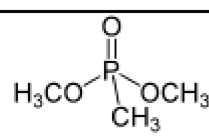	124.08	114.9

Pinacolyl methylphosphonate	616-52-4	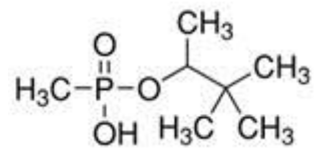	180.18	174.6
Soman (GD)	96-64-0	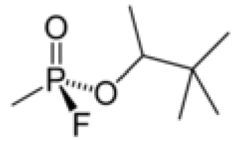	182.17	178.2
Tabun (GA)	77-81-6	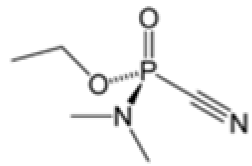	162.13	148.9

The performance of the hydrophobic binding interactions increases with the percentage of water in the solvent system used. Cyclophane **35** was able to tolerate up to 30% water in DMSO. A ^{1}H NMR titration experiment was designed in the mmol concentration range according to Table 4-2 to determine binding strength. The expected binding constant range for this molecule is 10^1 to 10^4 M^{-1}. EPP was held constant at 10 mmol while cyclophane **35** was varied from 0 to 50 mmol.

Table 4-2. ^{1}H NMR Titration of EPP with Cyclophane 35

Sample #	Cyclophane (mmol)	EPP (mmol)	Vol. Cyclophane Stock Solution (µL)	Vol. EPP Stock Solution (µL)	Vol. Blank Solvent (µL)
1	0	10	0	250	250
2	5	10	25	250	225
3	10	10	50	250	200
4	15	10	75	250	175
5	20	10	100	250	150
6	25	10	125	250	125
7	50	10	250	250	0

Four different concentrations of water in DMSO (95:5, 90:10, 85:15 and 80:20) were studied following the titration outlined in Table 4-2. The binding constant in each solvent system was determined using a non-linear least squares analysis. For EPP, the P-H bond becomes obscured as the concentration of cyclophane **35** increases. The binding constant was determined by measuring the rate at which this signal was obscured. The aromatic protons on the guest are not obscured and were normalized to 5. This provided a basis against which to determine the relative change. The following binding equation [1] was used to calculate the association constants,

$\Delta\delta = \Delta\delta_{obs} - \Delta\delta_0 = K_A[C]\ \Delta\delta_{max} / (1 + K_A[C])$, where the difference in the area ($\Delta\delta$) of the P-H signal in the presence of cyclophane **35** ($\Delta\delta_{obs}$) and in its absence ($\Delta\delta_0$) depends on the concentration of cyclophane **35** (C), the area of the P-H proton when it is completely bound to cyclophane **35** ($\Delta\delta_{max}$), and the binding constant of this complex (K_A). Table 4-3 shows the result from the integration of the ^{1}H NMR spectra of tubes 1 through 7. The ^{1}H NMR data for all the binding studies is available in Appendix A.

Table 4-3. ^{1}H NMR Analysis for the 95/5 DMSO-d_6 / D_2O Titration

Tube	[Cyclophane]	[EPP]	Guest Area Aromatic H	P-H Area obs.	Δ Area
1	0	10	5	0.437	0
2	5	10	5	0.241	0.196
3	10	10	5	0.137	0.3
4	15	10	5	0.094	0.343
5	20	10	5	0.082	0.355
6	25	10	5	0.076	0.361
7	50	10	5	0.078	0.359

The raw data was plotted using the non-linear least squares model below in Table 4-4.

Table 4-4. Non-linear Least Squares Model: Results for 95/5 DMSO-d_6 / D_2O

```
Nonlinear regression model
 model:  Y ~ P1 * P2 * X/(1 + P1 *X)
  data:  parent.frame()
    P1      P2
223.6079   0.4193
 residual sum-of-squares: 0.001997

Number of iterations to convergence: 6
Achieved convergence tolerance: 1.996e-06
```

*P1=K_a, P2= $(\Delta \text{ Area})_{Max}$, Y=(Δ Area), X=[Cyclophane 35]

The data was plotted and resulted in the following curve show in Figure 4-1. The residuals and fit values are shown in Figure 4-2.

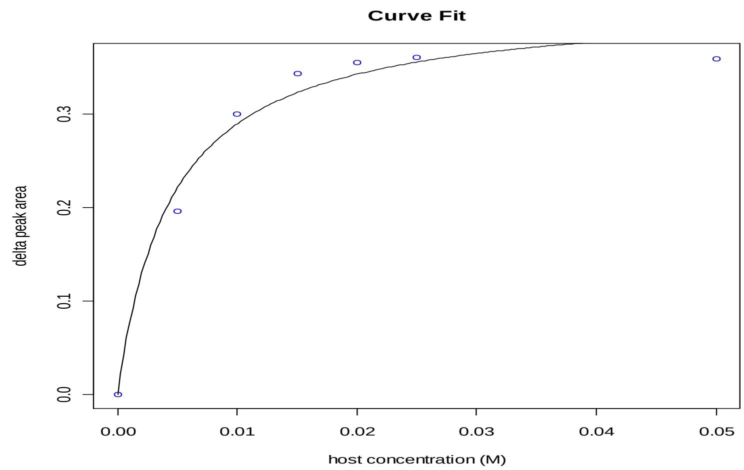

Figure 4-1. Binding Curve for Cyclophane 35 and EPP at 95/5 DMSO-d_6 / D_2O

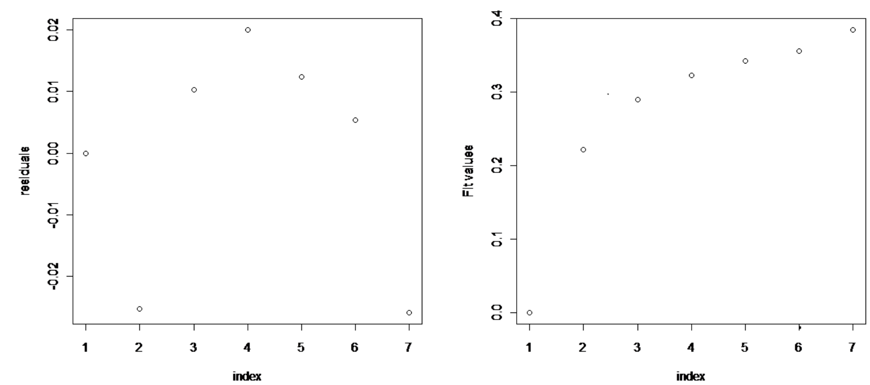

Figure 4-2. Residuals and Fit Values for Cyclophane 35 and EPP at 95/5 DMSO-d_6 / D_2O

The binding constants determined from all four water concentrations are shown in Table 4-5. The ^{1}H NMR data and binding curves are provided in Appendix A.

Table 4-5. Binding Constant Results for EPP and Cyclophane 35

% DMSO-d_6	**% D_2O**	**K_a, M^{-1}**
95	5	2.23×10^2
90	10	4.66×10^2
85	15	2.49×10^2
80	20	ND

ND=Not Determined

Results indicate the operational range for the cyclophane is between 5 and 15 percent water in DMSO. As expected, binding was not observed in 100% DMSO as water is necessary for a

hydrophobic interaction. Overall, the hydrophobic interaction is weak and the observed binding constants of this cyclophane are consistent with other cyclophanes reported in the literature. It is not entirely clear why the binding constant drops when the water concentration increases from 10% to 15% water. Closer review of the binding curve suggests that the curve at 15% water does not fit the data well. This can occur if the concentration of the titration is too high. In essence, the binding constant is much higher; thus, the titration needs to be performed at an order of magnitude lower in concentration to compensate. When the water concentration reached 20%, the data became erratic throughout the progression of the study. This was likely caused by formation of colloids and/or micelle complexes. Once this occurs, the binding interaction is no-longer a single kinetic event. Multiple different types of complexes with varying ratios of host to guest are present. The 1:1 binding model cannot account for such complex associations; thus, the model fails. It is important to note that the cyclophane precipitates out of solution at water concentrations of 30% or greater. Effectively, the operational range of the cyclophane was reached between 15% and 20% water.

4.2 Computational Study

A computational study was undertaken to understand the binding of cyclophane **35**. The following methods were used in this study. Molecular energies were computed with the Spartan software published by Wavefunction, Inc., using both molecular mechanics (MM3 parameter set) and quantum mechanics (using the MOPAC computational package with PM3 parameterization, no solvent simulation). These methods[2] were used to study cyclophane-guest complexes with the following guests: EPP, DMMP, GD and GA. Table 4-6 shows the calculated molecular energies (free and bound) and binding energy for each cyclophane-guest complex.

[2] The cyclophane-guest structure was entered manually, and optimized using molecular mechanics. Then, a molecular dynamics simulation (1 ps @ 300 K) was used to generate 25 new seed conformations. Each of these was minimized again using MM3, and the lowest energy of all of these conformations was used in all further calculations of that cyclophane-guest complex as the starting point for optimizations using the quantum method. Once bound structures were obtained for each complex using each of the computational methods, then each complex was subsequently “unbound” by simply relocating the guest 100 Angstroms away from the cyclophane. This “unbound” structure was then allowed to relax by re-optimizing it using the computational method that was used to generate that particular structure

Table 4-6. Calculated Molecular Energies and Binding Energies for Cyclophane 35

Species	Molecular Energies (kcal/mol) Bound	Free	Binding Energy (kcal/mol)
(**35**)-EPP (Ph in)	-393.7	-389.6	4.0
(**35**)-EPP (Et in)	-389.8	-389.6	0.2
(**35**)-DMMP	-484.4	-479.7	4.8
(**35**)-GA	-397.8	-392.2	5.6
(**35**)-GD	-526.0	-518.2	7.9

All of the complexes show stable binding, and the binding energies are of the order of magnitude expected for mainly hydrophobic interactions, 0 – 8 kcal/mol. This is consistent with the binding constants observed experimentally for cyclophane **35** with EPP. The EPP complex with the phenyl group inside the cyclophane is significantly more strongly bound than the EPP complex with the ethyl group inside the cyclophane[3]. The difference between the phenyl-bound and ethyl-bound complexes is likely due to π-π stacking interactions between the EPP phenyl group and the four phenyl rings of the cyclophane. From the experimental determination of the binding constants in Section 3.1, the aromatic protons on EPP did not show a change in chemical shift, which would suggest the mode of binding for EPP is a complex with the ethoxy bound into the cavity of the cyclophane.

Interestingly, the binding energy for the EPP-complex, calculated using the measured binding constants from Table 4-5 in the equation $\Delta G = -RT\ln(K_a)$ gives a result ranging from 3.2 to 3.6 kcal/mol (depending on the solvent ratio). This value is between the estimated values for the phenyl-bound and ethoxy-bound conformations shown in Table 4-6.

Because of the potential π-π stacking interactions of the phenyl-bound complex, EPP is not a good simulant for polar agents such as GA. Further, as DMMP is also a more polar molecule than EPP, it has little hydrophobic character, thus a weak complex with the cyclophane might be expected. This suggests that smaller, polar molecules will be out-competed for the pocket site. Note that this software package likely overestimates the binding energy of these molecules (DMMP and GA) because the computational methods used are not capable of simulating the solvent dipole field, and therefore do not take account of the solvent stabilization of the polar guest in the unbound complex (Williams, et al., 2004). This also has implications for the binding of GD in cyclophane **35**; however, the binding pocket is shown to be sufficiently large to fit the

[3] In the case of the EPP complex, the naturally optimized bound structure had the phenyl substituent inside the cyclophane ring. To ensure that this is really the minimum energy conformation of the complex, the structure was intentionally redrawn and optimized with the ethyl group inside the macrocyclic ring. In all other cases, the complex was allowed to optimize naturally without human intervention.

large pinacolyl group of GD and favor hydrophobic interactions. If the pocket were not sufficiently large, then the energy calculated for this complex would reflect the destabilization due to the repulsive van der Waals forces that would result from this overcrowding.

Figures 4-3 through 4-7 show a variety of views of the cyclophane-guest complexes for EPP (phenyl bound), EPP (ethyl bound), DMMP, GA, and GD, respectively. Each figure includes a top, bottom, and side view of the complex, rendered as both a ball-and-stick model (colored by atom type, all carbon-bound hydrogen atoms removed for clarity) and a space-filling model (Key to figures: carbon: grey; oxygen: red; nitrogen: blue; phosphorus: orange; fluorine: yellow; hydrogens omitted for clarity).

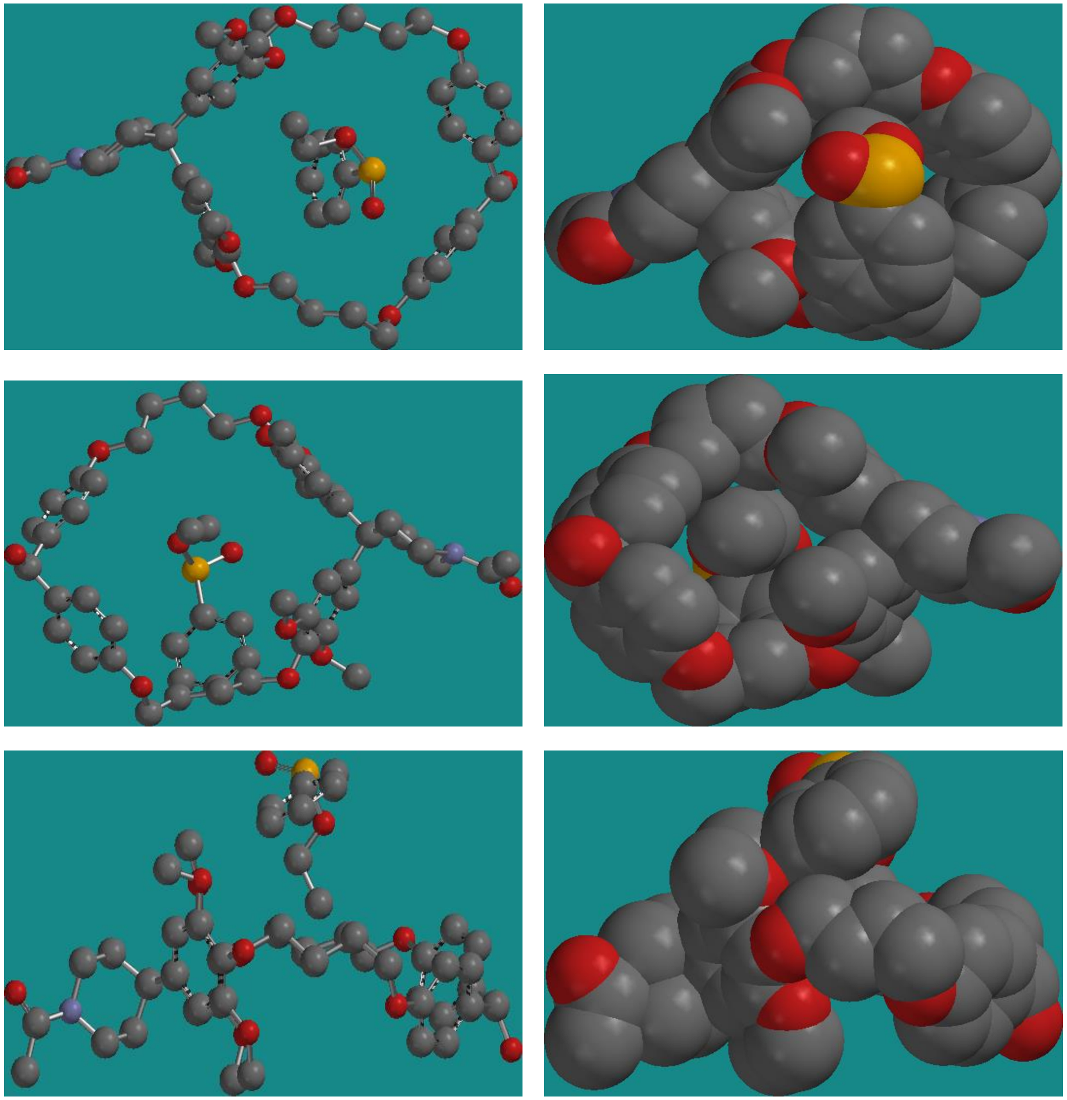

Figure 4-3. Optimized structure of the cyclophane-EPP complex (phenyl bound). Top: top view; middle: bottom view; bottom: side view. Note the P-OCH_2CH_3 group aligned along the rim of the cyclophane cavity, with the P-H and P=O exposed to the exterior.

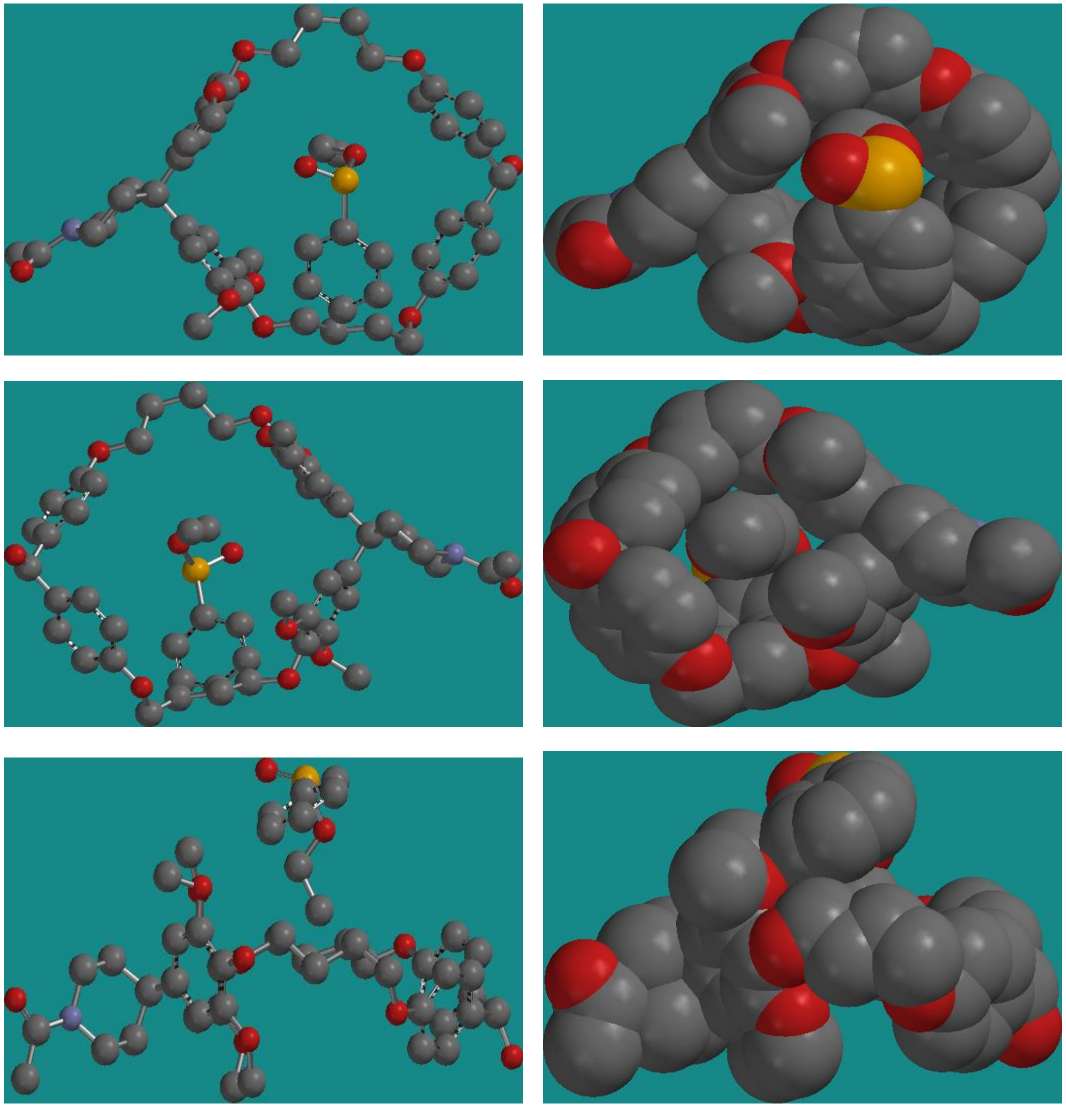

Figure 4-4. Optimized structure of the cyclophane-EPP complex (ethyl bound). Top: top view; middle: bottom view; bottom: side view. Note the P-C_6H_5 group aligned along the rim of the cyclophane cavity

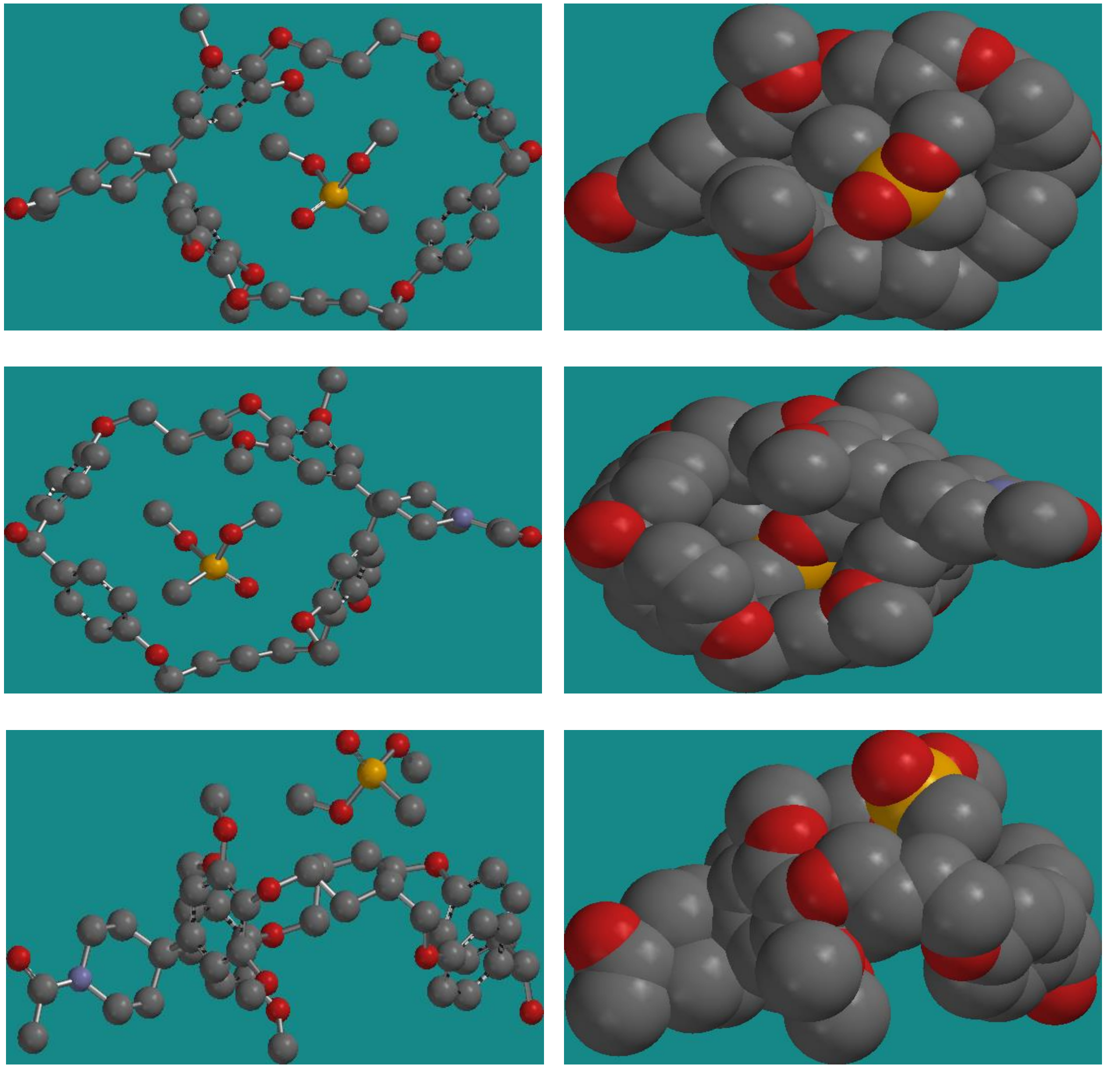

Figure 4-5. Optimized structure of the cyclophane-DMMP complex. Top: top view; middle: bottom view; bottom: side view. Note the P-CH_3 group buried in the cavity, and the P-OCH_3 and P=O groups exposed to the exterior.

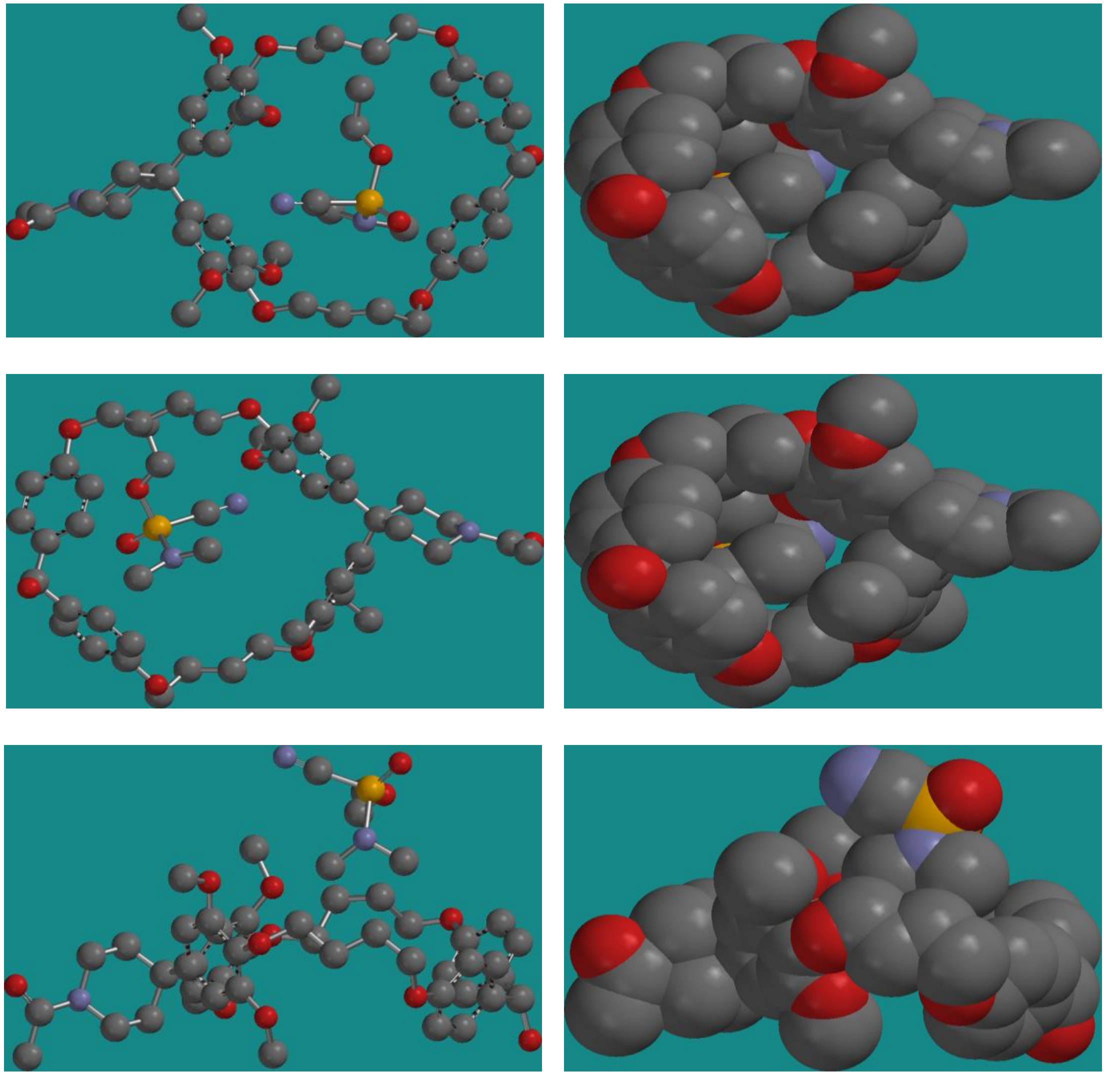

Figure 4-6. Optimized structure of the cyclophane-GA complex. Top: top view; middle: bottom view; bottom: side view. Note the P-OCH_2CH_3 group buried in the cyclophane cavity, with the P=O, P-$N(CH_3)_2$ and P-CN groups exposed to the exterior.

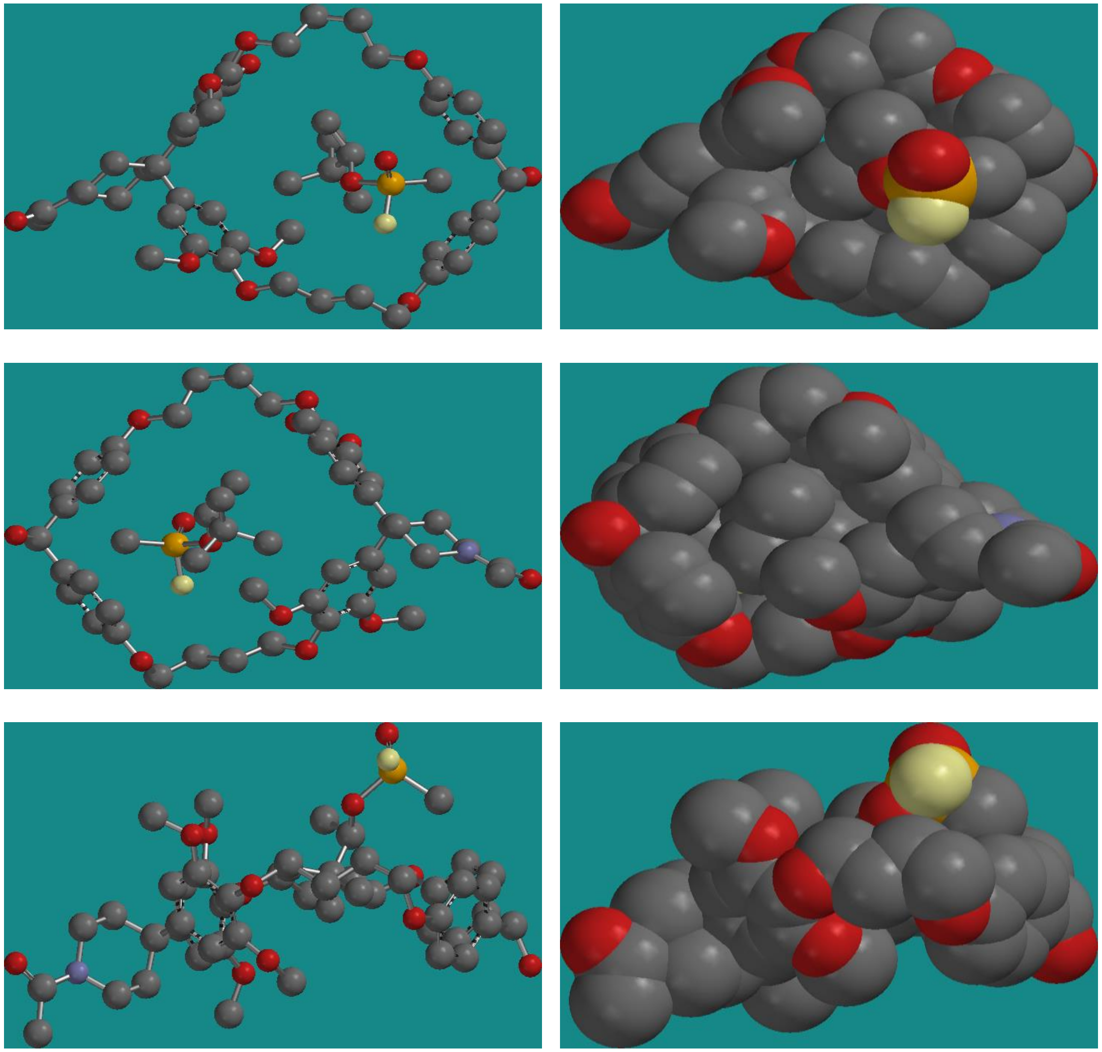

Figure 4-7. Optimized structure of the cyclophane-GD complex. Top: top view; Middle: bottom view; Bottom: side view

4.3 Agent Binding Studies

Due to the difficulty of attaching the fluorescent indicator group to the artificial receptor (discussed in Appendix A), there was no inherent signaling moiety on the receptor compound to evaluate agent binding. Direct measurement of the solutions by fluorescence was not possible. Further, typical measurements made by NMR (as discussed in the simulant study) were not feasible due to the lack of such instrumentation approved for chemical agent at the time of testing.

The only feasible method available to determine the agent binding involved extraction of solutions containing increasing concentrations of artificial receptor **1** and constant concentrations of the agent guest, followed by GC-MS analysis of the extracted agent. Quantification of unbound agent was determined by extracting mixed solutions of artificial receptor **1** and agent with hexane. The amount of unrecovered agent was assumed to be "bound" agent.

4.3.1 Methodology for Assessing Agent Binding Performance

The agent binding performance of artificial receptor **1** was assessed by challenging the receptor with chemical agents GD and GA at three sequentially lower concentration ranges. Assuming that assisted binding interactions occur, the association constant (K_a) for artificial receptor **1** was anticipated to be greater than the hydrophobic interactions determined for the cyclophane (i.e., in the 10^6 or 10^7 M^{-1} range). As such, the receptor was challenged at 10^{-5} M, 10^{-6} M and 10^{-7} M.

Two assumptions were used for this series of experiments:

1) The amount of unrecovered agent was equal to the agent bound by artificial receptor **1**.
2) The agent partition coefficient between hexane and water remained constant throughout the experiments.

Stock solutions for GD, GA and artificial receptor **1** were prepared in anhydrous DMSO at 10^{-3} M, 10^{-4} M and 10^{-5} M according to Tables 4-7 through 4-9.

Table 4-7. Stock Preparation for GD

Solution	Source of Agent	Volume of DMSO	Final Concentration
GD Dilution 1	17.75 µL Neat Material	1 mL	10 X 10^{-2} M
Stock GD 1	100 µL GD Dilution 1	900 µL	10 X 10^{-3} M
Stock GD 2	100 µL Stock GD 1	900 µL	10 X 10^{-4} M
Stock GD 3	100 µL Stock GD 2	900 µL	10 X 10^{-5} M

Table 4-8. Stock Preparation for GA

Solution	Source of Agent	Volume of DMSO	Final Concentration
GA Dilution 1	15.09 µL Neat Material	1 mL	10 X 10^{-2} M
Stock GA 1	100 µL GA Dilution 1	900 µL	10 X 10^{-3} M
Stock GA 2	100 µL Stock GA 1	900 µL	10 X 10^{-4} M
Stock GA 3	100 µL Stock GA 2	900 µL	10 X 10^{-5} M

Table 4-9. Stock Preparation for Artificial Receptor 1

Solution	Source of Agent	Volume of DMSO	Final Concentration
Stock AR	24.17 mg Neat Material	1 mL	10 X 10^{-3} M
Stock AR 1st dilution	100 µL Stock AR	900 µL	10 X 10^{-4} M
Stock AR 2nd dilution	100 µL Stock 1st dilution	900 µL	10 X 10^{-5} M

4.3.2 Artificial Receptor 1– Agent Binding

The binding experiment was conducted at target concentration ranges by mixing the agent and artificial receptor **1** in 1 mL of (95/5; H_2O/ DMSO) according to Table 4-10 (representative of 10^{-5} M concentration range). Binding studies with the 10^{-6} M and 10^{-7} M concentration ranges were performed using the same dilution volumes with the appropriate stock solutions (stocks numbered 2 and 3, respectively). The 95/5 H_2O/DMSO solvent mixture was prepared by adding 5 mL of DMSO to 95 mL of distilled water in a 100 mL volumetric flask. Each mixed solution stood at room temperature for 1 minute, then 1 mL of hexane was added. Each solution was manually shaken and extracted for 30 seconds, after which the hexane was transferred to a GC vial for analysis. GC-MS analysis was performed immediately on all extraction solutions to eliminate any loss of agent due to degradation.

Positive and negative controls were performed to establish baseline extraction efficiencies. A positive control containing only agent and solvent was extracted to confirm the extraction efficiency of agent into the hexane layer. A negative control containing only the receptor (at maximum test concentration) and solvent was extracted to determine any potential interference caused by the receptor in the extraction medium. Finally, a blank sample containing only solvent was extracted to ensure no solvent interferences.

Table 4-10. Solution Preparations for Binding Experiment at 10^{-5} M with GD

Sample #	Volume Solvent (95/5, H_2O/DMSO) (mL)	Volume Stock Solution AR 1 (µL)	Volume Stock Solution GD 1 (µL)	Control
AR-5RH-GD01	1	0	10	Positive
AR-5RH-GD02	1	5	10	N/A
AR-5RH-GD03	1	10	10	N/A
AR-5RH-GD04	1	15	10	N/A
AR-5RH-GD05	1	20	10	N/A
AR-5RH-GD06	1	30	10	N/A
AR-5RH-GD07	1	50	10	N/A
AR-5RH-GD08	1	50	0	Negative
AR-5RH-GD09	1	0	0	Blank

The experiment was repeated following the same procedures for GA, as shown in Table 4-11.

Table 4-11. Solution Preparations for Binding Experiment at 10^{-5} M with GA

Sample #	Volume Solvent (95/5, H_2O/DMSO) (mL)	Volume Stock Solution AR 1 (µL)	Volume Stock Solution GA 1 (µL)	Control
AR-5RH-GD01	1	0	10	Positive
AR-5RH-GD02	1	5	10	N/A
AR-5RH-GD03	1	10	10	N/A
AR-5RH-GD04	1	15	10	N/A
AR-5RH-GD05	1	20	10	N/A
AR-5RH-GD06	1	30	10	N/A
AR-5RH-GD07	1	50	10	N/A
AR-5RH-GD08	1	50	0	Negative
AR-5RH-GD09	1	0	0	Blank

Prior to the GC-MS run of each agent, a calibration curve was generated using standard agent solutions. In addition, calibration check verification (CCV) samples were run after every 5 samples.

4.3.3 Results

Tables 4-12 and 4-13 show the GC-MS results of GD and GA binding, respectively, with the artificial receptor **1**. The 10^{-5} M concentration range data show evidence of binding of GD by the receptor. GD concentrations are detected in the 10^{-6} M range samples; however, there is no difference between the positive control (no receptor) and the test samples, suggesting that binding does not occur in this concentration range. This is similar to the binding study of GA at the 10^{-5} M concentration, shown in Table 4-13, as there was no difference between the extracted

GA from the positive control and the GA test solutions. Calculated negative concentrations, difference between the starting agent concentration and the test sample concentration, were assumed to be zero.

It is apparent from the data that the GC-MS analysis is not an adequate method for low concentration studies (10^{-6} and 10^{-7} M) of either GD or GA. All extracted samples in these test ranges, including positive controls, were below the detection limit.

Table 4-12. Summary of GD Concentrations Determined via Extraction and GC-MS Analysis

sample name	Agent (Guest)	Volume of AR 1 (μL)	Volume of Guest (μL)	Peak area, Extracted GD	Δ peak area[1]	Analytical Result, Extracted GD (μg/mL)	Calculated Bound GD (μg/mL)
ART1011	GD	0	10	2419	0	1.14	0
ART1021	GD	5	10	1469	950	0.72	0.42
ART1031	GD	10	10	1443	976	0.71	0.43
ART1041	GD	15	10	2015	404	0.96	0.18
ART1051	GD	20	10	1759	660	0.85	0.29
ART1061	GD	30	10	1835	584	0.88	0.26
ART1071	GD	50	10	2752	-333	1.29	-0.15
ART1081	GD	50	0	0	ND	<0.01	ND
ART1091	GD	0	0	0	ND	<0.01	ND
ART1101	GD	0	10	15.5	0	<0.01	ND
ART1111	GD	5	10	23.3	-7.8	0.010	ND
ART1121	GD	10	10	23.7	-8.2	0.013	ND
ART1131	GD	15	10	31.4	-15.9	0.015	ND
ART1141	GD	20	10	31.5	-16	0.015	ND
ART1151	GD	30	10	39.2	-23.7	0.014	ND
ART1161	GD	50	10	38.6	-23.1	0.014	ND
ART1171	GD	50	0	0	ND	<0.01	ND
ART1181	GD	0	0	0	ND	<0.01	ND
ART1191	GD	0	10	ND	ND	<0.01	ND
ART1201	GD	5	10	ND	ND	<0.01	ND
ART1211	GD	10	10	ND	ND	<0.01	ND
ART1221	GD	15	10	ND	ND	<0.01	ND
ART1231	GD	20	10	ND	ND	<0.01	ND
ART1241	GD	30	10	ND	ND	<0.01	ND
ART1251	GD	50	10	ND	ND	<0.01	ND
ART1261	GD	50	0	ND	ND	<0.01	ND
ART1271	GD	0	0	ND	ND	<0.01	ND

[1]Determined by subtracting the sample peak area from the zero-host peak area.

Table 4-13. Summary of GA Concentrations Determined via Extraction and GC-MS Analysis

sample name	Agent (Guest)	Volume of AR 1 (μL)	Volume of Guest (μL)	Peak area, Extracted GA	Δ peak area[1]	Analytical Result, Extracted GA (μg/mL)	Calculated Bound GA (μg/mL)
ART1281	GA	0	10	1420	0	0.22	0
ART1291	GA	5	10	1103	317	0.18	0.05
ART1301	GA	10	10	1139	281	0.18	0.04
ART1311	GA	15	10	1432	-13	0.23	0.00
ART1321	GA	20	10	1454	-34	0.23	0.00
ART1331	GA	30	10	1115	305	0.18	0.05
ART1341	GA	50	10	1464	-45	0.23	-0.01
ART1351	GA	50	0	ND	ND	<0.01	ND
ART1361	GA	0	0	ND	ND	<0.01	ND
ART1371	GA	0	10	14	0	<0.01	ND
ART1381	GA	5	10	15	-1	<0.01	ND
ART1391	GA	10	10	15	-1	<0.01	ND
ART1401	GA	15	10	17	-3	<0.01	ND
ART1411	GA	20	10	17	-3	<0.01	ND
ART1421	GA	30	10	16	-2	<0.01	ND
ART1431	GA	50	10	14	0	<0.01	ND
ART1441	GA	50	0	ND	ND	<0.01	ND
ART1451	GA	0	0	ND	ND	<0.01	ND
ART1461	GA	0	10	ND	ND	<0.01	ND
ART1471	GA	5	10	ND	ND	<0.01	ND
ART1481	GA	10	10	ND	ND	<0.01	ND
ART1491	GA	15	10	ND	ND	<0.01	ND
ART1501	GA	20	10	ND	ND	<0.01	ND
ART1511	GA	30	10	ND	ND	<0.01	ND
ART1521	GA	50	10	ND	ND	<0.01	ND
ART1531	GA	50	0	ND	ND	<0.01	ND
ART1541	GA	0	0	ND	ND	<0.01	ND

[1]Determined by subtracting the sample peak area from the zero-host peak area.

4.4 GD Analysis

The results from the analysis of GD binding are plotted in Figure 4-7 as mmol artificial receptor **1** vs. Bound GD. Binding association typically results in increasing affinity between the host and bound guest at increasing host concentrations, demonstrated in the simulant binding studies in Section 4.1. As shown by the plot in Figure 4-8, the binding relationship for the host-[2]rotaxane and GD does not follow the expected trend for a 1:1 association constant.

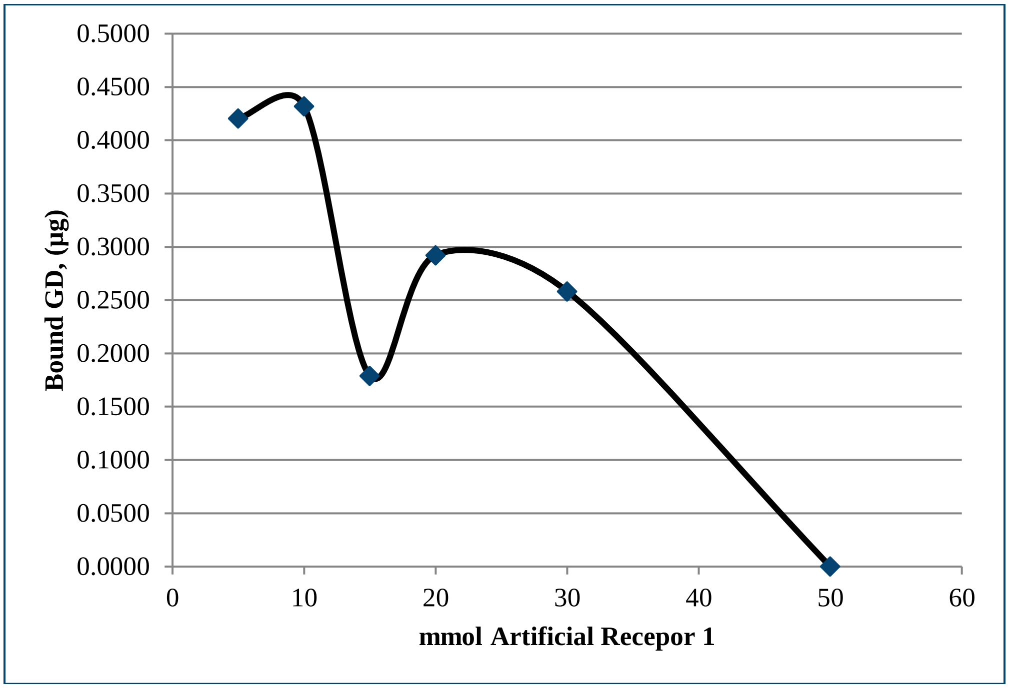

Figure 4-8. Plot of Artificial Receptor 1 (AR 1) Concentration versus Bound GD (calculated)

Similar behavior was observed for the EPP simulant binding with cyclophane **35** at 20 % water in DMSO (data shown in Appendix B, Figure B-64). In that case, it was observed that the cyclophane solubility was a limiting factor, and precipitation of the bound complex was observed at higher host-guest ratios. In this case, solubility of the artificial receptor **1** is not an issue and post addition precipitation was not observed.

Scatchard analysis is a method of linearizing data from a saturation binding experiment in order to determine binding and/or equilibrium constants (Wild, 2005). The plot is a “secondary” plot of specific binding/free host concentration (Y axis) vs. host binding (X axis). Typically, for each site where the guest binds to the host according to mass-action kinetics, the Scatchard plot is a straight line with a slope approximating the equilibrium constant/binding association constant (K_a) as shown in Equation 1.

$$K_a = \underline{[H \bullet G]} \qquad (1)$$

[H][G]

Since the form of the binding relationship in this study relies on the detection of the guest concentration, and not spectral changes due to host binding interactions, the slope of the line is actually the inverse of the association constant, aka the dissociation constant (K_D), Therefore, $K_D = 1/K_a$. A summary of calculated concentrations for GD binding are given in Table 4-14, and the Scatchard plot is shown in Figure 4-9.

Table 4-14. Summary of Calculated GD Concentrations used to determine the Scatchard Plot

mmol AR 1	mmol GD	mmol Bound GD	Scatchard Ratio (Bound GD/AR 1)	mmol unbound GD
5	0.0561	2.31E-06	4.62E-07	3.96E-06
10	0.0561	2.37E-06	2.37E-07	3.90E-06
15	0.0561	9.83E-07	6.55E-08	5.28E-06
20	0.0561	1.60E-06	8.02E-08	4.66E-06
30	0.0561	1.42E-06	4.73E-08	4.85E-06
50	0.0561	-8.07E-07	-1.61E-08	7.07E-06

The biphasic nature of the Scatchard plot in Figure 4-9 demonstrates that multiple binding events are occurring during the experiment involving GD and the host-[2]rotaxane. In DNA binding studies (Yang, et al., 2005) involving multiple binding motifs, it has been shown that the linear region of the plot is characteristic of the association binding constant.

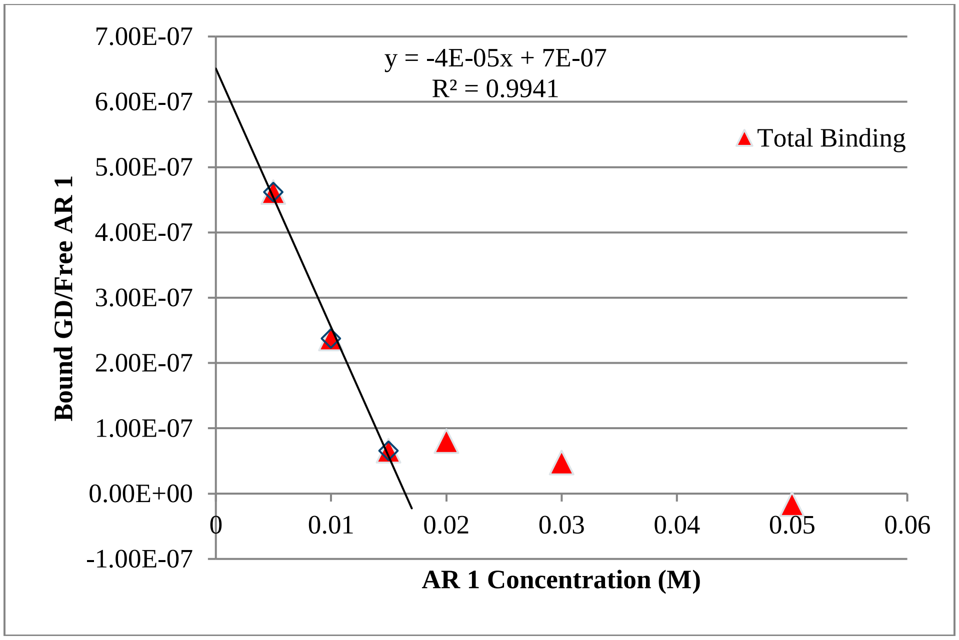

Figure 4-9. Scatchard Plot of Bound GD/Free AR 1 vs. AR 1 Concentration, Highlighting the Linear Region.

The resulting slope from the linear region in Figure 4-8 indicates a dissociation binding constant on the order of 4 x 10^{-5} M. Based on the inverse relationship of K_D to K_a, the association binding constant is estimated to be 25,000 M^{-1}. There have been a variety of studies performed to determine the binding/reactivation or degradation of nerve agents using enzymes or antibodies. Reported binding association constants between nerve agents and oximes are in the range of 10^5 to 10^9 M^{-1} (Luo, et al., 2007). A review of the catalyzed degradation of nerve agents with various enzymes (Dawson, et al., 2008) suggested that Soman binding was among the lower range of binding efficiencies (ca. 10^2 – 10^4 M^{-1}), contributing to lower degradation in targeted systems than the other nerve agents.

The free energy of binding (ΔG) for GD by the artificial receptor **1** is calculated with Equation 2, and is estimated to be ~ 6 kcal/mol. This value is higher than simple hydrophobic interactions estimated in Table 4-6 for either of the simulant compounds (EPP and DMMP).

$$\Delta G = -RT\ln(K_a) \qquad (2)$$

In addition, the calculated free energy of binding of GD by cyclophane **35** is 7.9 kcal/mol (see Table 4-6). Remembering that the calculations only take into account the non-covalent interactions of the cyclophane, if we assume the effects of solvent stabilization and potential cooperative binding due to the guanidine pendant groups on the sliding ring of AR **1**, the measured binding energy of 6 kcal/mol for GD by AR **1** is not unreasonable. Note also, that because the experiment relied upon saturation binding, the actual binding energy may be higher.

4.5 Binding Study Lessons Learned

The binding association kinetics are more complex than the 1:1 mathematical model can accommodate. The system shows strong evidence of multi-configurational binding behavior. This observed behavior is likely due to pocket conformational changes as binding occurs. This interaction is also influenced by the assisted binding of the guanidine moeities on the sliding ring. This complex kinetic behavior would be better evaluated using a direct spectroscopic method, with the assistance of a signaling indicator. Further, lower concentration test exposures would more accurately depict binding kinetics, whether results are due to intermolecular or intramolecular forces, such as conformational changes, single complex binding, or other interactions.

The data suggests that binding in this system is selective. GD was bound whereas GA was not. It would be advantageous to further evaluate the binding behavior of AR 1 with a broader range

of analytes, including VX, GB, Cyclosarin, and other toxic materials of interest. The nature of this selectivity is likely due to pocket size and / or electronic influences.

5.0 Conclusions

Battelle investigated the development of a tunable artificial receptor designed with a sliding ring (e.g., Host-[2]rotaxane) to detect the presence of nerve agents. Evaluation of artificial receptor **1** with GD and GA indicated that this artificial receptor will bind GD effectively in water at 10^{-5} M. The measured binding constant is 25,000 M^{-1}, two orders of magnitude greater than the hydrophobic binding of the cyclophane pocket moiety alone. It is suggested that the artificial receptor system captures GD through use of two cooperative non-covalent interactions: hydrophobic binding and a salt-bridging interaction. Figure 5-1 depicts these binding interactions.

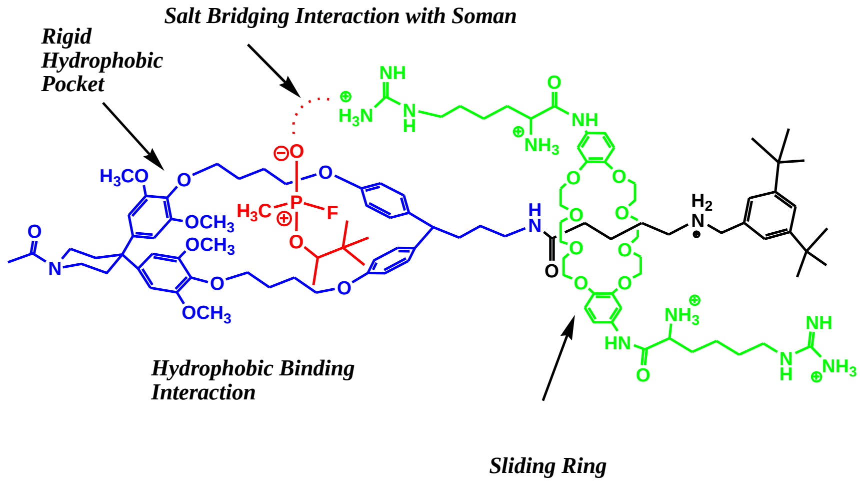

Figure 5-1. Artificial Receptor 1 Binding Interactions

Artificial receptor **1** has demonstrated, in these initial studies, the ability to sequester GD in water for subsequent removal or decontamination. The receptor was not effective in binding GA at these concentration levels. Differences in binding could be due to either steric or electronic differences. Higher concentration studies using the GC-MS methodology may provide a range in which to measure the association constant with GA; however, definitive proof of binding interactions will only be possible using a direct spectroscopic method (i.e., NMR, fluorescence quenching, or similar method).

It is important to note that the confirmation of “assisted” binding suggests that molecular motion is occurring within the rotaxane upon detection of CWAs. To understand this behavior, it is necessary to study the baseline response of the host-[2]rotaxane in the presence of various types of CWAs (i.e., Sarin (GB), Cyclosarin (GF), VX, and advanced threats). Direct measurements

by spectroscopic methods are needed for determination of binding kinetics at low concentration levels. This could also provide more clarity into the binding mechanism and understanding of the artificial receptor's intramolecular mobility.

This compound could be compared against commercially available systems to benchmark binding efficiency. The strength of this approach is that once binding with different CWA/advanced threats are characterized; strategies can be formulated to change the pocket design to accommodate different threat materials and comparisons made on improvements relative to a baseline performance. Further, the implication of intramolecular motion in this compound is a compelling platform for the development of advanced novel decontaminants. If design elements to incorporate decontamination strategies were made within the molecule, the initiation of decontamination could be driven by the capture of threat materials.

6.0 Recommendations for Future Work

This research has established ground work towards the development of a durable artificial catalytic system that efficiently destroys chemical agents. Critical to the development of this system is mastering the underlying chemistry of 1) selective molecular recognition of chemical agents 2) controlled shuttling of the ring between two points along the axle and 3) catalysis which uses environmentally available water to render chemical agent inert.

Thus far it has been shown that chemical agent can be trapped by a host-[2]rotaxane system with a moderately strong association constant of 2.5 X 10^4 M^{-1}. Further research is warranted to optimize the cavity size to accommodate the agent(s) of interest. There are a few commercially available low-cost cyclophanes with various pocket sizes, such as cyclodextrins, calixarenes, and cucurbiturils. It will be advantageous to purchase these materials and perform binding studies with chemical agent to determining their strength. This information will provide an optimized cavity size which can be translated into the artificial receptor's cyclophane pocket.

Control of the ring movement within a rotaxane system is required to develop a system that can cycle. To artificially create the "catalytic motion" observed in the backbone of enzymes, the electronics of the ring and axle have to favor the ring in a bound position in the presence of agent. Once the agent is hydrolyzed into multiple components, the electronics must switch to favor an open state.

There are multiple examples of simple shuttling systems in the recent literature which can move from one position to another with the help of an external trigger. Two examples of axles upon which modified DB24C8 rings can shuttle have been reported this year in the literature (Zhu 2012; Zhang 2012). A [2]rotaxane system designed by Zhang et al. uses a counterion-induced switching strategy to control ring motion (Figure 6-1). This rotaxane also has a fluorescent indicator included as a blocking element. Both NMR and fluorescent information was obtained demonstrating control of the shuttling motion of the modified DB24C8 ring (Figure 6-2 and 6-3, respectively).

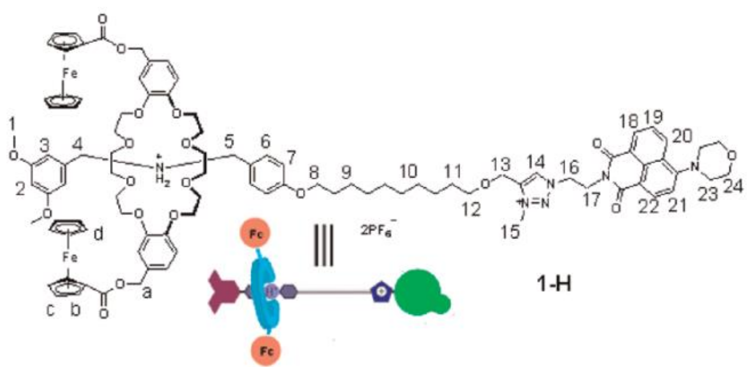

Figure 6- 1. Rotaxane Shuttling System using Counterion-induced

Switching Strategy (Zhang, et al., 2012)

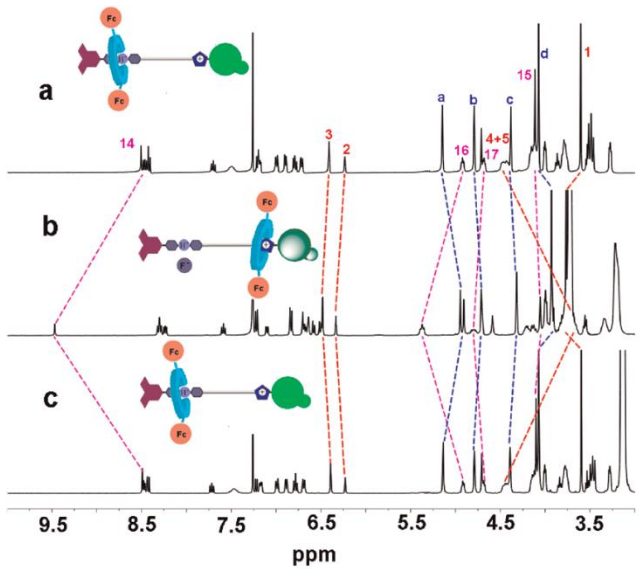

Figure 6- 2. NMR Data of Shuttling Motion: Partial ^{1}H NMR spectra (400 MHz, 298 K, $CDCl_3$) of (a) [2]rotaxane 1-H, (b) the solution obtained after adding 2 equiv of TBAF to the solution of (a), and (c) the solution obtained after adding 4 equiv of $Ca(PF_6)_2$ to the solution of (b). (from Zhang et al., 2012)

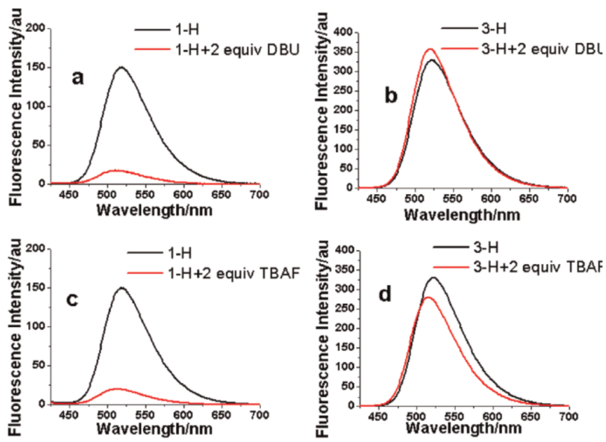

Figure 6- 3. Fluorescent Signaling of Shuttling Motion: Fluorescence spectral changes in CH_2Cl_2 (a) from[2]rotaxane 1-H to the mixture obtained after adding 2 equiv of DBU to the solution of 1-H, (b) from dumbbell 3-H to the mixture obtained after adding 2 equiv of DBU to the solution of 3-H, (c)from [2]rotaxane 1-H to the mixture obtained after adding 2 equiv of TBAF to the solution of 1-H, and (d) from dumbbell 3-H to the mixture obtained after adding 2 equiv of TBAF to the solution of 3-H. Excitation wavelength of all fluorescence spectra was 398 nm. (from Zhang et al., 2012)

In a [2]rotaxane system designed by Stephen Loeb, control over the shuttling motion and configuration changes in DB24C8 was accomplished by changing the electronic properties on the axle component (Zhu et al., 2012). This pincer motion is a good mimetic for the shifting which occurs in the backbones of enzymes. Figure 6-4 shows the shuttling motion along with the induced configuration change. Note the control over the "C" shape configuration in the ring. Designing this motion into AR 1 could have a significant impact on the pocket's ability to cycle out the agent hydrolysis product.

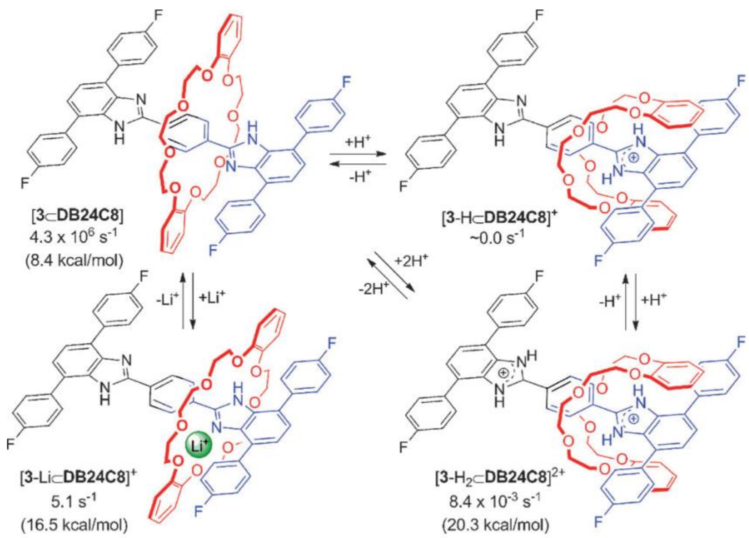

Figure 6- 4. Shuttling in H-shaped [2]rotaxane (from Zhu et al., 2012)

Both of these examples demonstrate the use of a DB24C8 ring system in a shuttling system. The design elements (an appropriately modified DB24C8 ring) which are most compatible with the decontamination goals of the system being evaluated at Battelle could be incorporated into a simple model system of the rotaxane element. Once proof of shuttling control is established the system will be built into an artificial catalytic system.

Catalytic hydrolysis of CWA materials has been and continues to be studied in multiple research groups (Kim, et al., 2011), and provides a strong baseline understanding of the kinetics required to break P-O and P-F bonds. For an oscillating catalytic system, it would be advantageous for the non-covalent interactions leading to hydrolysis to be of lower energy than the energy required to move the ring. This will help reduce product inhibition and promote catalytic cycling. As hydrolysis has been performed in both acidic and basic media, the catalysis mechanism can be designed as to not interfere with the shuttling and configuration motion of the DB24C8 ring. A small series of DB24C8 rings modified with varying catalytic groups selected from the literature will need to be evaluated for their ability to hydrolyze agent under acidic and basic reaction conditions. The rings do not need to be locked into a rotaxane for their initial evaluation thus simplifying synthetic preparation. The down-selected catalyst(s) can then be incorporated into the artificial receptor compound and performance assessed.

Overall, the development of a catalytic agent decontaminant molecular machine based on [2]rotaxanes is easily compartmentalized into small research efforts. None of the components are wholly dependent on the development of the others. Because of this convergent ideology, there may be several approaches developed that are amenable to resolving challenges. This will ultimately yield numerous potentially interchangeable components to the system. Several different decontaminant systems could be developed and assessed.

7.0 References

Clemente-León, M.; Credi, A.; Martínez-Díaz, M-V.; Mingotaud, C.; Stoddart, J. F.; "Towards Organization of Molecular Machines at Interfaces: Langmuir Films and Langmuir–Blodgett Multilayers of an Acid–Base Switchable Rotaxane," *Adv. Mater.* 2006, *18*, 1291–1296.

Dawson, R.M., Pantelidis, S., Rose, H.R., Kotsonis, S. E.., "Degradation of Nerve Agents by an Organophosphate-degrading Agent (OPdA)," *J. Hazardous Materials*, 2008, (157), 308-314).

Diederich, F. Cyclophanes; The Royal Society of Chemistry: Cambridge 1991. Ferguson, S. B.; Sanford, E. M.; Seward, E.; Diederich, F. J. Am. Chem. Soc. 1991, 113, 5410-5419. Mattei, P.; Diederich, F. *Helv. Chim. Acta*, 1997, 80, 1555-1588.

Dvornikovs, V.; House, B.; Kaetzel, M.; Dedman, J.R.; Smithrud. D. "Host−[2]Rotaxanes as Cellular Transport Agents" *J. Am. Chem. Soc.*, 2003, 125 (27), 8290-8301.

Kim, K., Tsay, O.G., Atwood, D.A., Churchill, D. G., "Destruction and Detection of Chemical Warfare Agents" *Chemical Reviews*, 2011, 111(9), 5345-5403.

Luo, C., Tong, M., Chilukuri, N., Brecht, K., Maxwell, D. M., Saxena, A. "An In Vitro Comparative Study on the Reactivation of Nerve Agent-Inhibited Guinea Pig and Human Acetylcholinesterases by Oximes," *Biochemistry*, 2007, 46, 11771-11779.

Wild, D., The Immunoassay Handbook, Elsevier Inc., San Diego, CA, 2006, 8-10.

Williams, D. H., Stephens, E., O'Brien, D. P., Zhou, M., "Understanding Noncovalent Interactions: Ligand Binding Energy and Catalytic Efficiency from Ligand-Induced Reductions in Motion within Receptors and Enzymes," *Angew. Chemie, Int. Ed.*, 2004, 43,6596-6616.

Yang, Y., Sass, L.E., Du, C., Hsieh, P., and D.A. Erie, "Determination of protein-DNA binding constants and specificities from statistical analyses of single molecules": MutS-DNA Interactions, Nucleic Acids Research, 2005, Vol. 33, No. 13, 4322- 4334.

Zhang, H.; Qu, Da-Hui,"Dual-Mode control of PET process in a ferrocene-functionalized [2]rotaxane with high-contrast Fluorescence output" *Organic letters*, 2001, *3*(16), 2485-7.

Zehnder, D W, and Smithrud, D B. "Facile synthesis of rotaxanes through condensation reactions of DCC-[2]rotaxanes." *Organic letters*, 2012, 14(9), 2334-2337.

Zhu, K.; Vukotic, V.N.; Loeb, S.J. "Molecular Shuttling of a compact and Rigid H-shaped [2]Rotaxane" *Angew. Chemie, Int. Ed.*, **2012**, 51(9), 2168-2172

Appendix A: Synthesis Experimental Procedures for Preparation of Artificial Receptor 1

(19): To a stirring solution of dibenzo-24-crown-8-ether (5.1 g, 11 mmol) dissolved in chloroform (50 mL) was added a mixture of concentrated nitric acid (7 mL) and acetic acid (20 mL) drop-wise over 30 minutes at ambient temperature. The mixture was heated under reflux for 3 hours then stripped of solvent under reduced pressure. The crude solids were solvated with chloroform (100 mL), sonicated then precipitated with ethanol 150 mL to afford **19** a quantative yield (5.87 g).

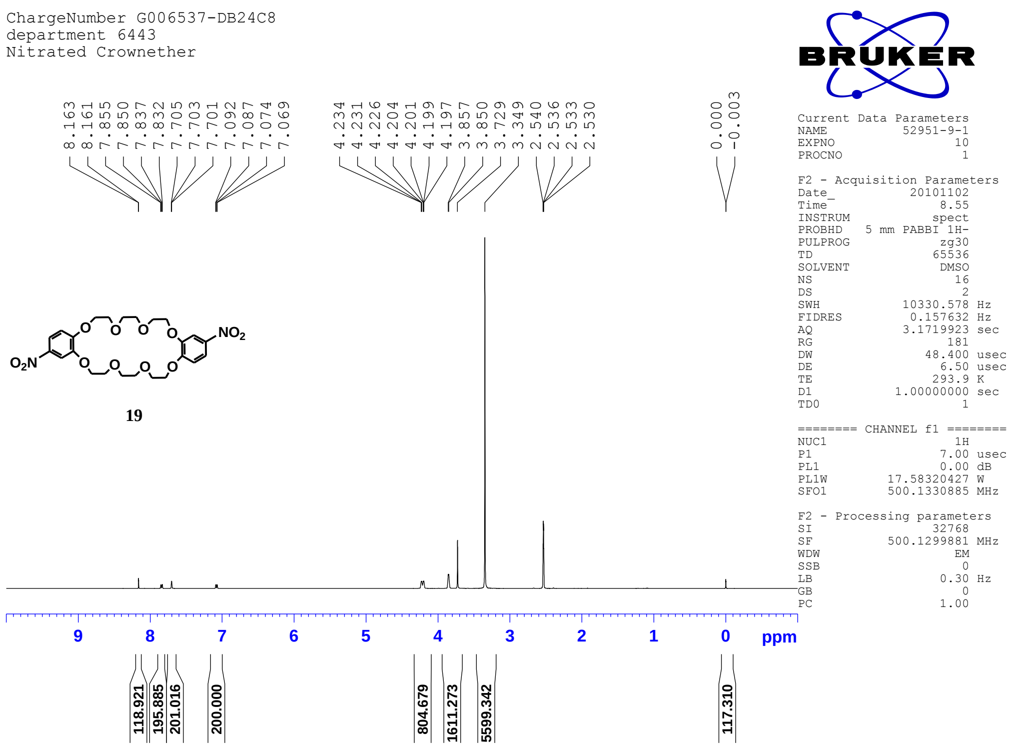

Figure A-1. ^{1}H NMR for compound **19** in DMSO-d_6

(20): Compound 19 (6 g, 11.1 mmol) was mixed with Boc_2O (6 g, 27 mmol) and 10% Pd/C (500 mg) in 75mL of anhydrous THF/CH_3OH (50/50) solvent mix. Mixture was placed under a hydrogen atmosphere (50 psi) for 12 hours. The material was filtered through a celite pad then concentrated. The material was solvated in chloroform then precipitated with a 50/50 solvent mixture of diethylether/hexane. Material was isolated by filtration to give **20** (4.98 g, 95% yield) as a white free flowing powder.

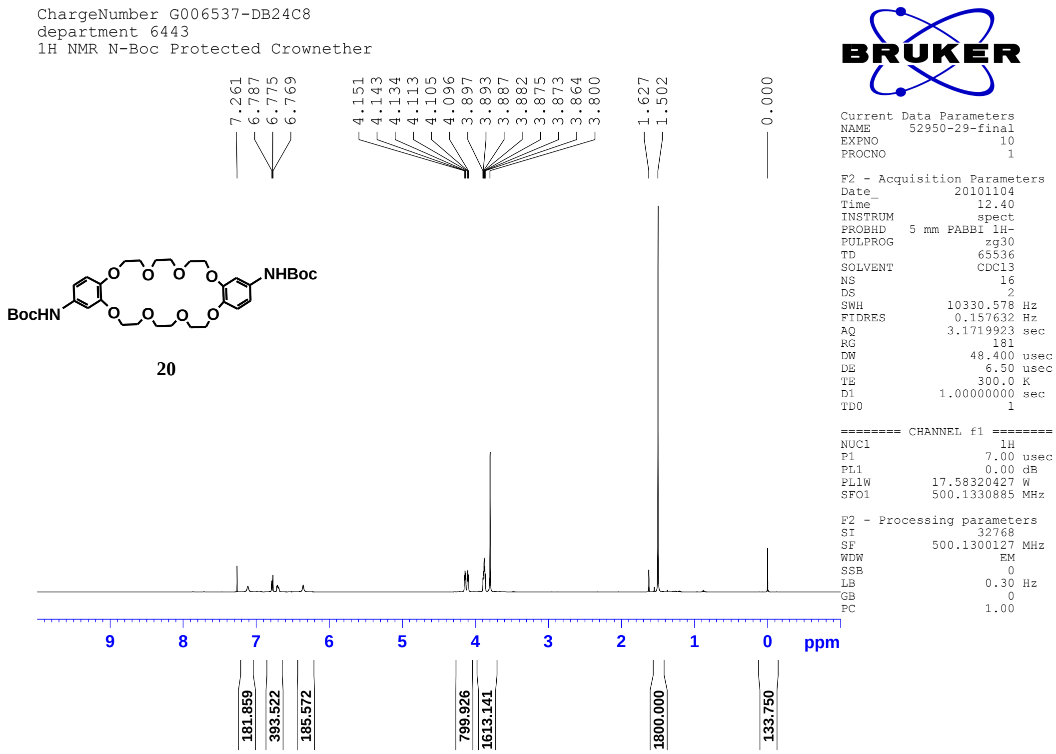

Figure A-2. ^{1}H NMR for compound **20**

(21): *N*-Acetyl-4-piperidinone (5.3g, 37.5 mmol) and 2,6 dimethoxyphenol (11.56 g, 75 mmol) were mixed in a 150 mL beaker using a thick glass rod. While mixing, concentrated sulfuric acid (7 mL) was added slowly in small portions. An ice bath was used to keep the temperature below 10 °C. After addition was complete, the thick material sat at ambient temperature for 16 hours and hardened. This material was solvated in a 4L beaker using acetone / methanol (70:30 mix) then neutralized to pH 7 with 1N sodium carbonate. Water (2L) was added to induce precipitation. The material was collected using a medium porosity frit and rinsed with diethyl ether to help dry the compound. Reaction afforded **21** (13.1 g, 81% yield) as a white powder.

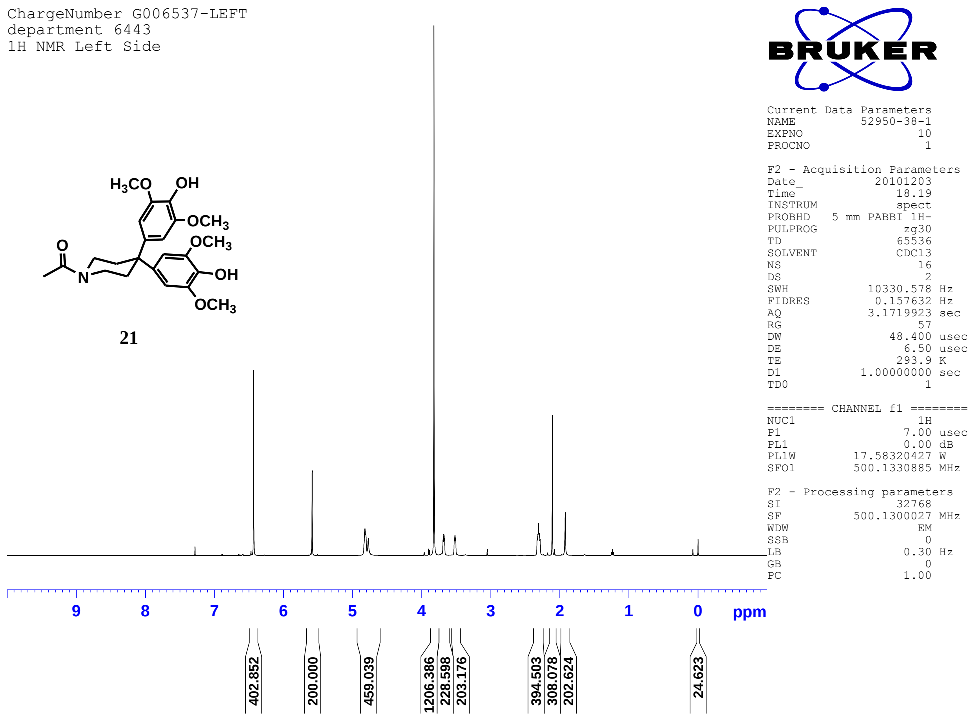

Figure A-3. ^{1}H NMR of compound **21** in $CDCl_3$

(22): Compound 21 (13.1 g, 30.38 mmol) was mixed with 1,4-dibromobutane (32.5 g, 151 mmol) then treated with cesium carbonate (21 g, 66.8 mmol) in DMF (200 mL) and then stirred for 16 hours at ambient temperature. Solvent was removed under reduced pressure, and then the crude was extracted between water (200 mL) and chloroform (3x100 mL). The combined organics were dried with magnesium sulfate, filtered then concentrated. Final purification by column chromatography (silica gel, $CHCl_3$: CH_3OH 98:2) afforded **22** (17 g, 80% yield). ^{1}H NMR analysis is consistent with literature reported values.

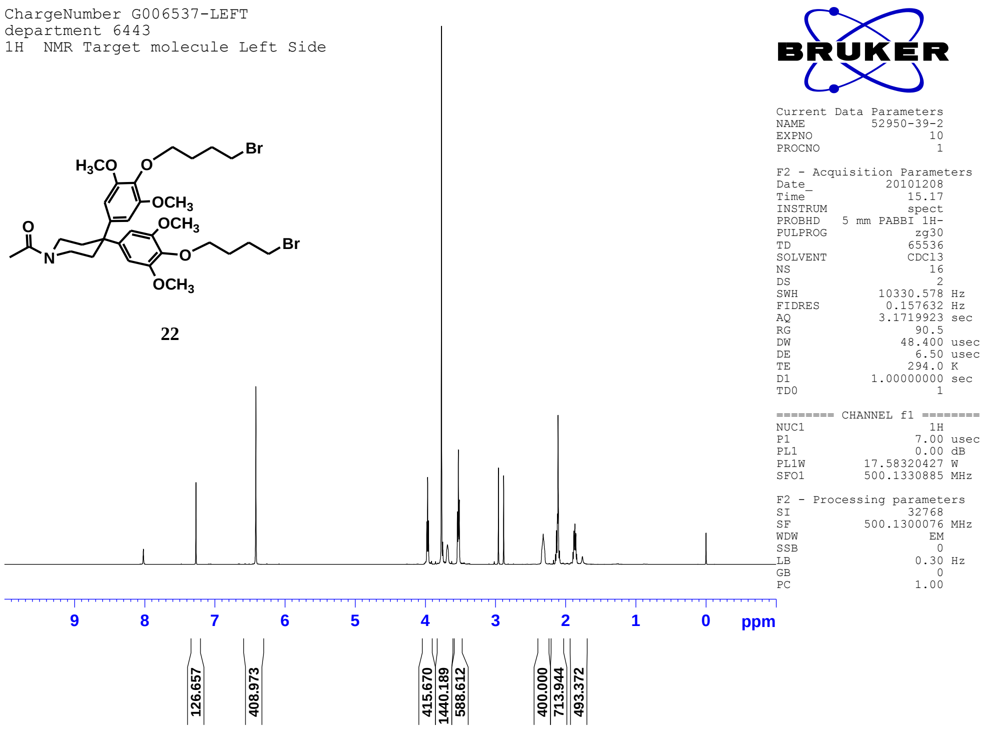

Figure A-4. ^{1}H NMR of compound **22** in $CDCl_3$

(23a): To a solution 4,4-dihydroxybenzephone (23.96 g, 111.85 mmol) dissolved in $CHCl_3/CH_3OH$ 50:50 solvent mixture (400 mL) was added benzyl bromide (34.59 mL, 290.81 mmol) and cesium carbonate (108.96 g, 334.43 mmol). This mixture was heated to reflux for 16 hours. After removing the solvent, the crude material was extracted with 2L of chloroform and 600 mL of water. Note it is necessary to use 2L of chloroform to solvate the material. Organics were dried with magnesium sulfate, filtered and concentrated. This material was washed with diethyl ether (200 mL) decanted then dried. Reaction produced 34.62 g, 78% yield. ^{1}H NMR analysis is consistent with literature reported values.

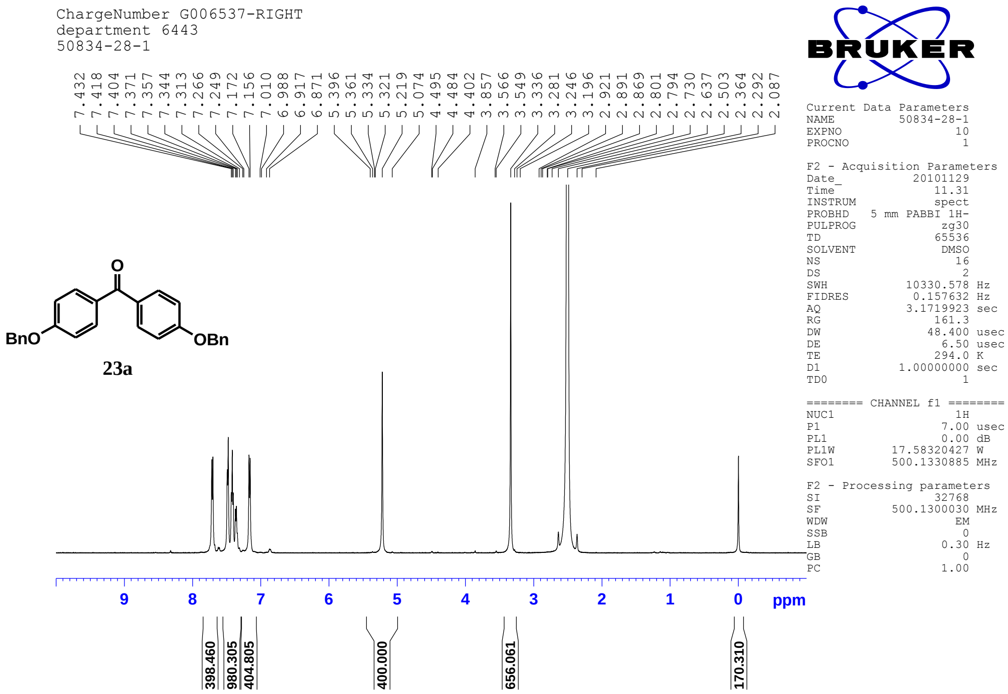

Figure A-5. [1]H NMR for compound **23a** in DMSO-d_6

(23): Compound **23a** (34.62 g, 87.77 mmol) was dissolved in CH_2Cl_2/EtOH, 50:50 solvent mixture (400 mL) then mixed with sodium borohydride (3.32 g, 87.77 mmol) and heated to reflux for 16 hours. Solution was diluted with DCM (250 mL) then extracted with water (150 mL). Organics were dried over magnesium sulfate, filtered then dried to afford **23** (34.36 g, 98% yield) as a white solid. [1]H NMR analysis is consistent with literature reported values.

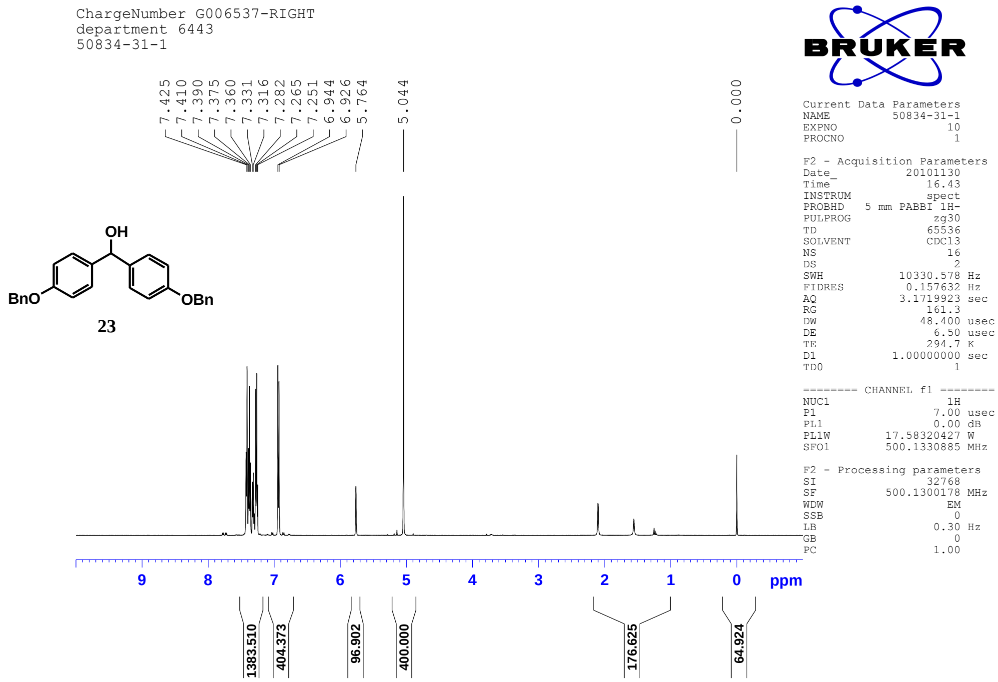

Figure A-6. ^{1}H NMR for compound **23** in $CDCl_3$

(24): Alcohol **23** (34.36 g, 96.7 mmol) and allyl trimethylsilane (27.55 mL, 173.34 mmol) were mixed in DCM (350 mL) then treated with trifluoroacetic acid (3.34 mL, 114.02 mmol) in DCM (6 mL) drop-wise over 15 minutes. During the addition the solution turned bright red. Reaction was stirred for 2 days. Solvents were removed under reduced pressure affording **24** (36.78 g, 99% yield). No further purification was performed. ^{1}H NMR analysis is consistent with literature reported values.

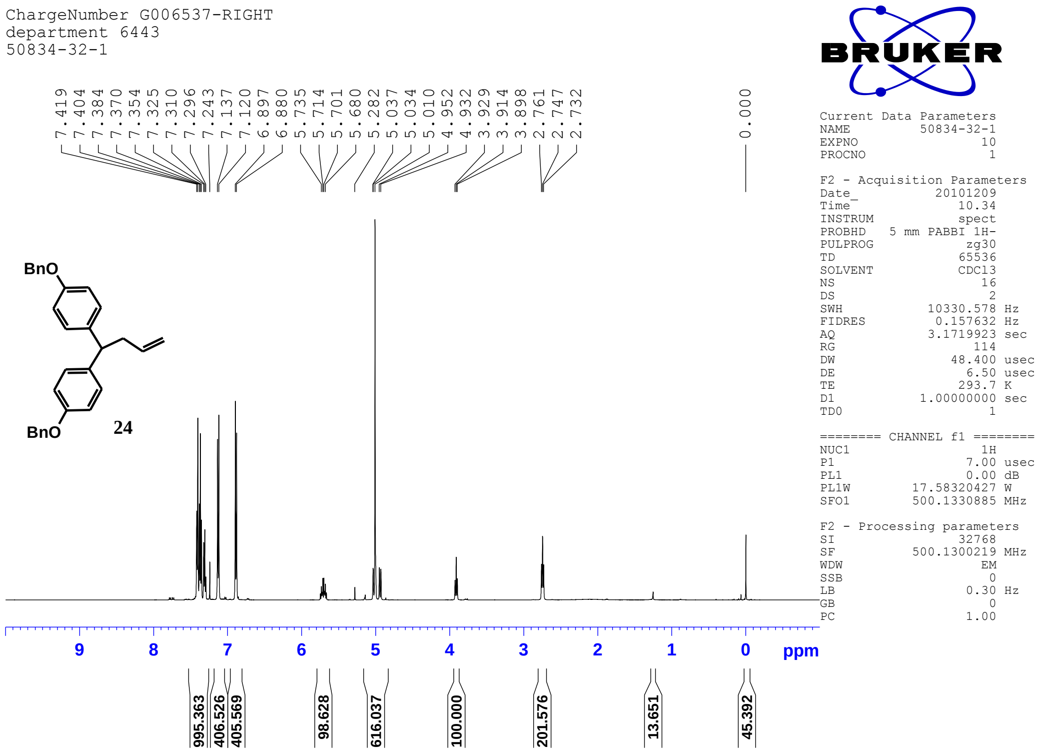

Figure A-7. ^{1}H NMR for compound **24** in $CDCl_3$

(25): Compound **24** (36.72 g, 87.32 mmol) dissolved in anhydrous tetrahydrofuran (THF) (87 mL) was treated with borane-DMS (2M, 47 ml in THF) drop-wise via addition funnel over 15 minutes. Temperature was maintained at 20 °C while stirring for 6 hours. The solution was cooled to 2 °C then hydrogen peroxide (30%, 21.7 mL) was added slowly; CAUTION reaction will exotherm here. Sodium hydroxide (2M, 21.7 mL) was added slowly immediately following the peroxide. Reaction was stirred for 16 hours in the melting ice bath, then extracted with DCM (3X150 mL). The combined organics were washed with brine (200 mL), dried with magnesium sulfate, filtered and concentrated. Purification by column chromatography (silica gel, Hexane:EtoAc gradient 0% to 50 % EtoAc) afforded **25** (17.66 g, 46% yield) as a heavy oil. 1H NMR analysis is consistent with literature reported values.

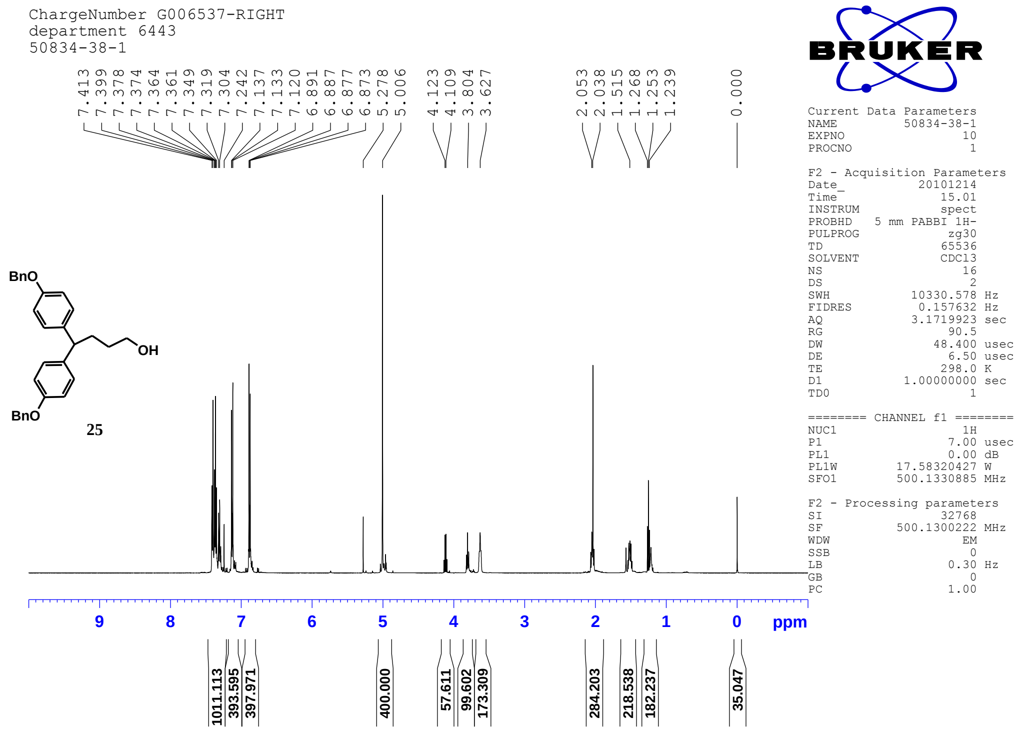

Figure A-8. ^{1}H NMR for compound **25** in $CDCl_3$

(25a): Compound **25** (17.66 g, 40.27 mmol) was mixed with triphenylphosphine (13.73 g, 52.35 mmol) in acetonitrile (CH_3CN) (100 mL). Carbon tetrabromide (17.36 g, 52.35 mmol) in CH_3CN (10 mL) was added to the stirring solution at ambient temperature over 15 minutes. A slight exotherm of 20 °C was noted. The solution was stirred for 5 hours then stripped of solvents under reduced pressure. The concentrated was purified by column chromatography (silica gel, hexane/EtoAc gradient 10-40% EtoAc) which gave **25a** (16.9 g, 84% yield) as a yellow solid. ^{1}H NMR is consistent with literature reported values.

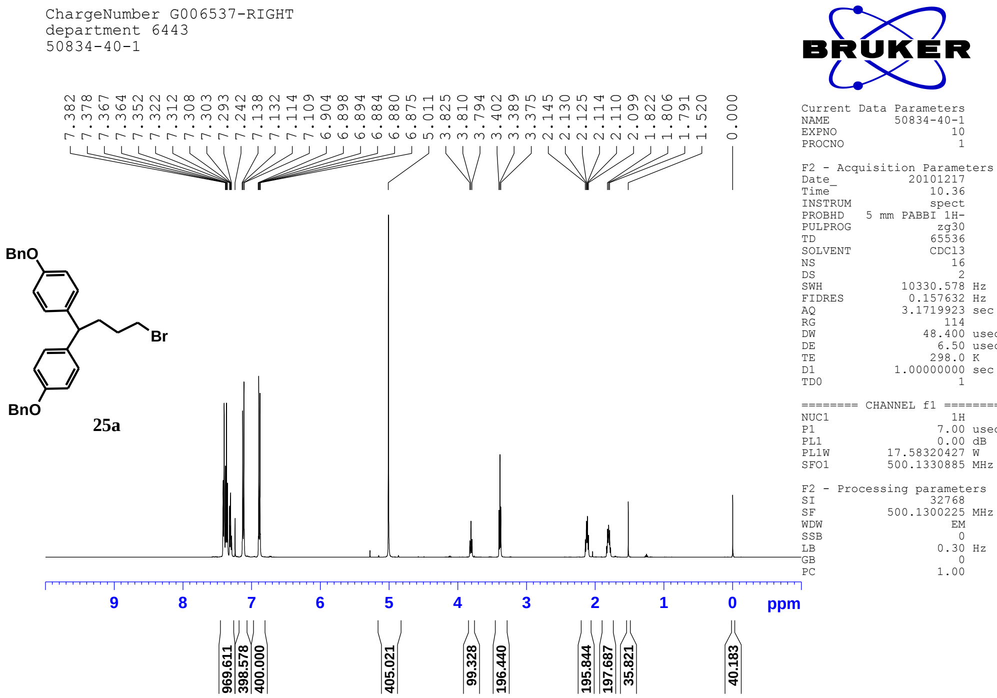

Figure A-9. ^{1}H NMR of compound **25a** in $CDCl_3$

(26): Compound **25a** (16.9 g, 33.70 mmol) in acetonitrile (70 mL) was treated with sodium azide (13.15 g, 202.2 mmol) then heated to reflux for 12 hours. The precipitates were filtered and the solution was concentrated under reduced pressure to afford **26** (15.62 g, 99% yield). The material solidified to a white solid upon standing. No further purification was performed. ^{1}H NMR was consistent with literature reported values.

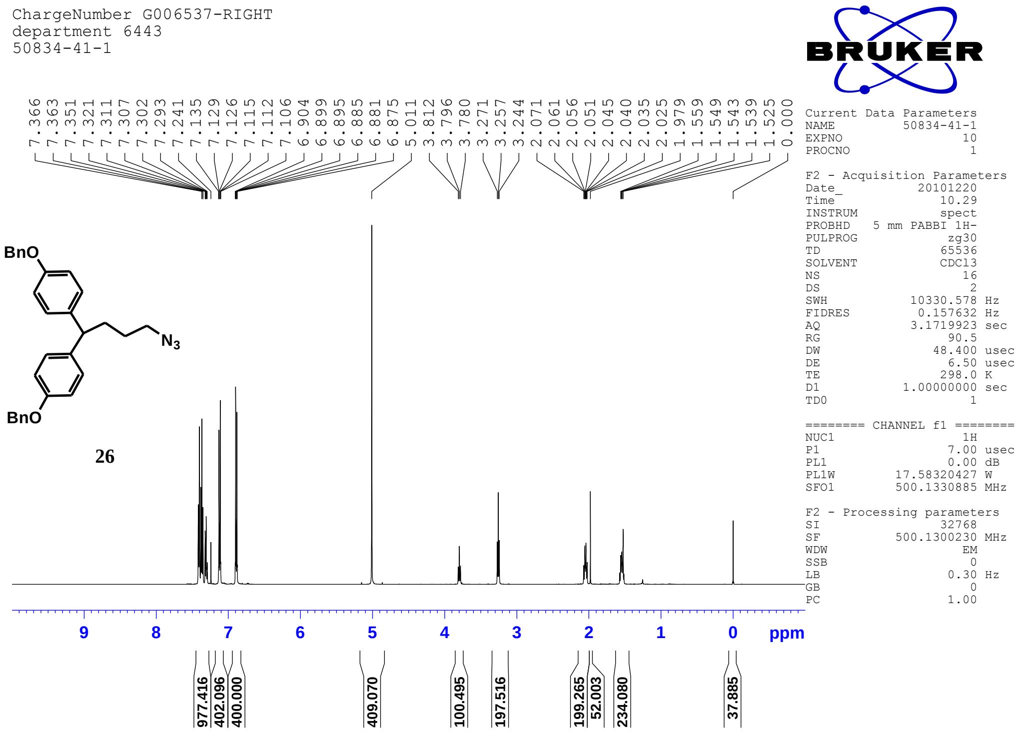

Figure A-10. ^{1}H NMR for compound **26** in $CDCl_3$

(27): Compound **26** (12 g, 25.9 mmol) dissolved in methanol/THF 50:50 solvent mixture (100 mL) was combined with palladium black (1.2 g) then shaken under a hydrogen atmosphere (60 psi) for 5 days. After filtering through a celite pad, TEA (50 mL) and BOC_2O (13.4 g, 61.8 mmol) were added then mixed for 16 hours at room temperature. The reaction solution was added to chloroform (300 mL) then extracted with water (2 X 300 mL). The combined organics were dried with magnesium sulfate, filtered and concentrated. Purification by column chromatography (silica gel, $CHCl_3$: CH_3OH 95:5) afforded 14.25 g 83% yield. Reaction was repeated on the same scale to generate more material: afforded 16.1 g, 95% yield.
^{1}H NMR data is shown below.

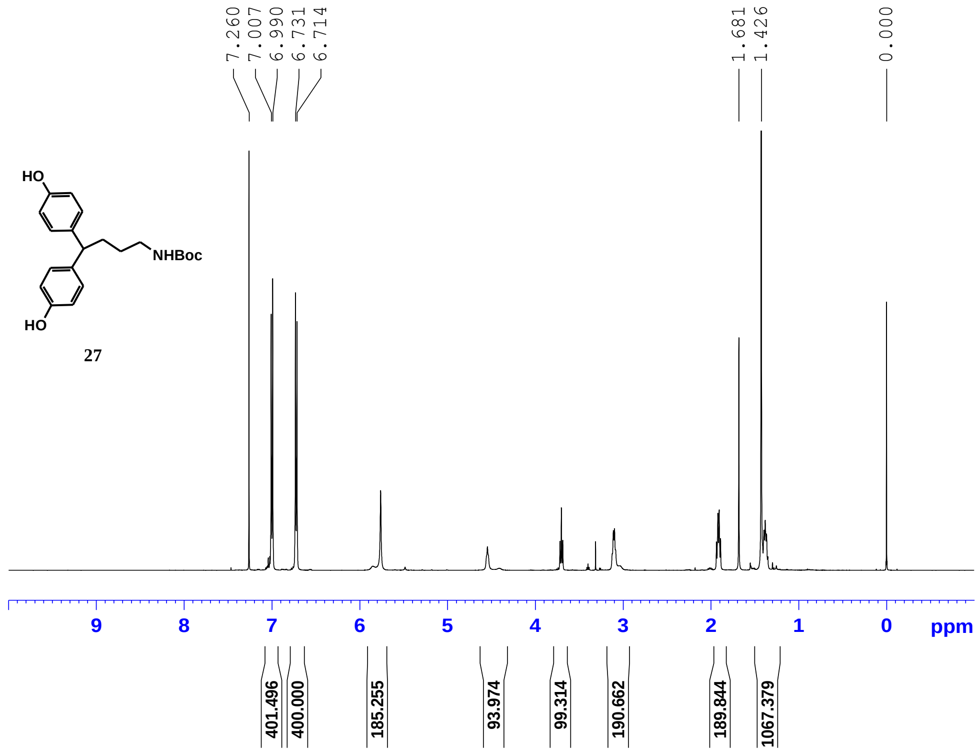

Figure A-11. ¹H NMR of Compound **27** in $CDCl_3$

(31): 3,5-di-tert-butyltoluene (10 g, 49 mmol) was mixed with NBS (9.16 g, 51.4 mmol) along with a catalytic amount of benzyl peroxide (300 mg) in carbon tetrachloride (200 mL) then heated to reflux for 6 hours. A white precipitate had formed and was removed by filtration. The solvents were removed to give a thick clear oil. ¹H NMR analysis showed the material was 85% pure (Figure A-12). No further purification was performed.

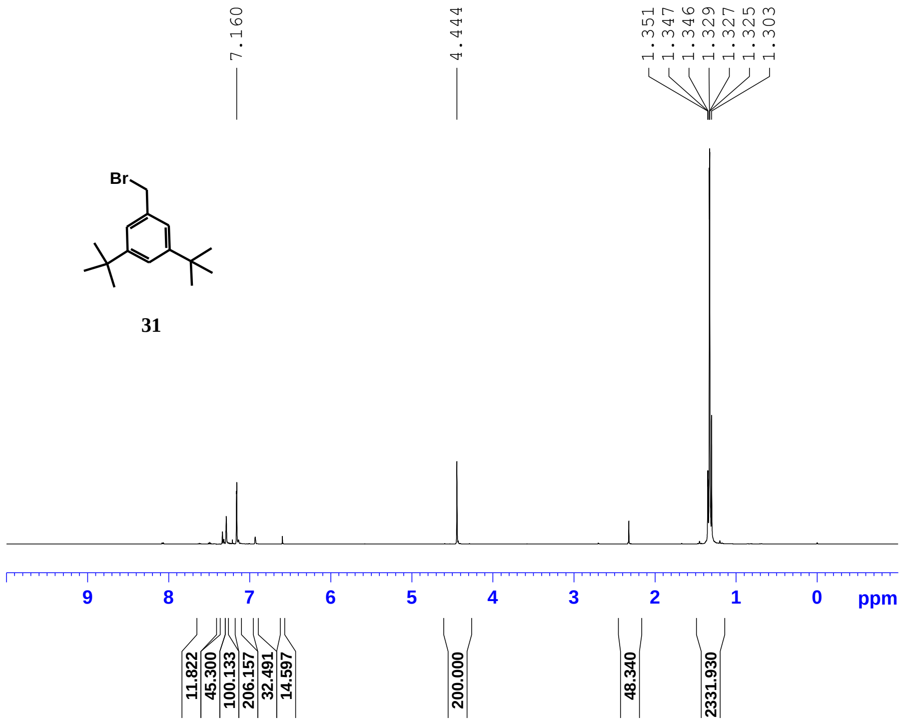

Figure A-12. [1]H NMR of Compound 31

(32): Valerolactam (4.55 g, 46 mmol) in anhydrous DMF (100 mL) at 0 °C was treated with sodium hydride (1.16 g, 46 mmol) in small portions over 20 minutes. Precipitates formed which impeded stirring. After breaking up the precipitates with a glass stir rod, the solution was stirred for 1 hour. Bromide **31** (13 g, 46 mmol) in DMF (50 mL) was added then the solution was stirred at room temperature for 16 hours. The solvent was removed under reduced pressure leaving a thick crude material. Material was solvated in chloroform (100 mL) then extracted with distilled water (100 mL). Combined organics were dried with magnesium sulfate, filtered then concentrated. Purification by column chromatography (silica gel, $CHCl_3$:CH_3OH 95: 5) afforded **32** (10.3 g, 74% yield). ^1H NMR is shown in Figure A-13.

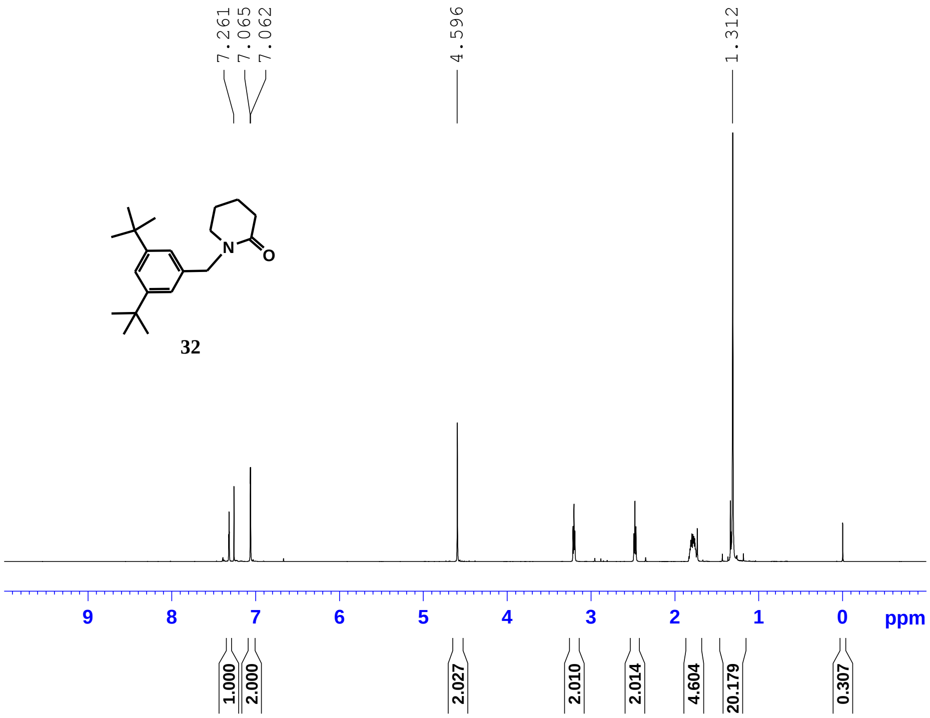

Figure A-13. ^{1}H NMR of Compound 32

(33): Lactam 32 (10.3 g, 34.2 mmol) was mixed in 6N HCl (100 mL) then heated to reflux for 12 hours. Reaction was monitored by ^{1}H NMR for completion by sampling the hot aqueous mixture. After cooling to room temperature, the material was extracted with chloroform (3X75mL). The organics were dried with magnesium sulfate, filtered and concentrated to 50 mL under reduced pressure. Diethylether (200 mL) was added to precipitate the product. Material was collected by filtration and then dried under reduced pressure. Reaction generated 11g 90% yield of 95% pure **33**. No further purification was necessary. ^{1}H NMR is shown in Figure A-14.

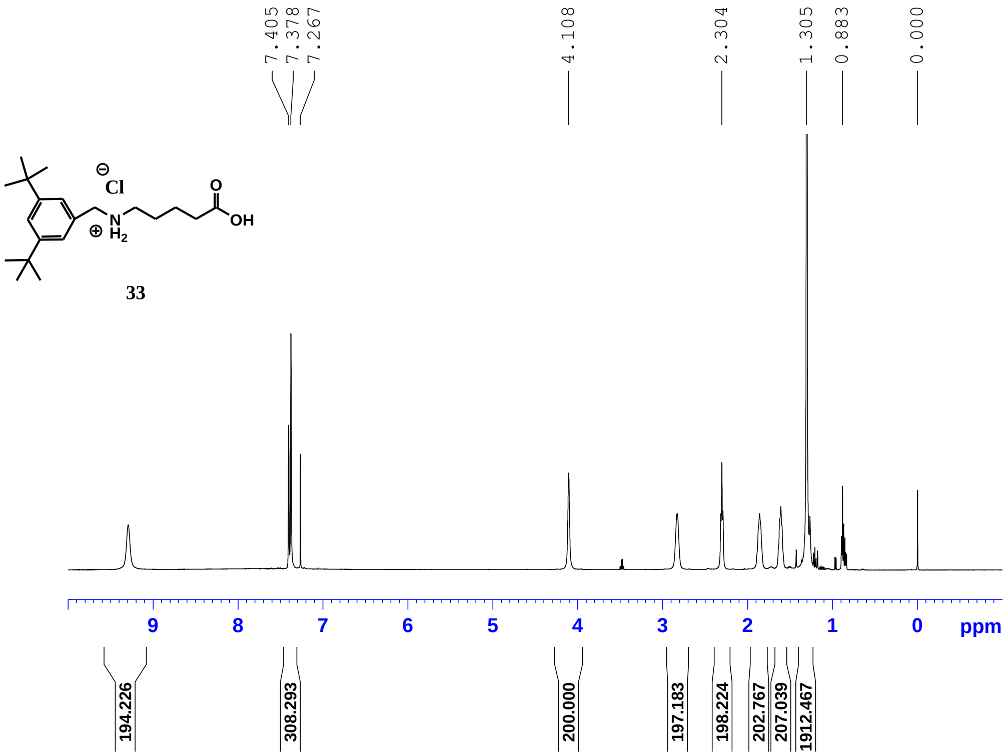

Figure A-14. [1]H NMR of the Simple Tether Compound 33

(34): Left half **22** (13.35 g, 19.04 mmol) and right half **27** (6.8 g, 19.04 mmol) were mixed in DMF (750 mL) with Cs_2CO_3 (12.64 g, 41.8 mmol) for 15 days. Solvent was removed under reduced pressure leaving a thick crude material. Crude material was extracted between water (300 mL) and chloroform (2 X 300 mL). The combined organics were dried with magnesium sulfate, filtered and then concentrated. Purification by column chromatography (silica gel, $CHCl_3$: CH_3OH 95:5) afforded cyclophane **34** (10.4 g, 60% yield). ^{1}H NMR is shown below.

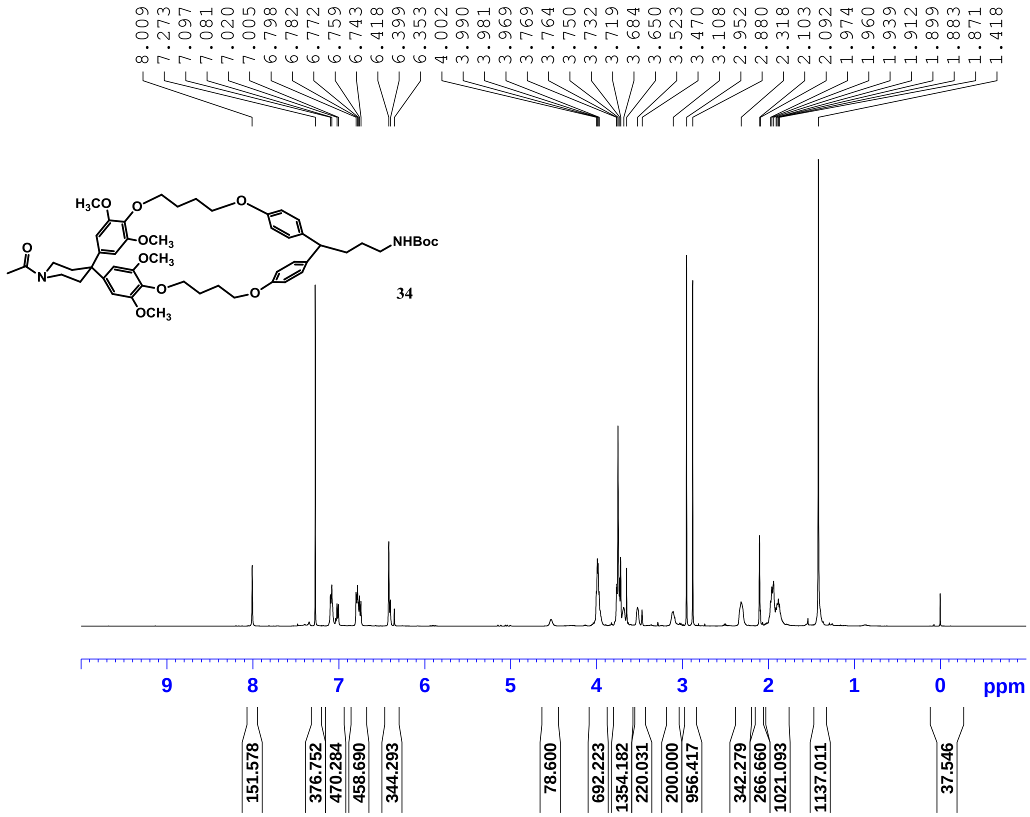

Figure A-15. ^{1}H NMR of Cyclophane 34

(35): TFA (5 mL) was added to Cyclophane **34** (5 g, 5.4 mmol) in chloroform (75 mL) then stirred at room temperature for 16 hours. Solution was extracted with 2N NaOH (100 mL), dried with magnesium sulfate, filtered and concentrated. Material was used without further purification.

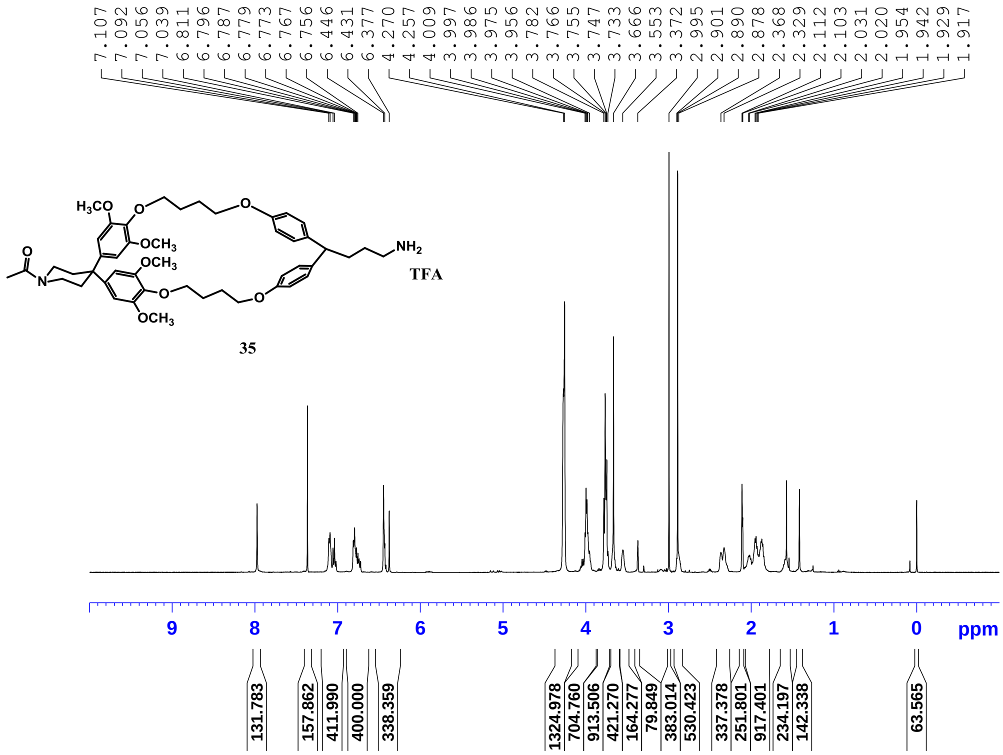

Figure A-16. ^{1}H NMR of Cyclophane 35

(36) Tether 33 (1.2 g, 3.32 mmol) was added to ammonium hexafluorophosphate (3 eq.) in 5% aq. HCl (50 mL). Note: Tether 33 is not soluble. The suspension was mixed vigorously with diethyl ether (50 mL) until all the solids were solvated, approximately 20 minutes. The organics were dried with magnesium sulfate, filtered and concentrated to afford an off-white solid. Crown ether **20** (2.25 g, 3.32 mmol) was added to the off-white tether salt then solvated with $CDCl_3$. Pseudo-rotaxane formation was followed by ^{1}H NMR.

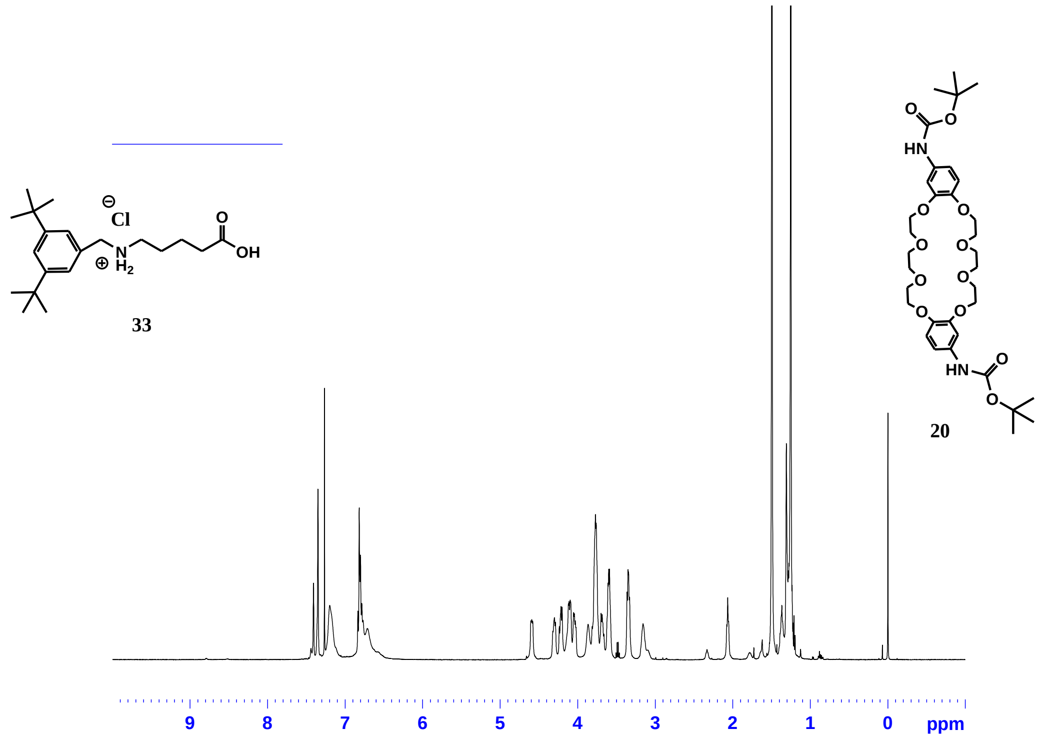

Figure A-17. ^{1}H NMR of Tether 33 Complexed with Crown Ether 20

In Figure A-17, note the ^{1}H NMR signal at δ 4.6 ppm. This chemical shift is the result of a threaded pseudo-rotaxane state. DCC (686 mg, 3.32 mmol) was then added to the mixture. ^{1}H NMR is shown in Figure A-18 below. Note the tall sharp singlet overlapping the broad multiplet is compound **32**. This is formed as a result of the threading equilibrium. Non-Threaded tether is immediately converted to 33. This is very good as it eliminates potential byproducts from the step in the reaction. All recovered **32** can be recycled back into tether **33** on large scale production.

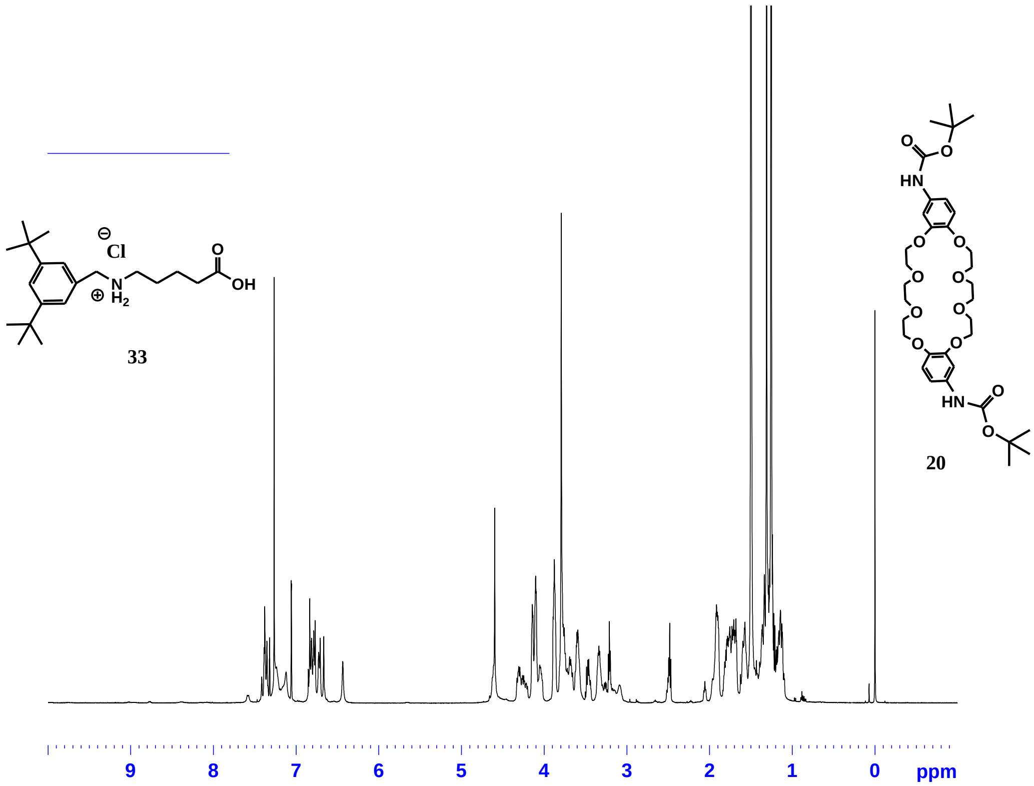

Figure A-18. ^{1}H NMR of the DCC-Rotaxane Reagent

The mixture was stirred for three days at room temperature to facilitate a complete conversion. A small amount of white precipitate (dicyclohexylurea, DCU) had formed, indicating the coupling reaction had occurred. DCU was completely removed by exchanging solvents to acetonitrile and then filtering. After purification by column chromatography, three compounds were recovered: cyclophane **35**, DCC-rotaxane reagent and the host-[2]rotaxane **36**. No other by-products were found. The un-reacted cyclophane **35** was estimated at 83% based on the amount of host-[2]rotaxane recovered. This un-reacted material was recycled in repeat reactions which generated more material. The isolated yield of host-[2]rotaxane was (1.0 g, 17%); ^{1}H NMR of host-[2]rotaxane **36** is show in Figure A-19. host-[2]rotaxane **36** is an amorphous pink-colored glass.

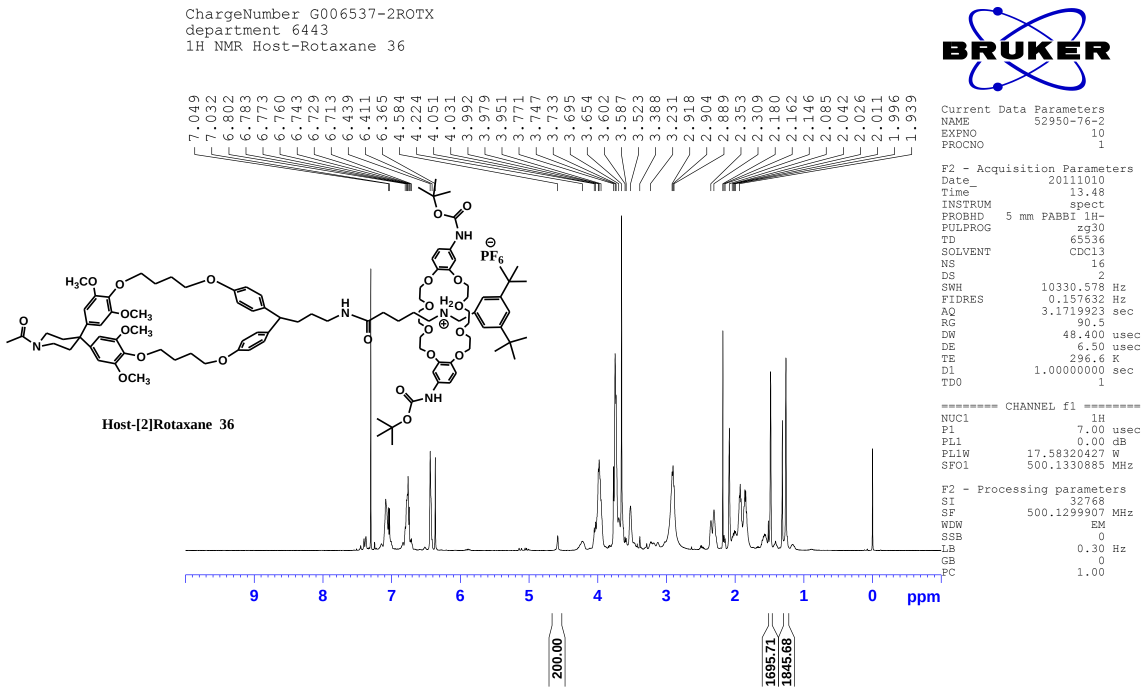

Figure A-19. ^{1}H NMR of Host-[2]Rotaxane 36

(37): TFA (3 mL) was added to host-[2]rotaxane **36** (3 g) in chloroform (50 mL) then stirred at room temperature for 3 hours. Solution was quenched with 10% aq KOH (100 mL) then extracted with chloroform (2 X 50 mL). Combined organics were dried with magnesium sulfate, filtered and concentrated. No further purification was necessary. ^{1}H NMR shown below, note the loss of BOC protecting group functionality.

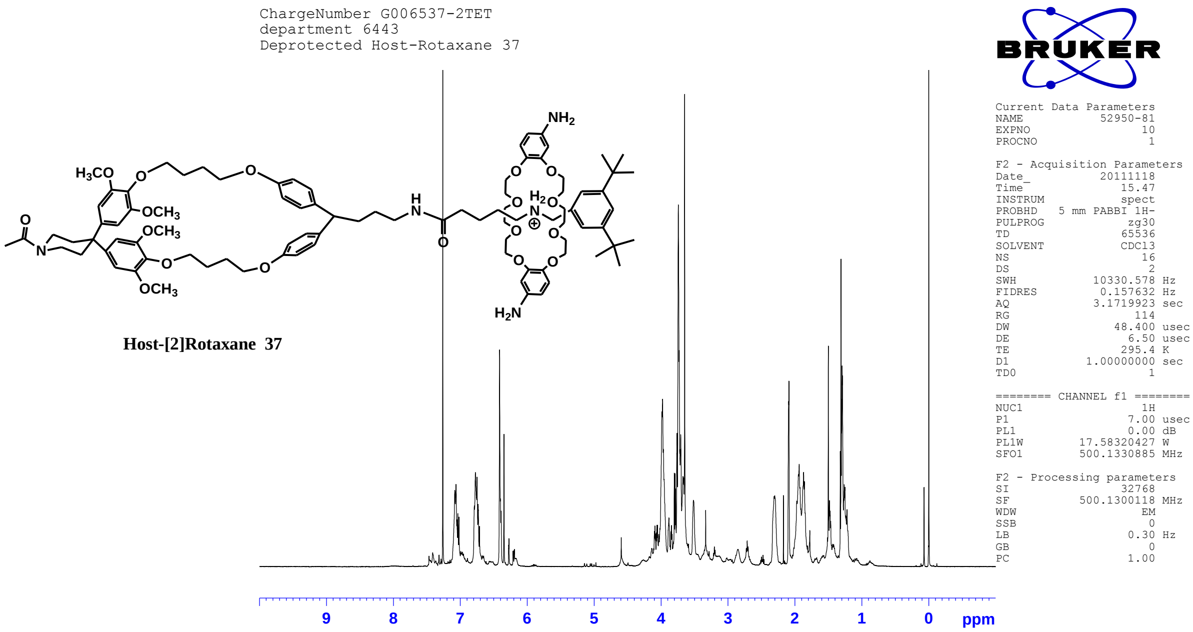

Figure A-20. ^{1}H NMR of Host-[2]Rotaxane 37

(38): Tri-Boc-Arginine (1.3 g, 2.74 mmol), Host-[2]rotaxane **37** and 1-hydroxybenzotriazole hydrate (74 mg, 0.5 mmol, 0.2 eq) were mixed in chloroform at room temperature. DCC (566 mg, 2.74 mmol) dissolved in chloroform was added add at once and the solution was stirred for 16 hours at room temperature. Chloroform was removed under reduced pressure and replaced with acetonitrile. The DCU byproduct was filtered and concentrated. Purification by column chromatography afforded **38** in 70% yield. ^{1}H NMR spectrum is shown in Figure A-21. Note the presence of the multiple BOC t-butyl groups on the arginine at δ 1.5.

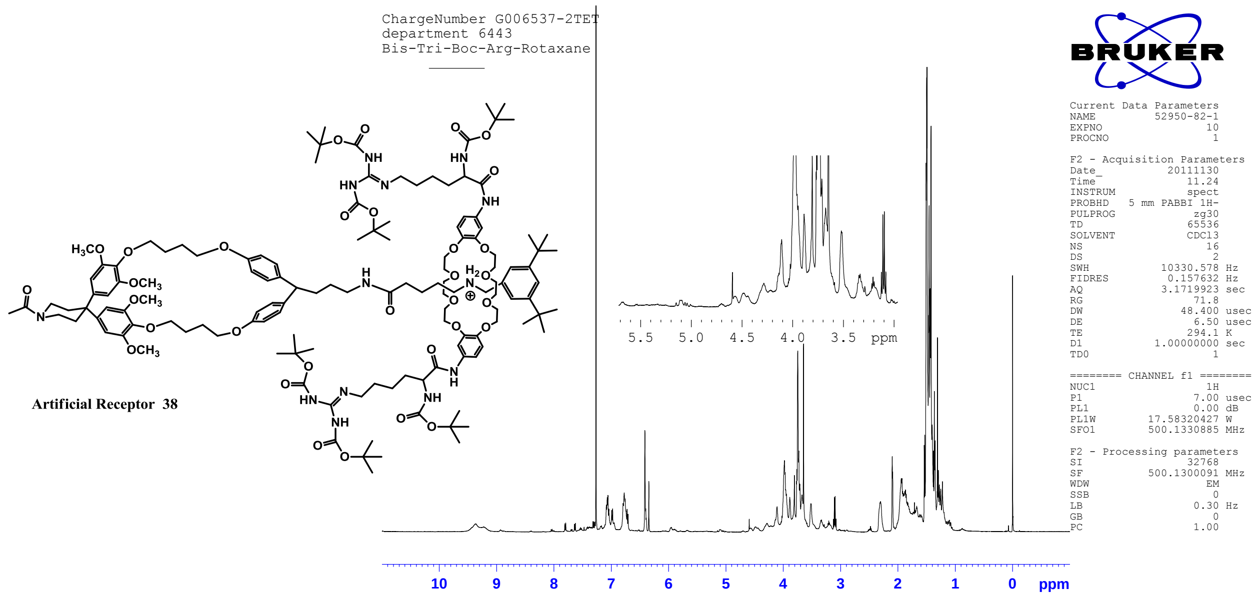

Figure A-21 [1]H NMR of Bis-Tri-Boc-Arg-Host-[2]Rotaxane 38

Artificial Receptor **(1):** Bis-Boc-Arg-Host-[2]Rotaxane **38** (2 g) was mixed in chloroform (20 mL) with 20 mL of 50:50 TFA/AcOH for 5 days at room temperature. Solvents were removed under reduced pressure to give a think amorphous glass. Material was solvated with 5 mL of DMSO then precipitated with hexane. After decanting the solvent the material was dried under hi-vac. No further purification was performed. Reaction provided **1** (1.9 g, 98%) as a red-brown amorphous glass. ^{1}H NMR for **1** is show below.

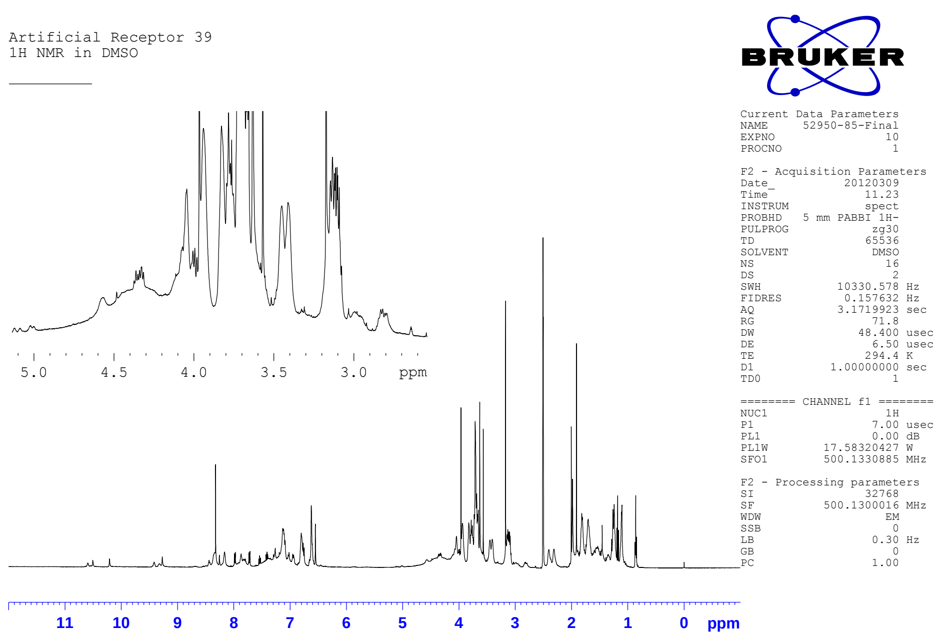

Figure A-22. [1]H NMR of Bis-Tri-Boc-Arg-Host-[2]Rotaxane 38

Appendix B: Binding Study Data on Cyclophane 35 with Ethyl Phenylphosphinate

Binding Study using 95% DMSO-d_6 / 5% D_2O

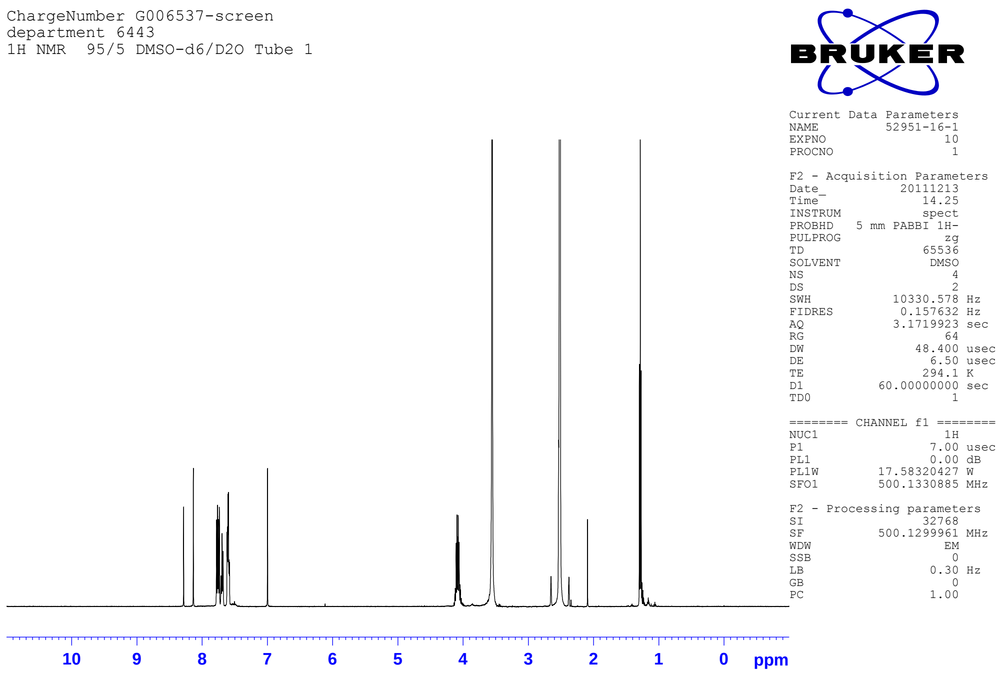

Figure B-1. ^{1}H NMR Tube 1: (10 mmol) EPP, (0 mmol) of 35

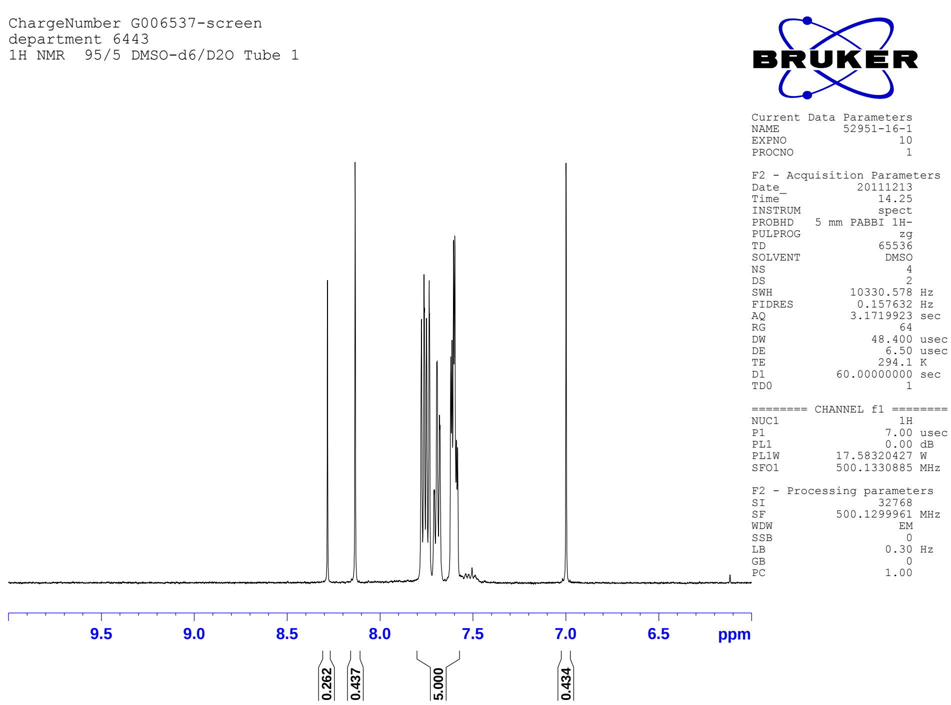

Figure B-2. Expanded View of ^{1}H NMR Tube 1: (10 mmol) EPP, (0 mmol) of 35

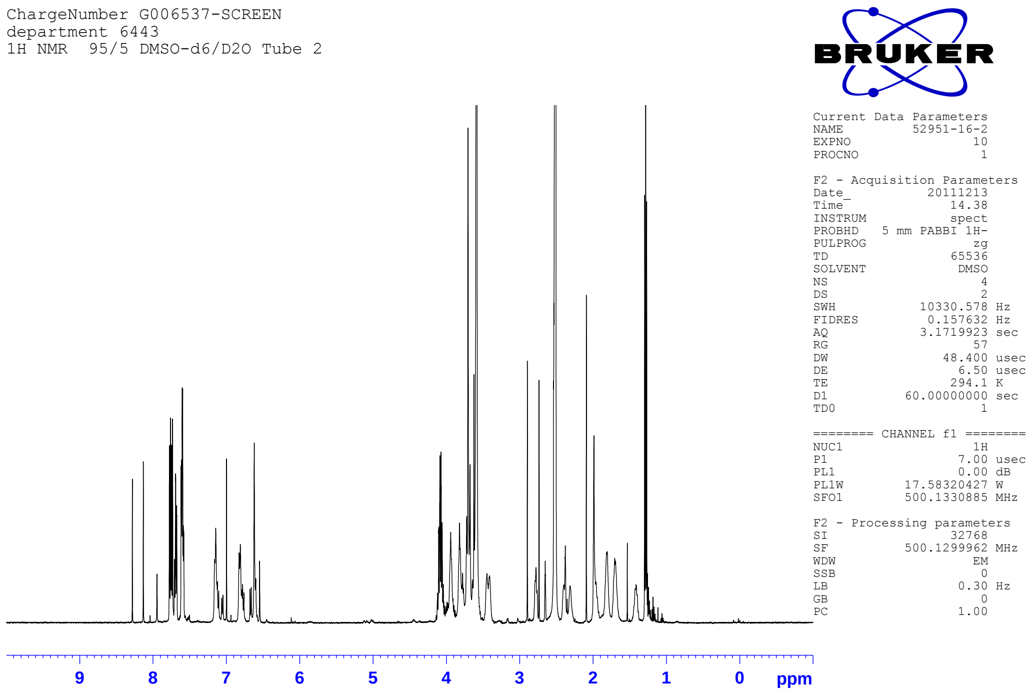

Figure B-3. ^{1}H NMR Tube 2: (10 mmol) EPP, (5 mmol) of 35

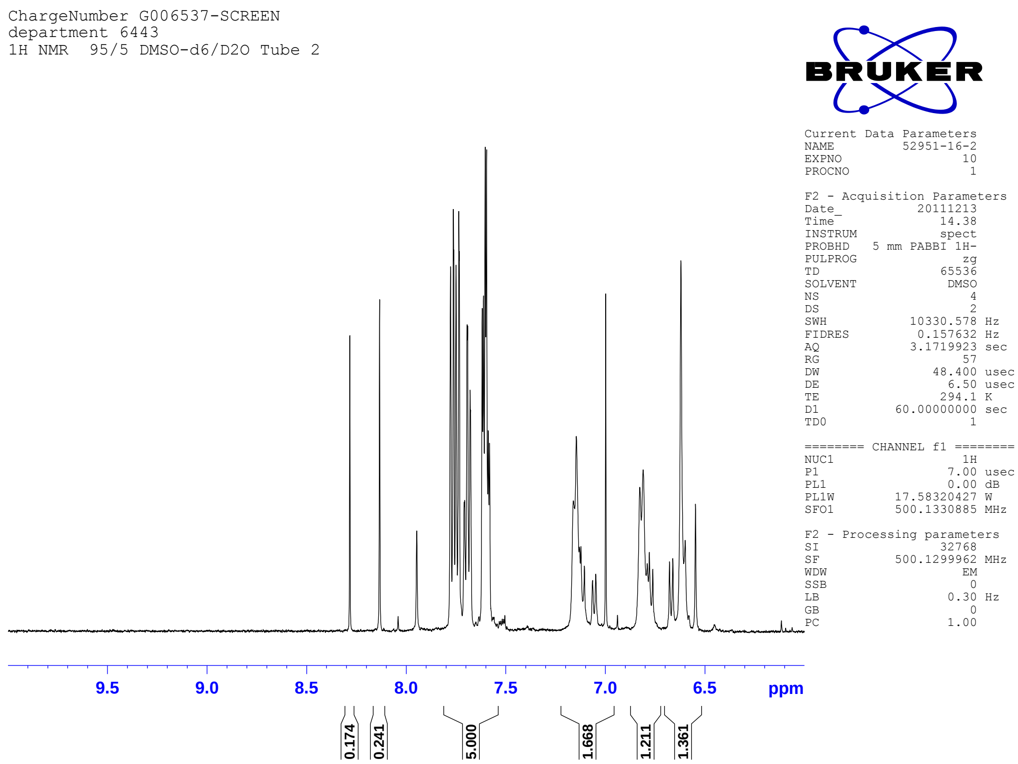

Figure B-4. Expanded View of ^{1}H NMR Tube 2: (10 mmol) EPP, (5 mmol) of 35

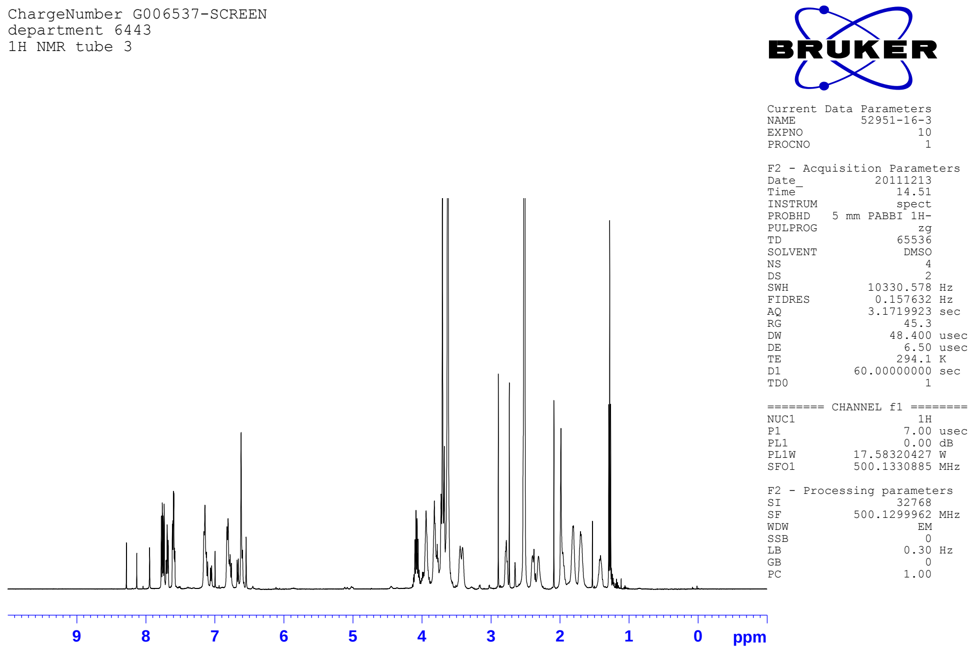

Figure B-5. ^{1}H NMR Tube 3: (10 mmol) EPP, (10 mmol) of 35

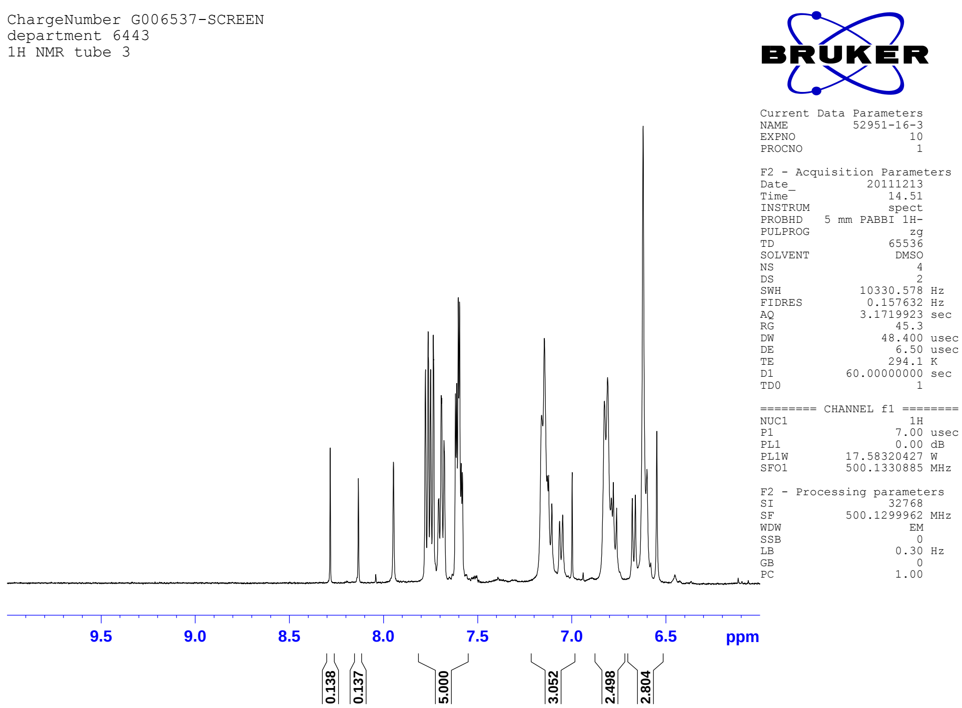

Figure B-6. Expanded View of ^{1}H NMR Tube 3: (10 mmol) EPP, (10 mmol) of 35

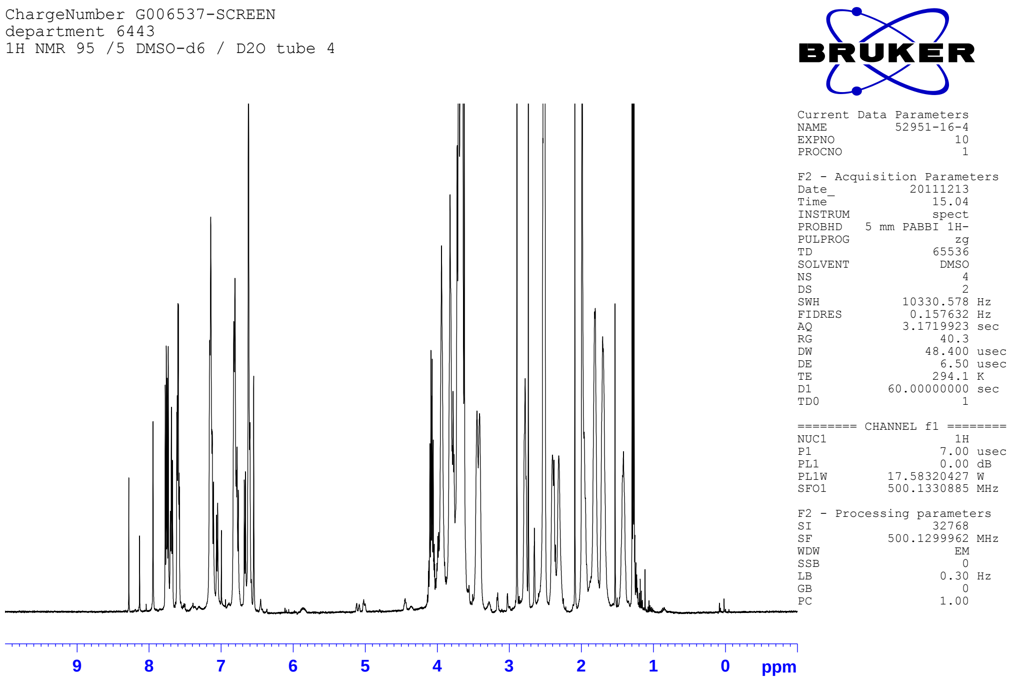

Figure B-7. ^{1}H NMR Tube 4: (10 mmol) EPP, (15 mmol) of 35

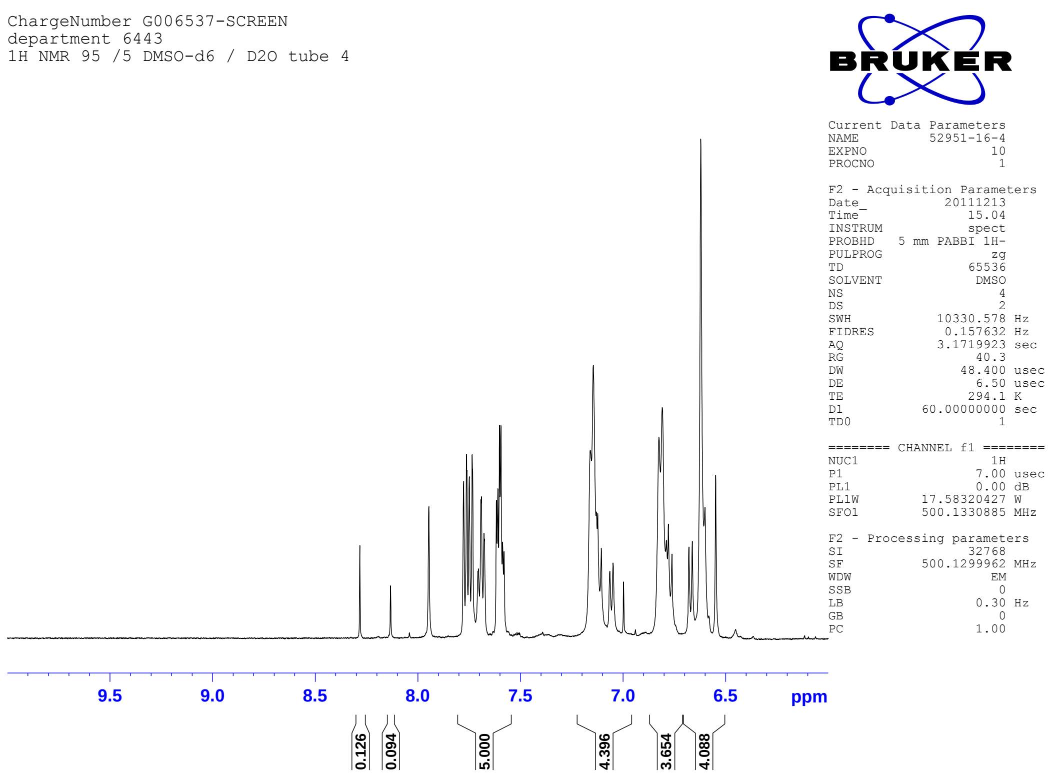

Figure B-8. Expanded View of ^{1}H NMR Tube 4: (10 mmol) EPP, (15 mmol) of 35

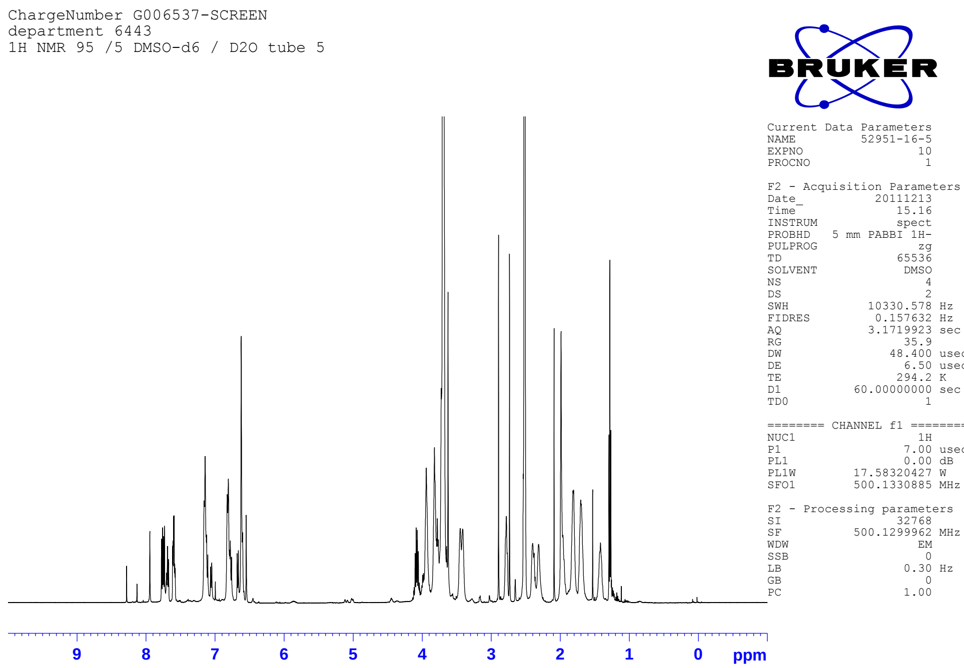

Figure B-9. ¹H NMR Tube 5: (10 mmol) EPP, (20 mmol) of 35

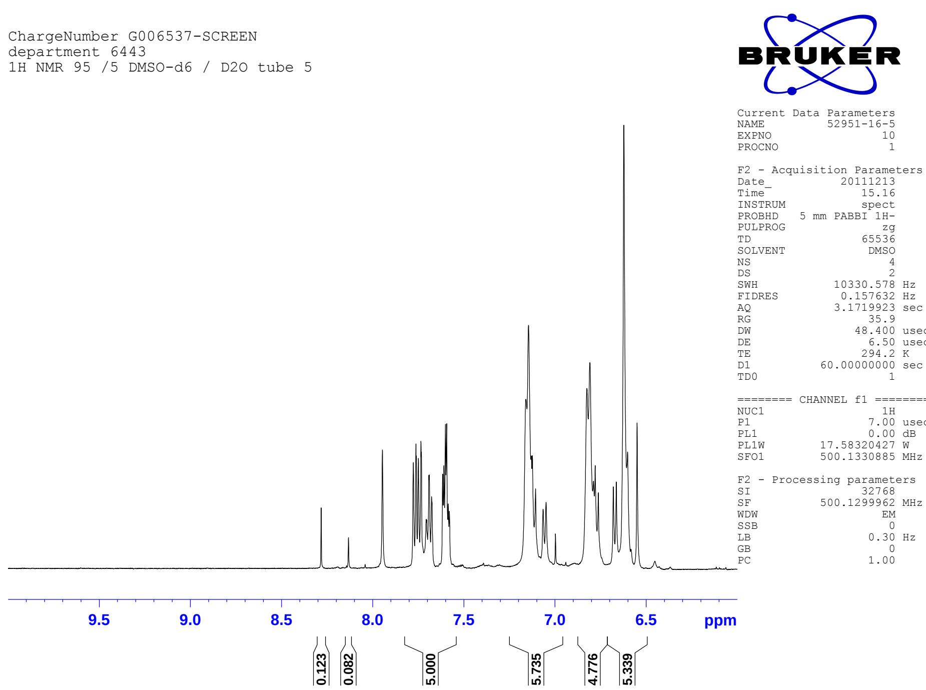

Figure B-10. Expanded View of ¹H NMR Tube 5: (10 mmol) EPP, (20 mmol) of 35

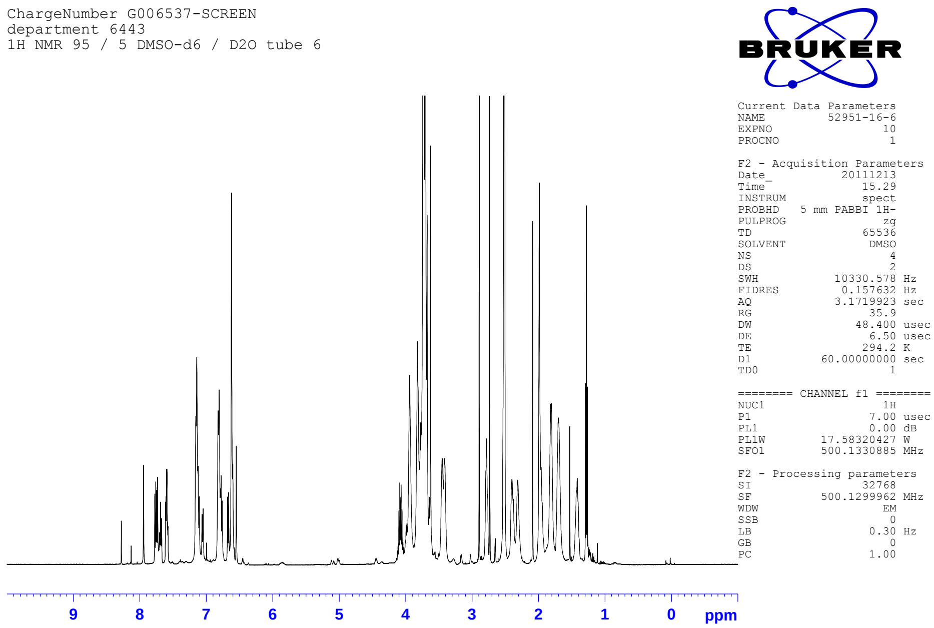

Figure B-11. ^{1}H NMR Tube 6: (10 mmol) EPP, (25 mmol) of 35

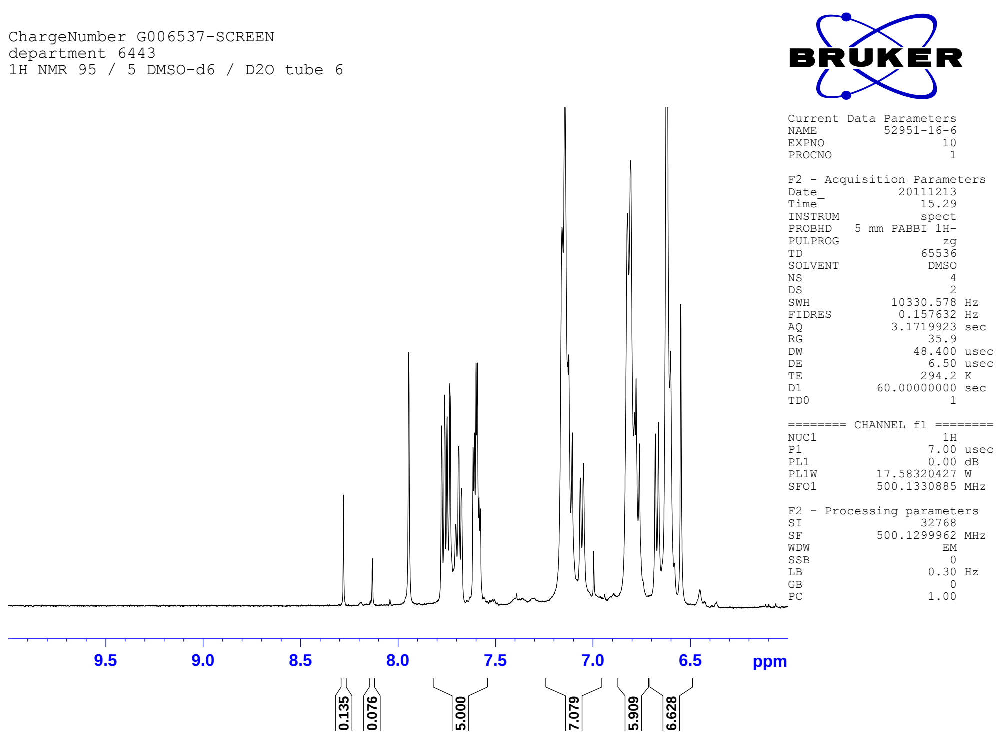

Figure B-12. Expanded View of ^{1}H NMR Tube 6: (10 mmol) EPP, (25 mmol) of 35

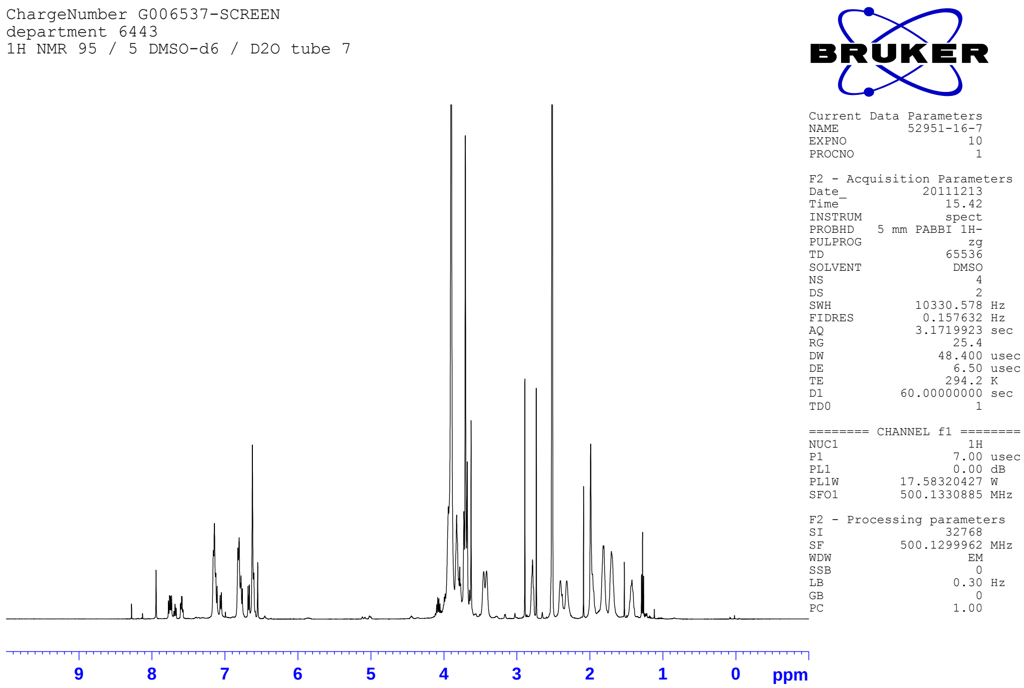

Figure B-13. ^{1}H NMR Tube 7: (10 mmol) EPP, (50 mmol) of 35

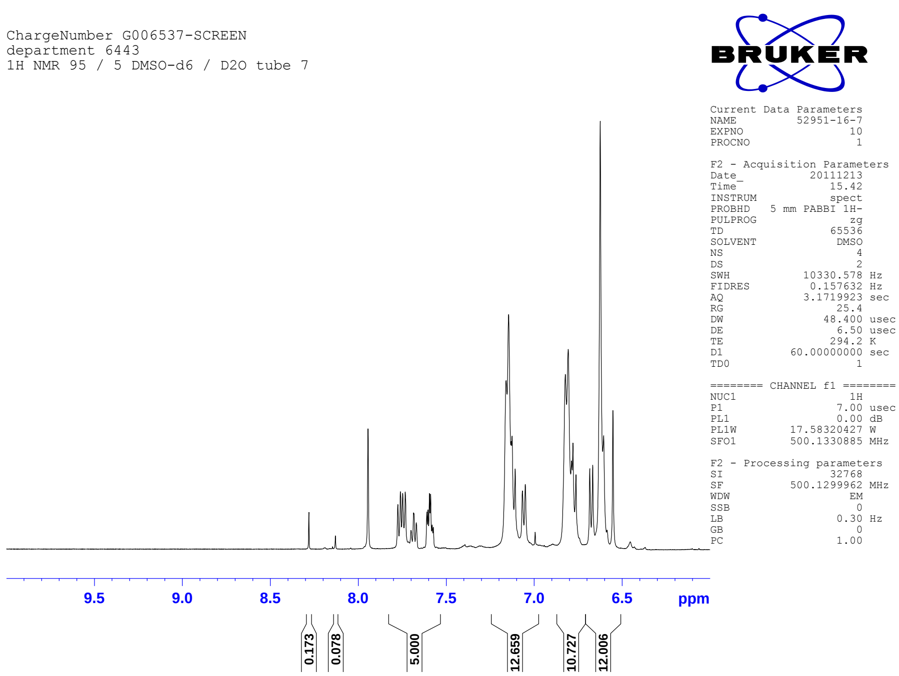

Figure B-14. Expanded View of ^{1}H NMR Tube 7: (10 mmol) EPP, (50 mmol) of 35

```
Nonlinear regression model
 model:  Y ~ P1 * P2 * X/(1 + P1 *X)
   data:  parent.frame()
     P1       P2
223.6079   0.4193
 residual sum-of-squares: 0.001997

Number of iterations to convergence: 6
Achieved convergence tolerance: 1.996e-06
```

*P1=K_a, P2= $(\Delta \text{ Area})_{Max}$, Y=$(\Delta \text{ Area})$, X=[Cyclophane 35]

Figure B-15. Non-Linear Least Squares Analysis

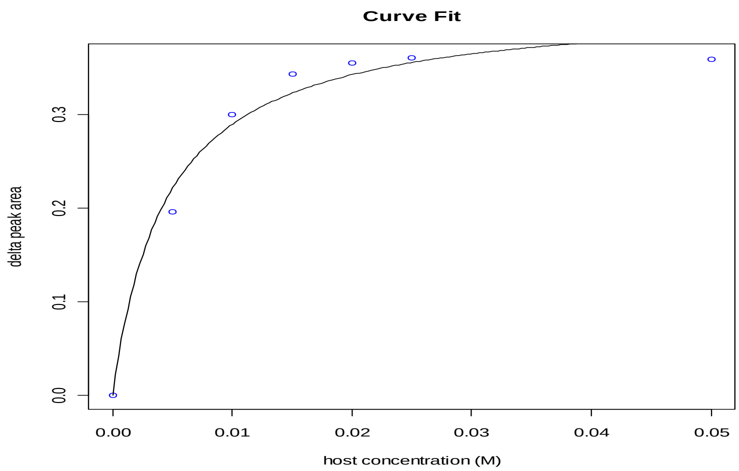

Figure B-16. Binding Curve for Cyclophane 35 and EPP at 95/5 DMSO-d_6 / D_2O

Binding Study using 90% DMSO-d_6 / 10% D_2O

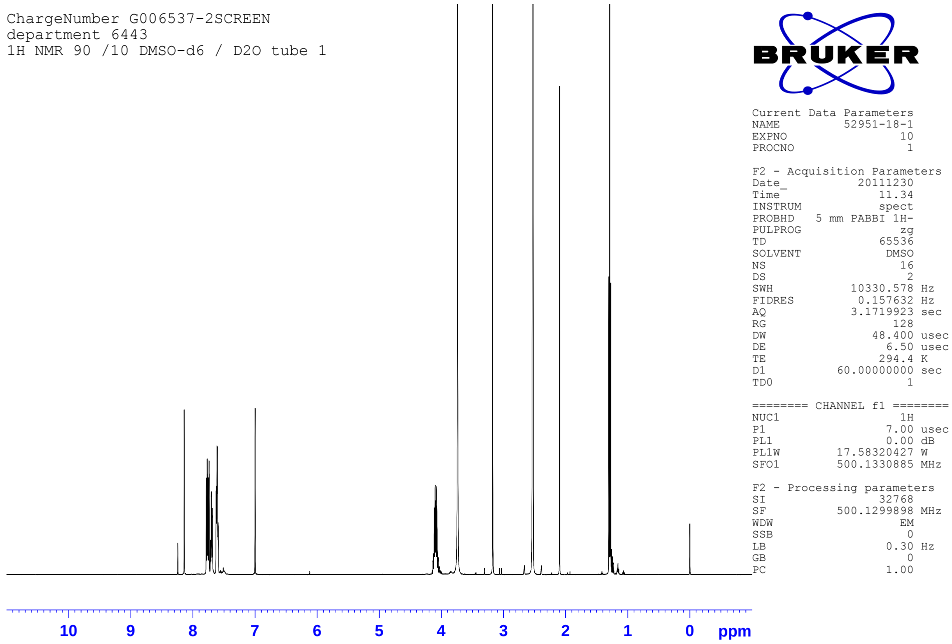

Figure B-17. ^{1}H NMR Tube 1: (10 mmol) EPP, (0 mmol) of 35

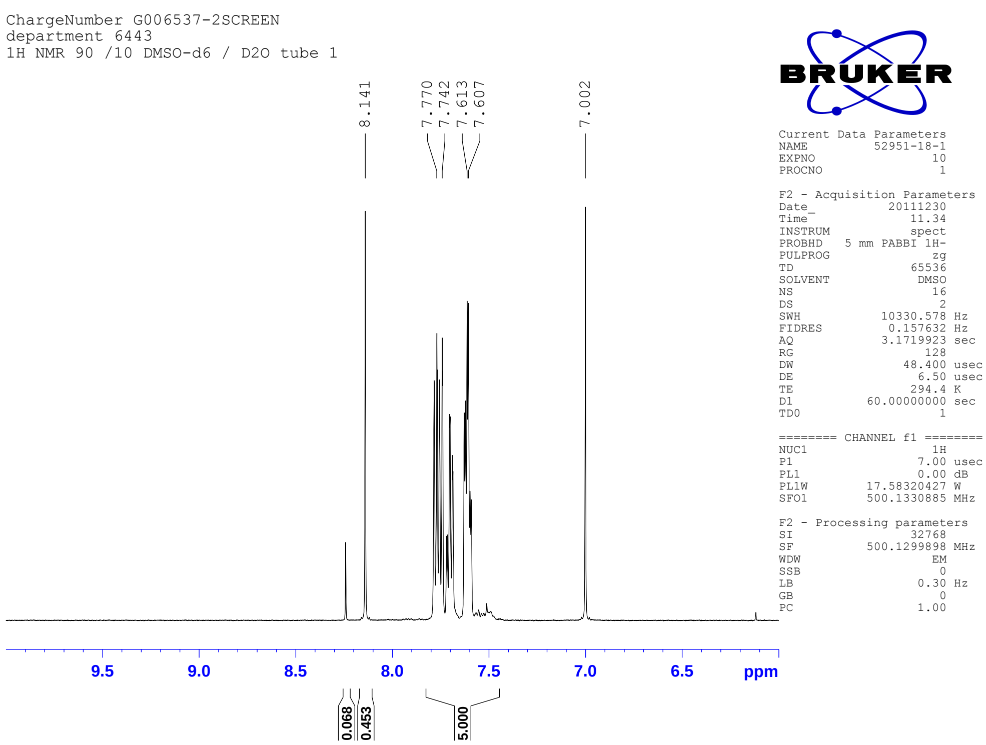

Figure B-18. Expanded View of ^{1}H NMR Tube 1: (10 mmol) EPP, (0 mmol) of 35

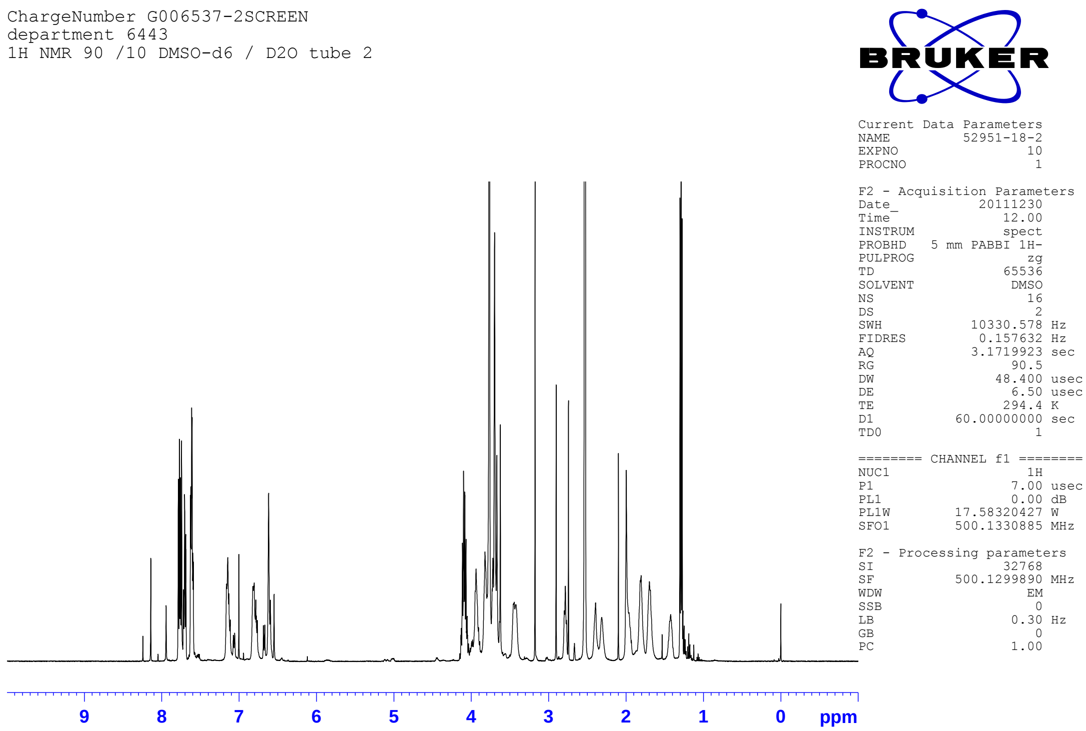

Figure B-19. ^{1}H NMR Tube 2: (10 mmol) EPP, (5 mmol) of 35

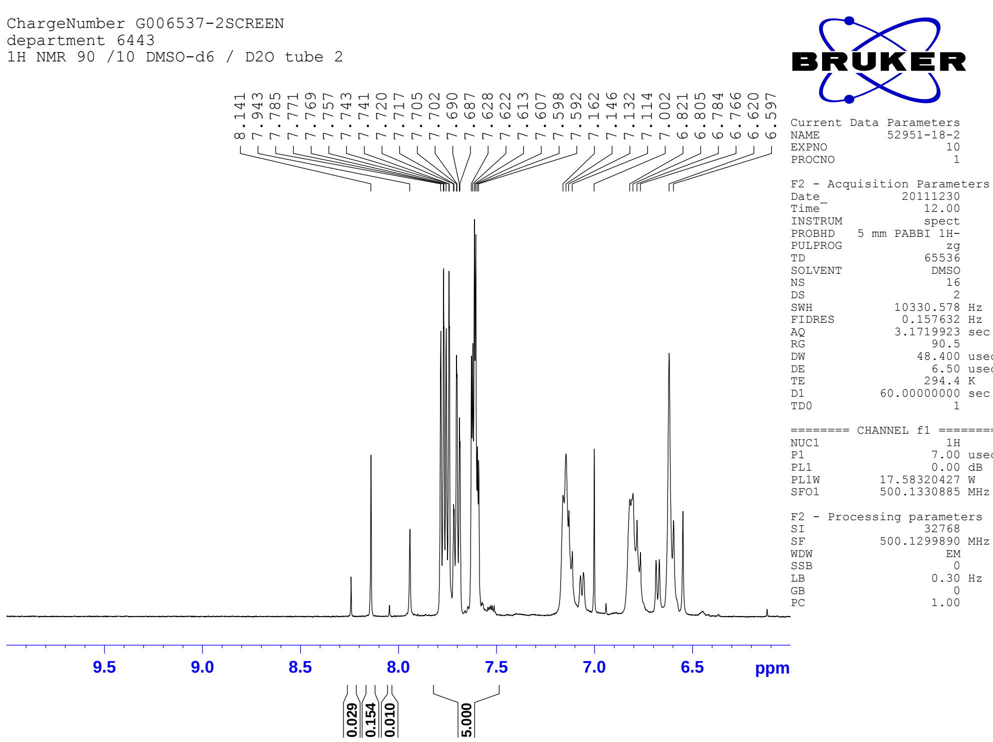

Figure B-20. Expanded View of ^{1}H NMR Tube 2: (10 mmol) EPP, (5 mmol) of 35

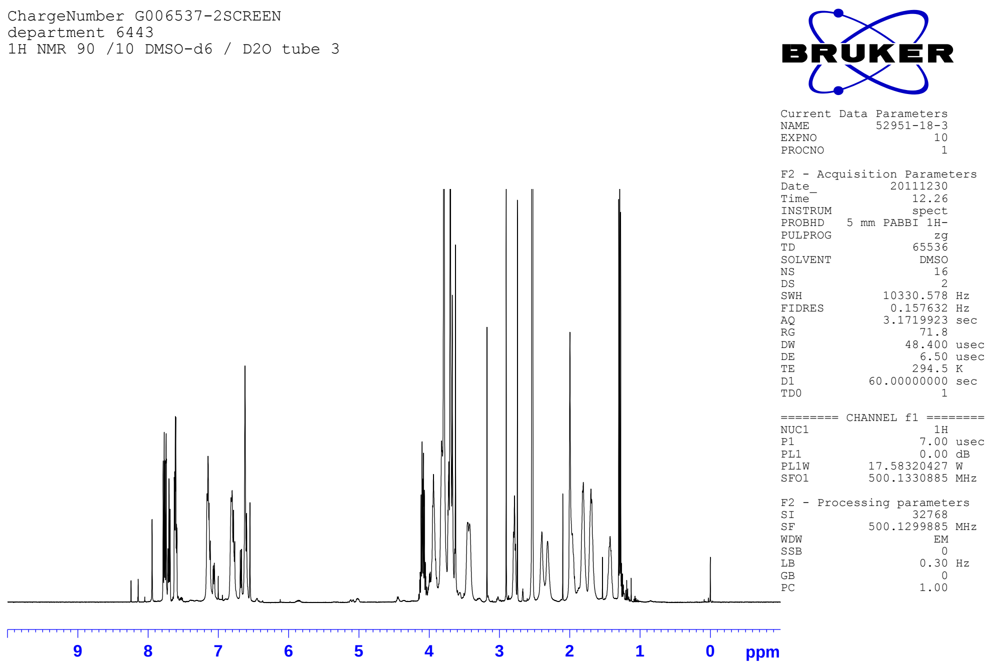

Figure B-21. [1]H NMR Tube 3: (10 mmol) EPP, (10 mmol) of 35

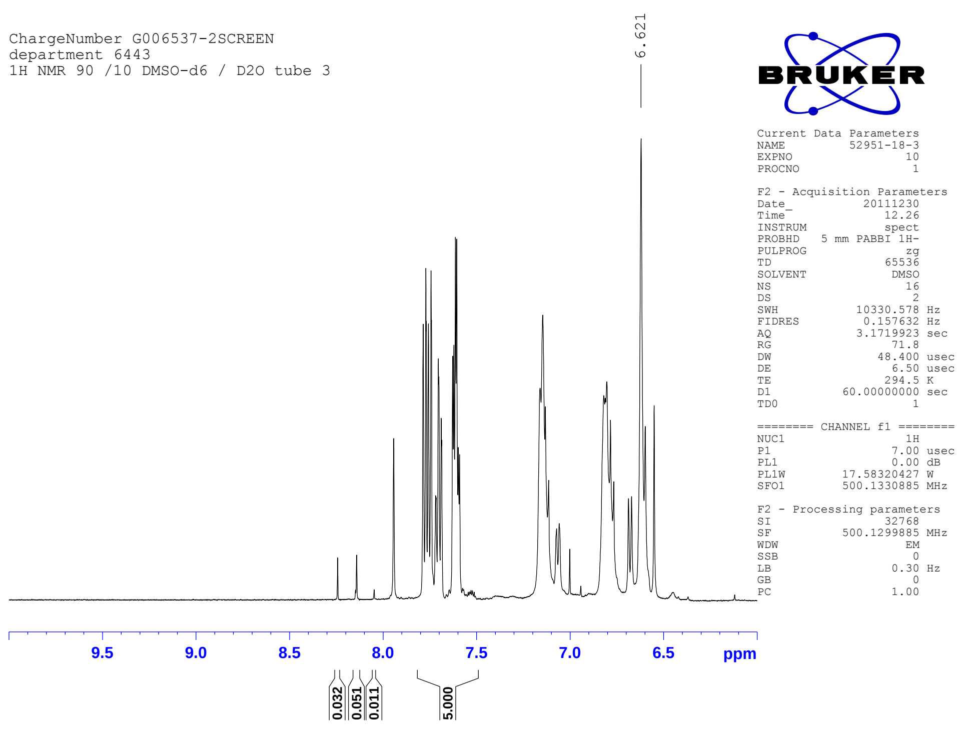

Figure B-22. Expanded View of [1]H NMR Tube 3: (10 mmol) EPP, (10 mmol) of 35

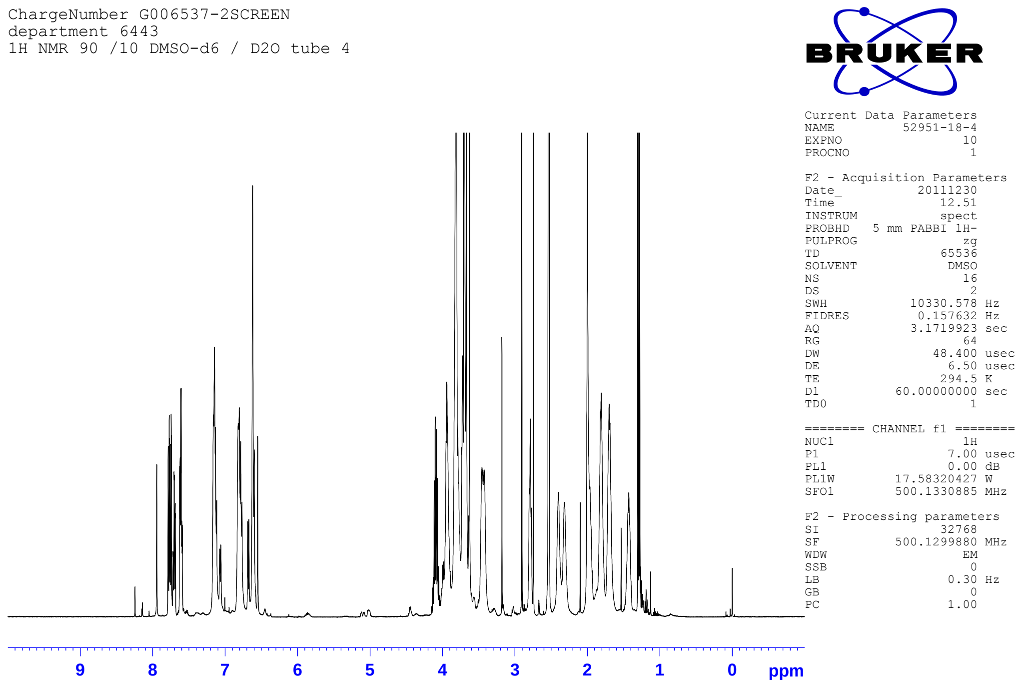

Figure B-23. ^{1}H NMR Tube 4: (10 mmol) EPP, (15 mmol) of 35

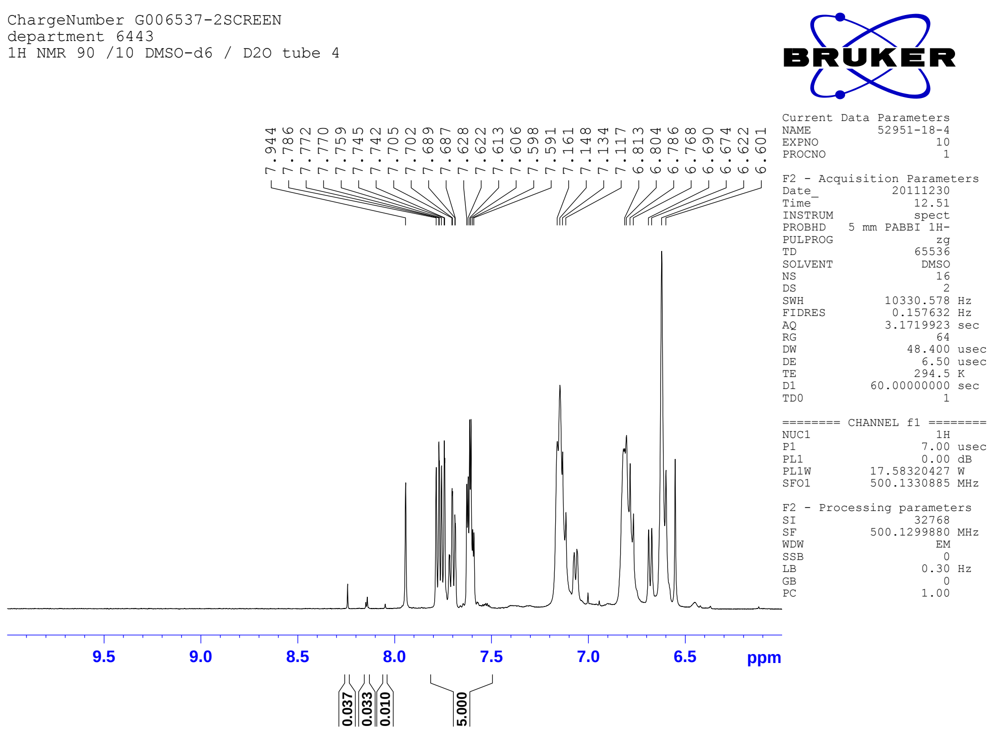

Figure B-24. Expanded View of ^{1}H NMR Tube 4: (10 mmol) EPP, (15 mmol) of 35

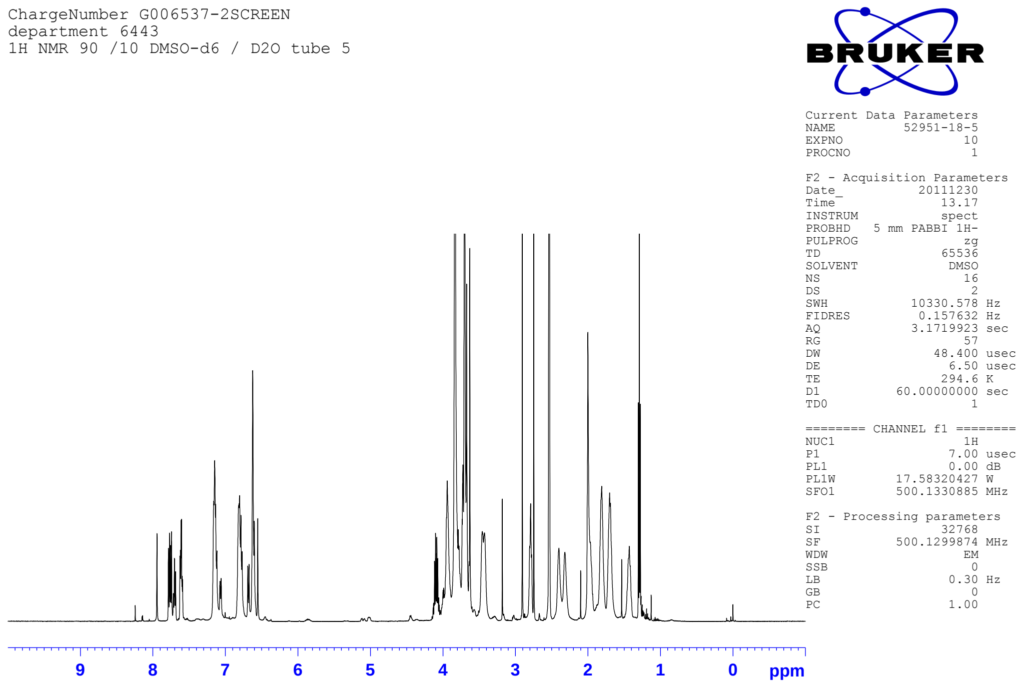

Figure B-25. ^{1}H NMR Tube 5: (10 mmol) EPP, (20 mmol) of 35

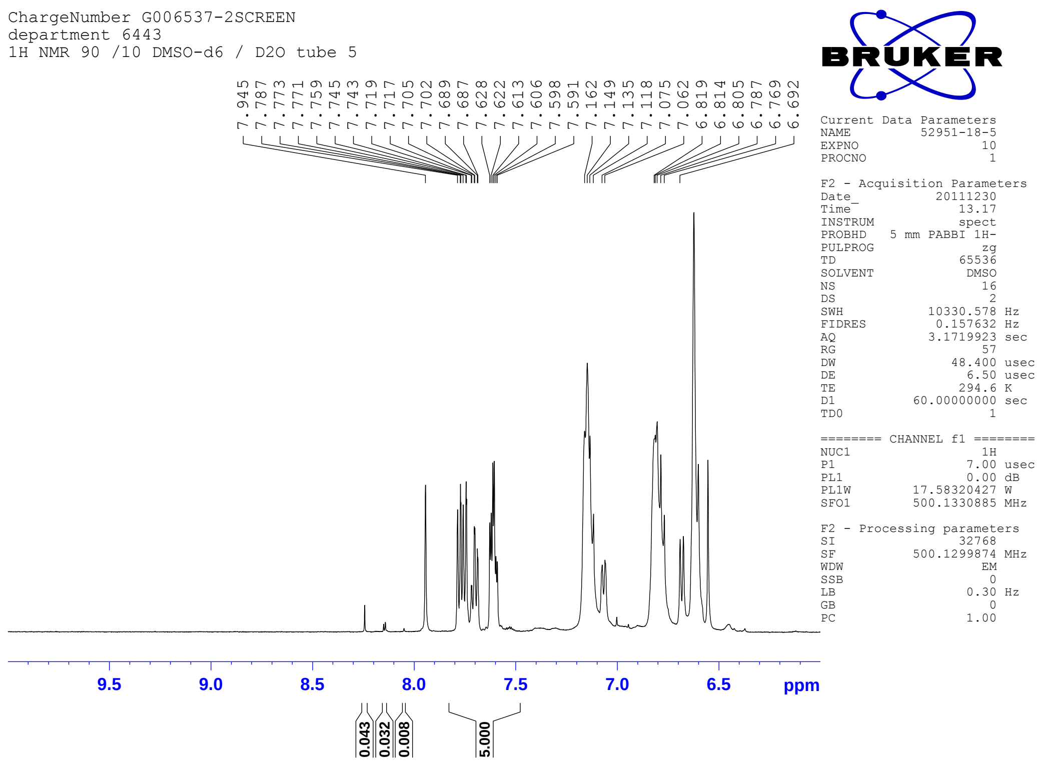

Figure B-26. Expanded View of ^{1}H NMR Tube 5: (10 mmol) EPP, (20 mmol) of 35

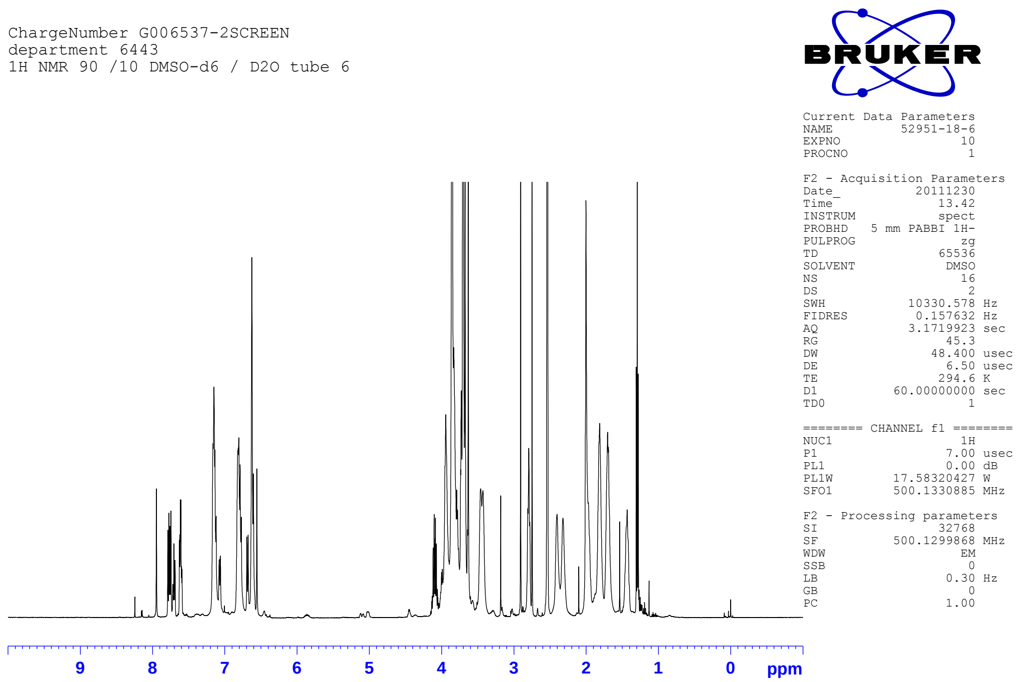

Figure B-27. ^{1}H NMR Tube 6: (10 mmol) EPP, (25 mmol) of 35

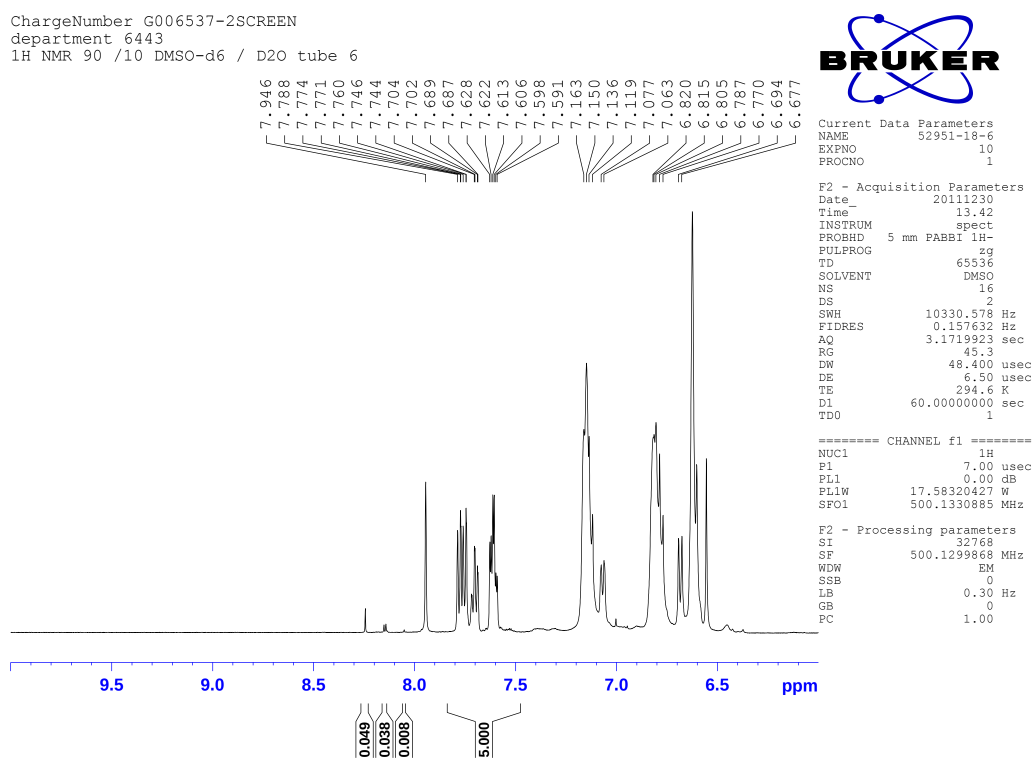

Figure B-28. Expanded View of ^{1}H NMR Tube 6: (10 mmol) EPP, (25 mmol) of 35

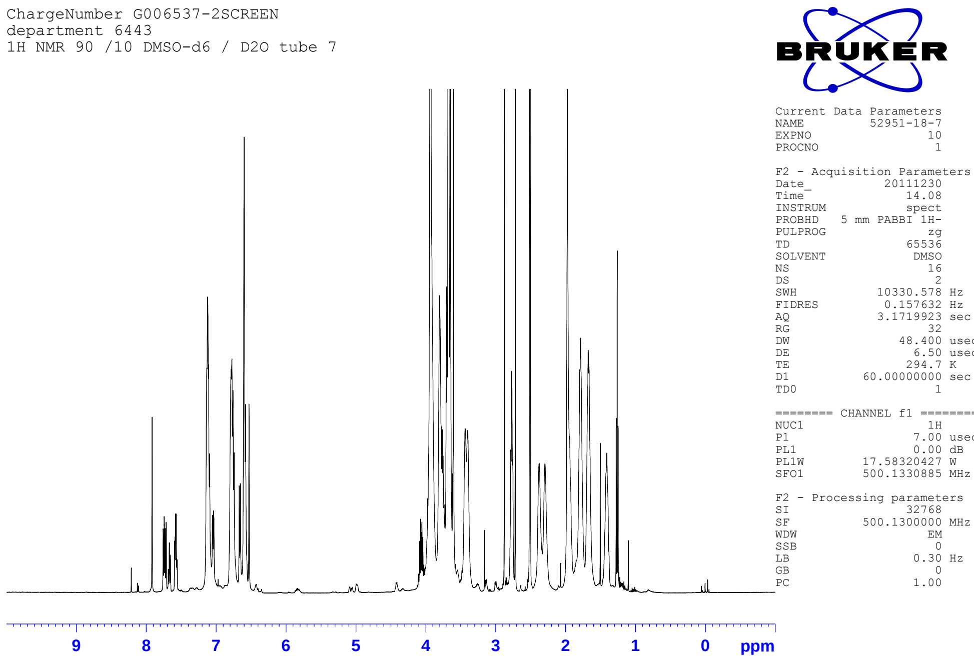

Figure B-29. ^{1}H NMR Tube 7: (10 mmol) EPP, (50 mmol) of 35

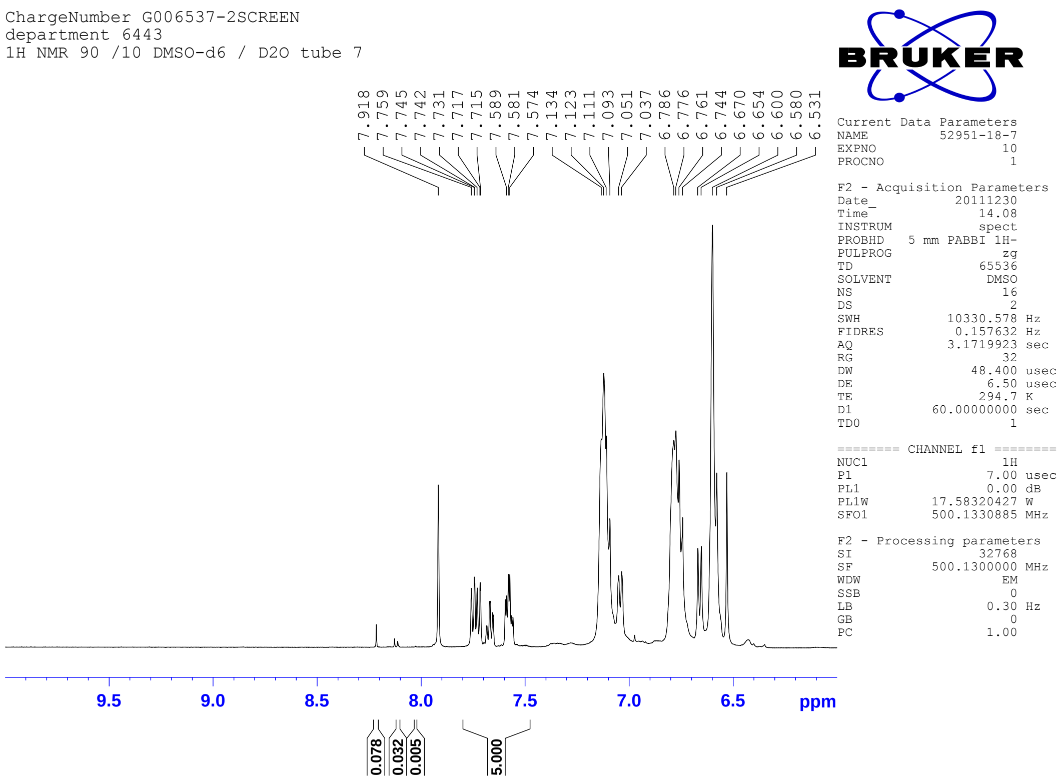

Figure B-30. Expanded View of ^{1}H NMR Tube 7: (10 mmol) EPP, (50 mmol) of 35

```
Nonlinear regression model
  model:  Y ~ (P1 * P2 * X)/(1 + P1 * X)
   data:  parent.frame()
     P1       P2
466.4152   0.4591
 residual sum-of-squares: 0.001879

Number of iterations to convergence: 6
Achieved convergence tolerance: 1.320e-06
```

*P1=K_a, P2= $(\Delta\ Area)_{Max}$, Y=(Δ Area), X=[Cyclophane 35]

Figure B-31. Non-Linear Least Squares Analysis

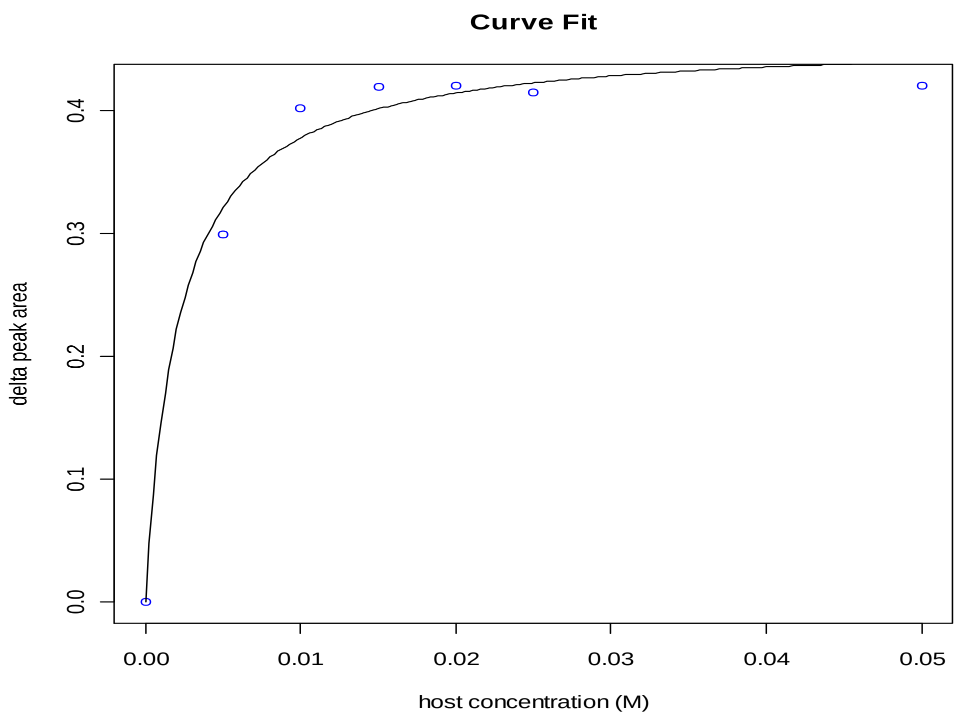

Figure B-32. Binding Curve for Cyclophane 35 and EPP at 90/10 DMSO-d_6 / D_2O

Binding Study using 85% DMSO-d_6 / 15% D_2O

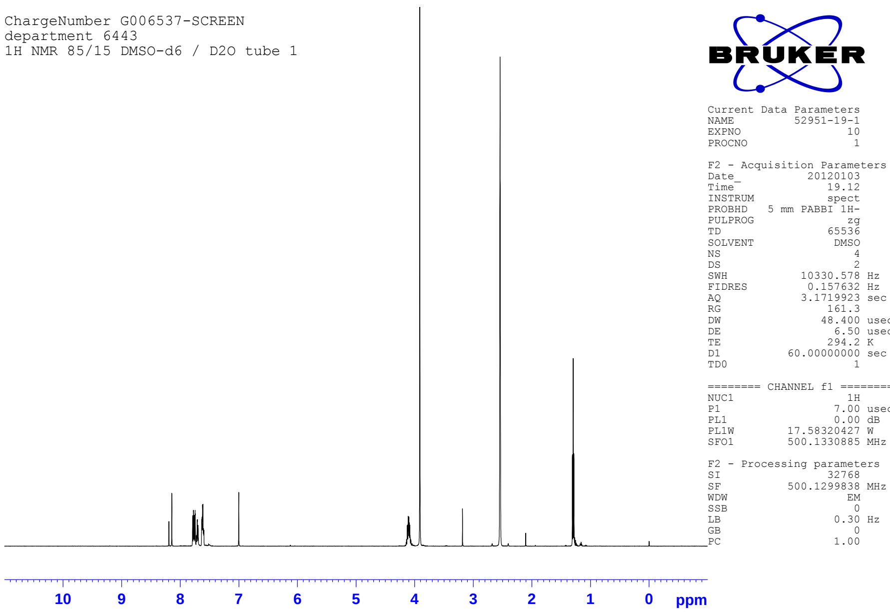

Figure B-33. [1]H NMR Tube 1: (10 mmol) EPP, (0 mmol) of 35

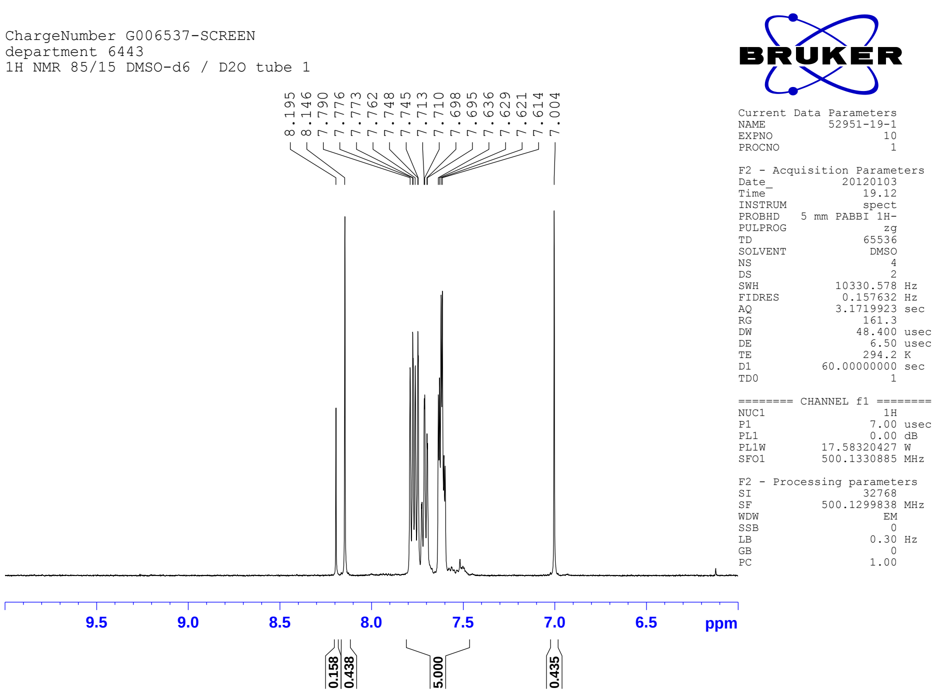

Figure B-34. Expanded View of [1]H NMR Tube 1: (10 mmol) EPP, (0 mmol) of 35

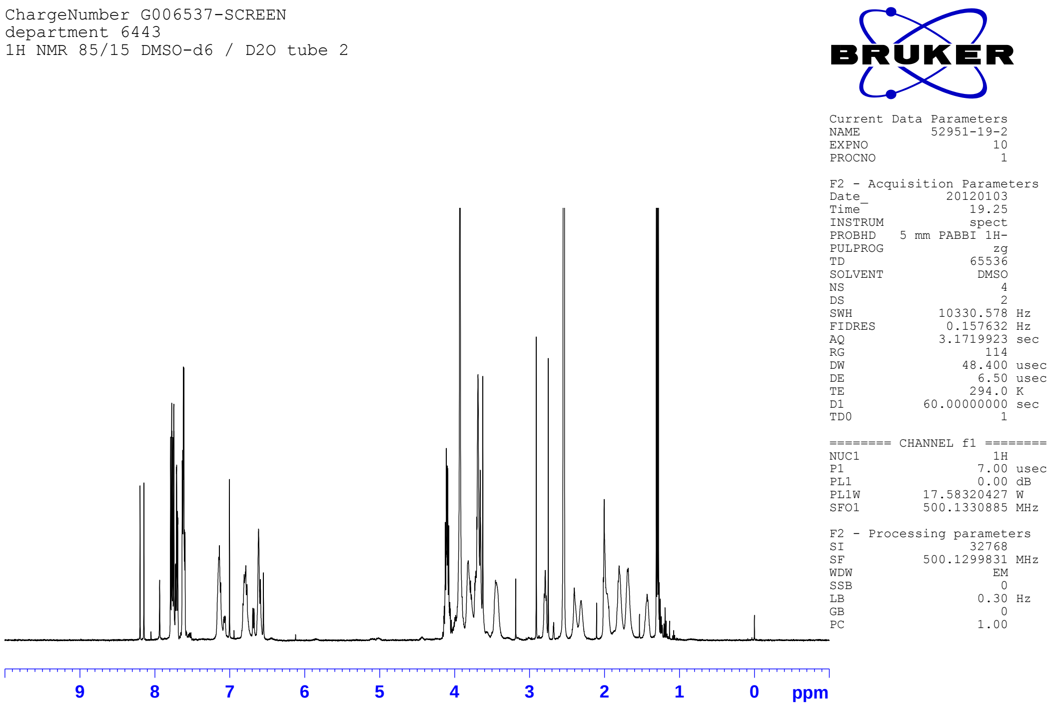

Figure B-35. ^{1}H NMR Tube 2: (10 mmol) EPP, (5 mmol) of 35

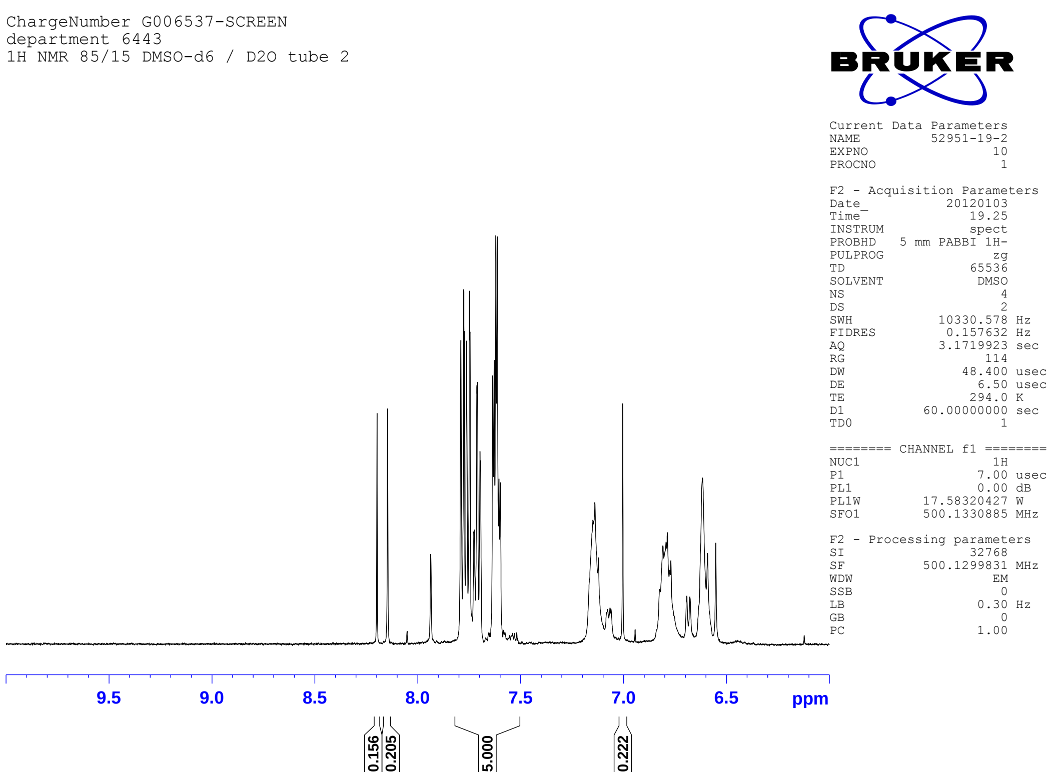

Figure B-36. Expanded View of ^{1}H NMR Tube 2: (10 mmol) EPP, (5 mmol) of 35

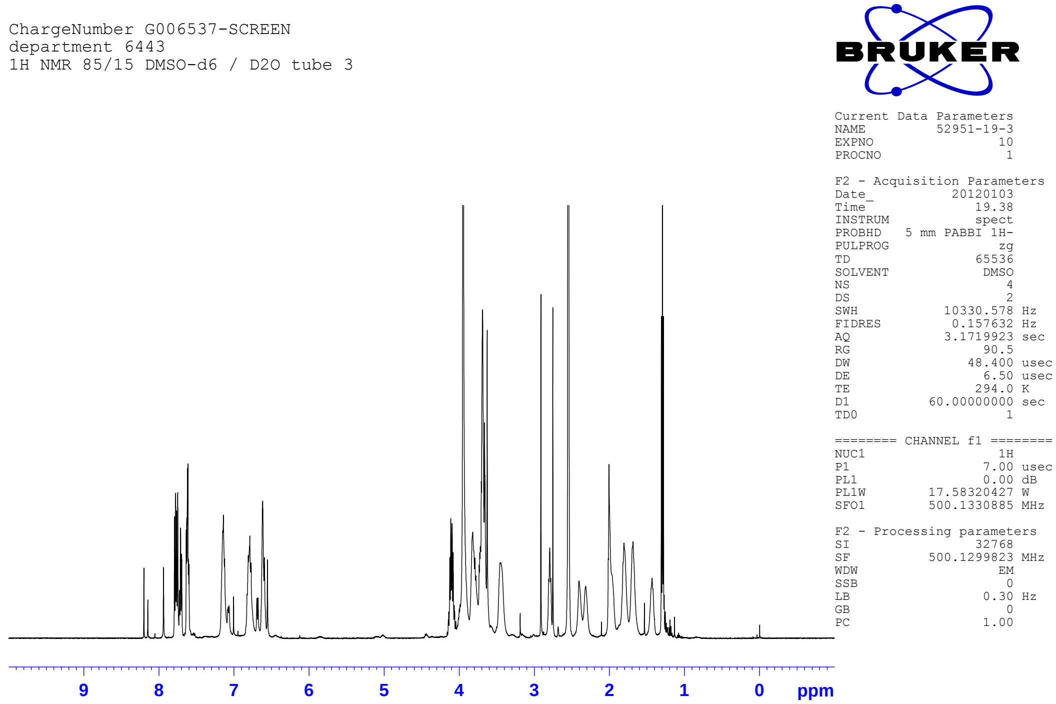

Figure B-37. ^{1}H NMR Tube 3: (10 mmol) EPP, (10 mmol) of 35

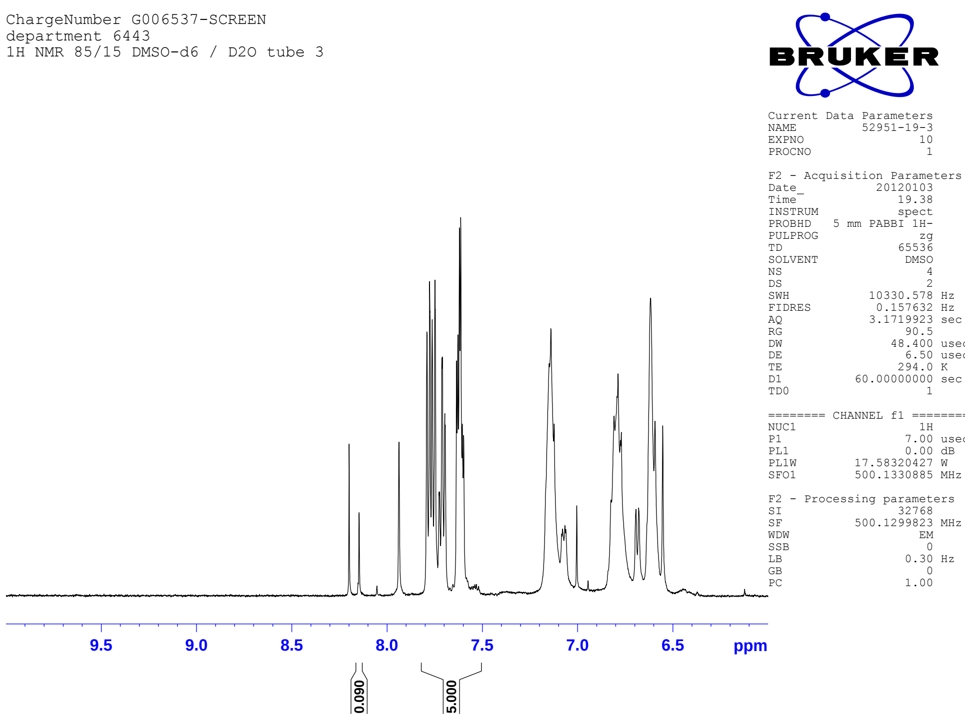

Figure B-38. Expanded View of ^{1}H NMR Tube 3: (10 mmol) EPP, (10 mmol) of 35

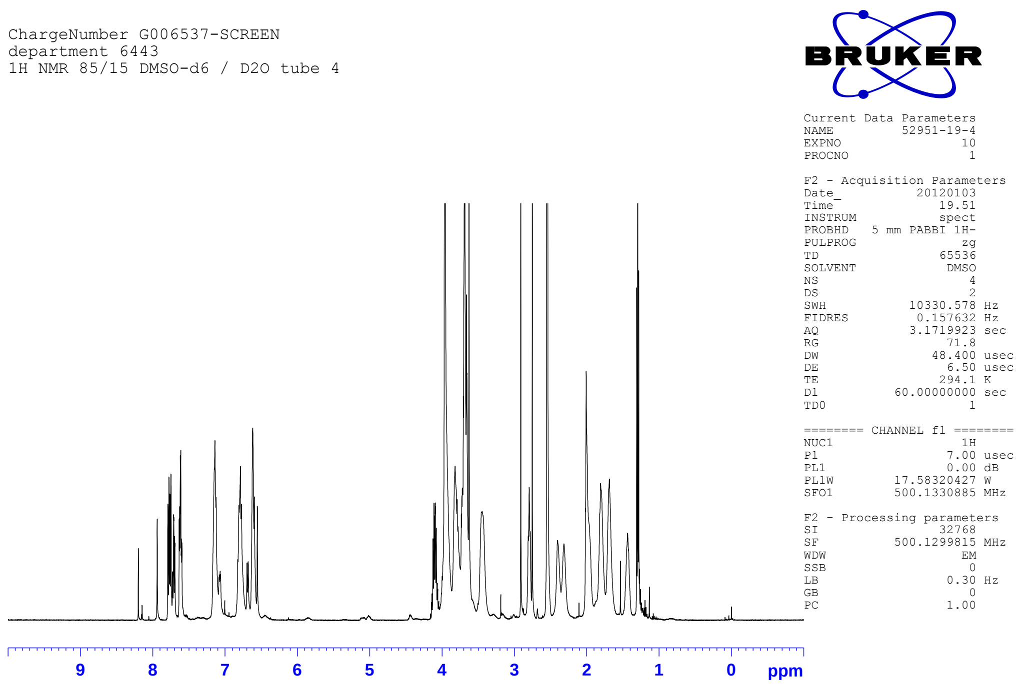

Figure B-39. ^{1}H NMR Tube 4: (10 mmol) EPP, (15 mmol) of 35

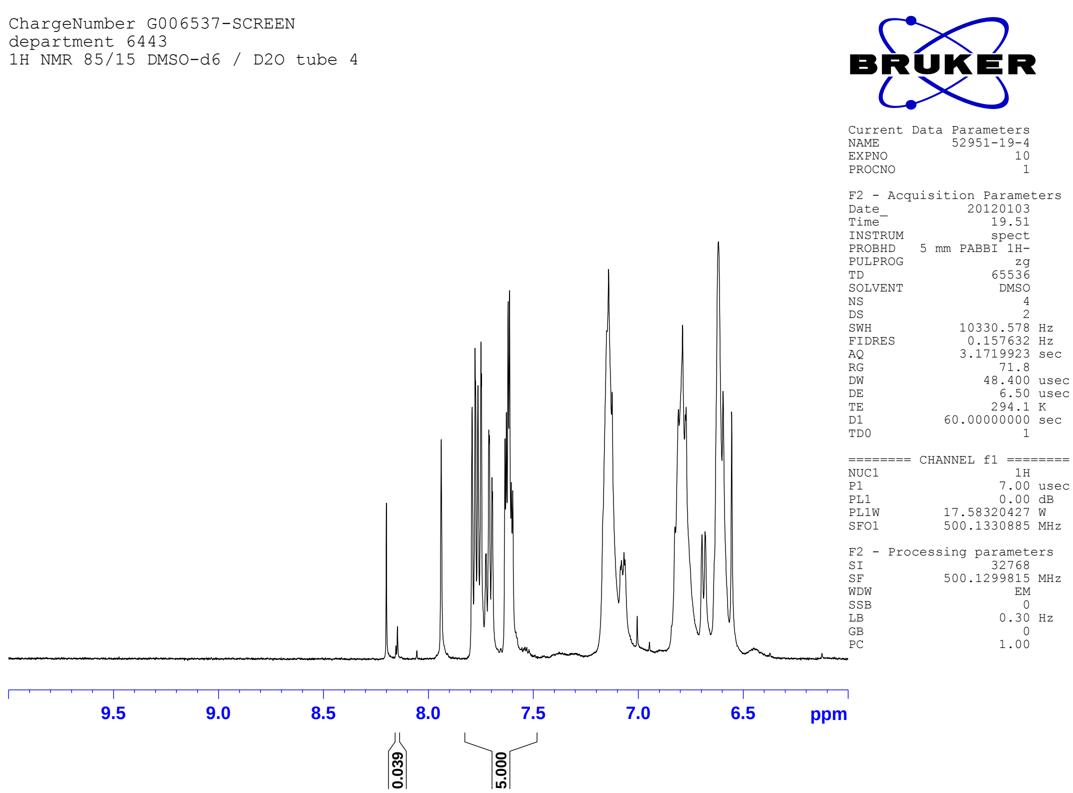

Figure B-40. Expanded View of ^{1}H NMR Tube 4: (10 mmol) EPP, (15 mmol) of 35

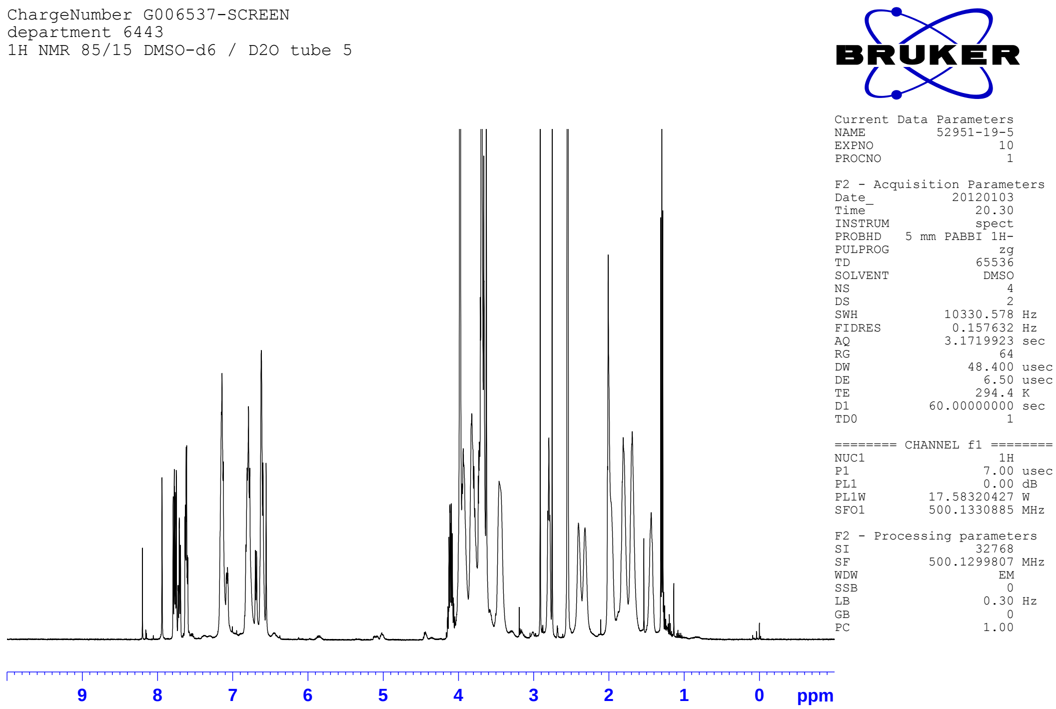

Figure B-41. ^{1}H NMR Tube 5: (10 mmol) EPP, (20 mmol) of 35

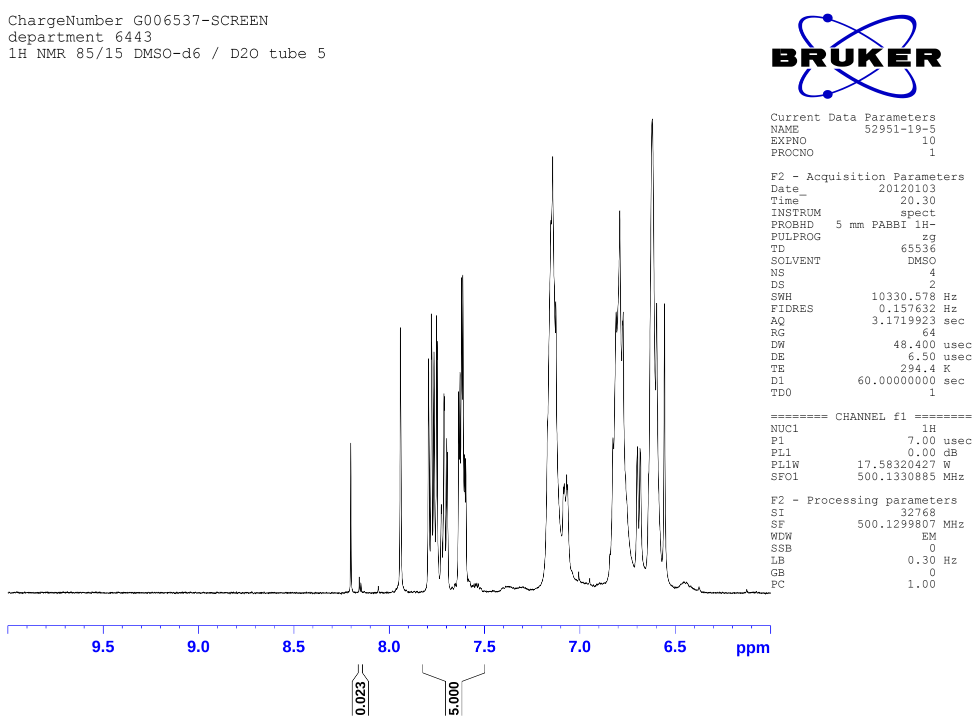

Figure B-42. Expanded View of ^{1}H NMR Tube 5: (10 mmol) EPP, (20 mmol) of 35

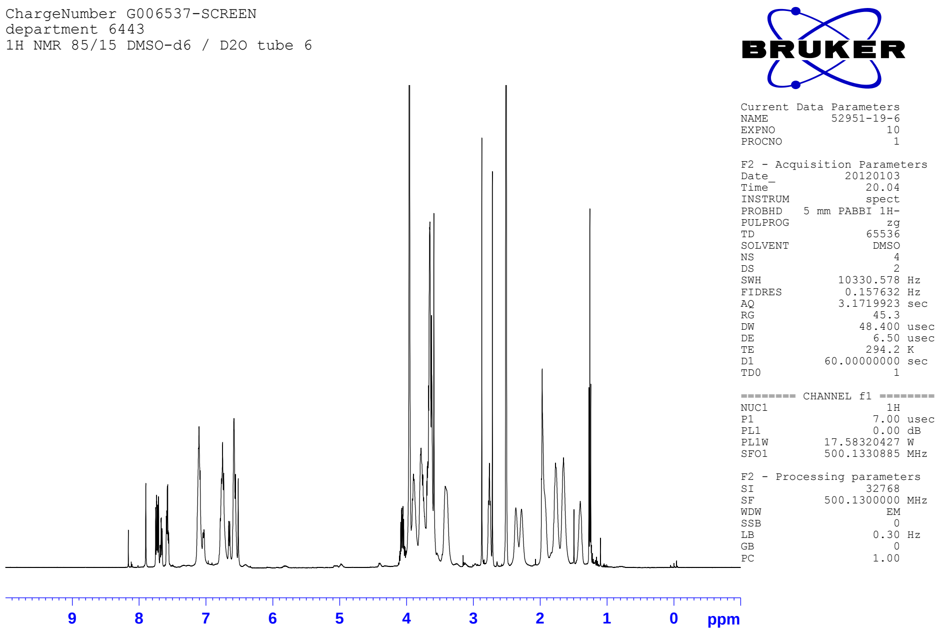

Figure B-43. [1]H NMR Tube 6: (10 mmol) EPP, (25 mmol) of 35

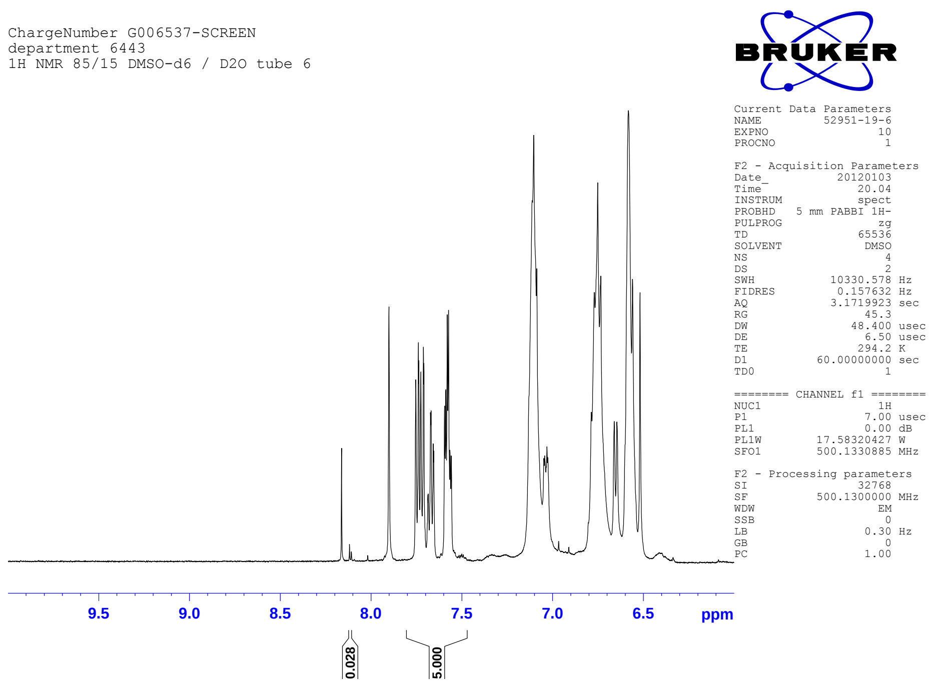

Figure B-44. Expanded View of [1]H NMR Tube 6: (10 mmol) EPP, (25 mmol) of 35

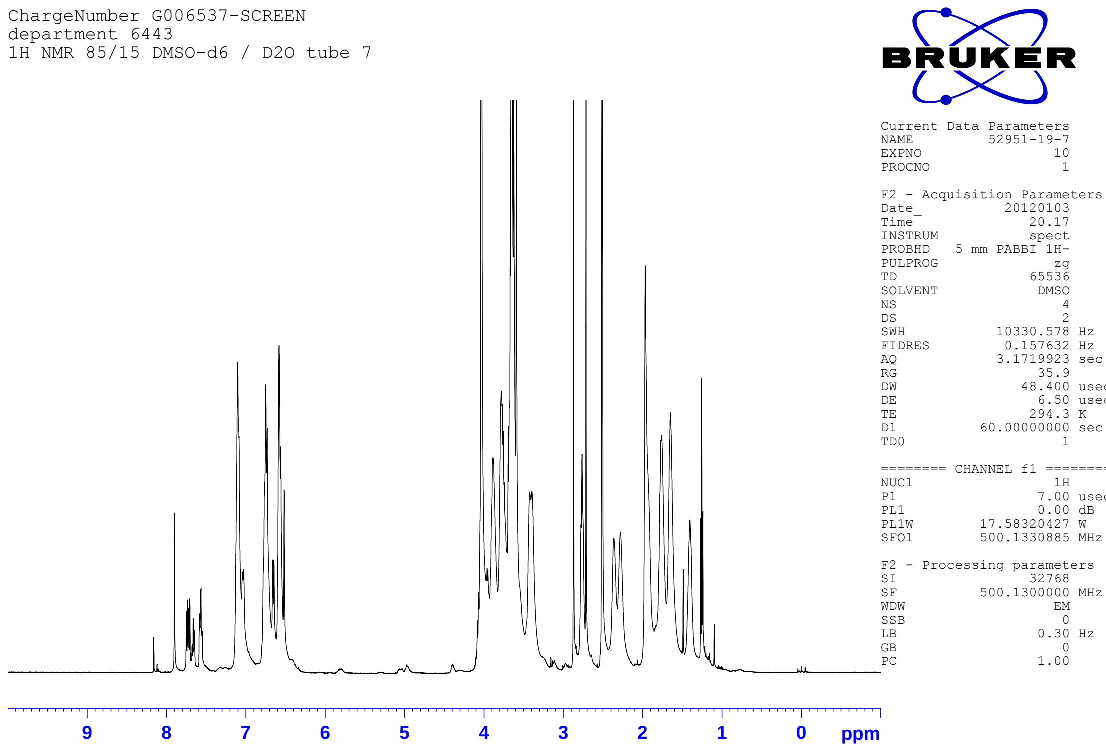

Figure B-45. [1]H NMR Tube 7: (10 mmol) EPP, (50 mmol) of 35

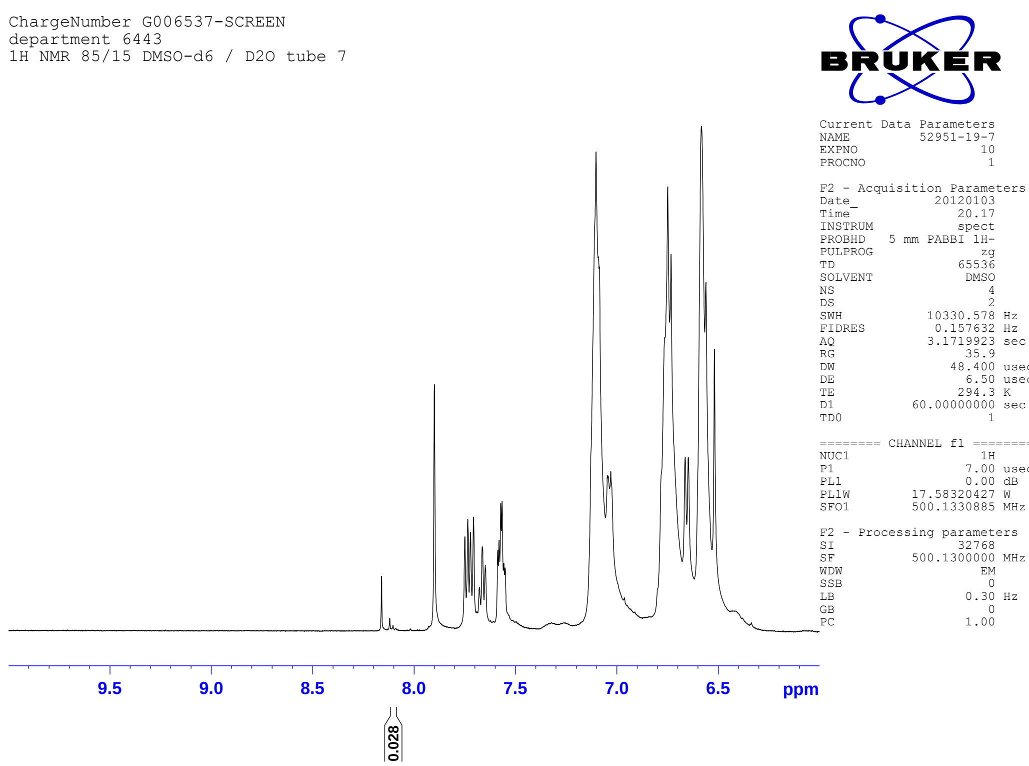

Figure B-46. Expanded View of [1]H NMR Tube 7: (10 mmol) EPP, (50 mmol) of 35

```
Nonlinear regression model
  model:  Y ~ (P1 * P2 * X)/(1 + P1 * X)
   data:  parent.frame()
      P1       P2
249.9242   0.4699
 residual sum-of-squares: 0.003317

Number of iterations to convergence: 8
Achieved convergence tolerance: 1.510e-06
```

*P1=K_a, P2= (Δ Area)$_{Max}$, Y=(Δ Area), X=[Cyclophane 35]

Figure B-47. Non-Linear Least Squares Analysis

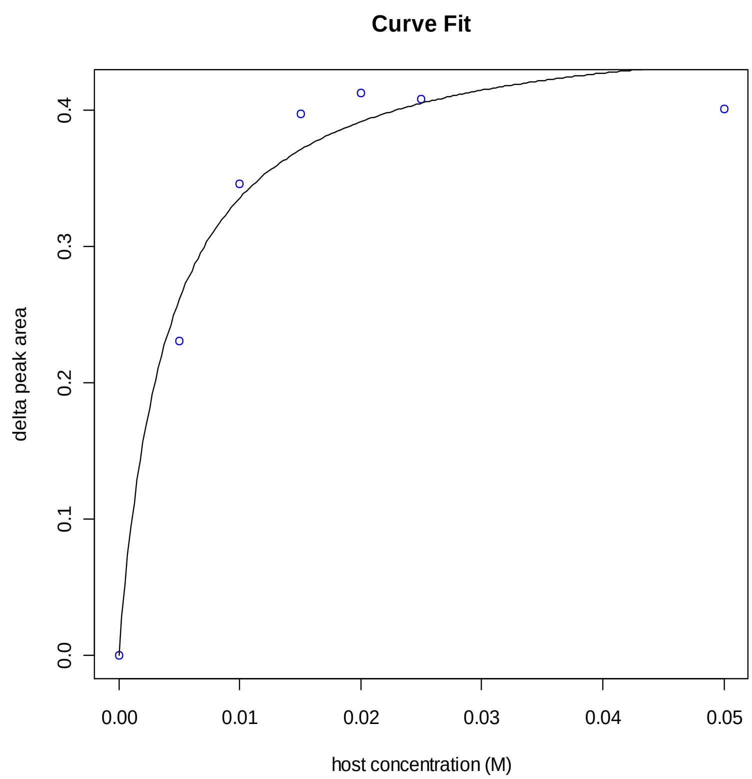

Figure B-48. Binding Curve for Cyclophane 35 and EPP at 85/15 DMSO-d_6 / D_2O

Binding Study using 80% DMSO-d_6 / 20% D_2O

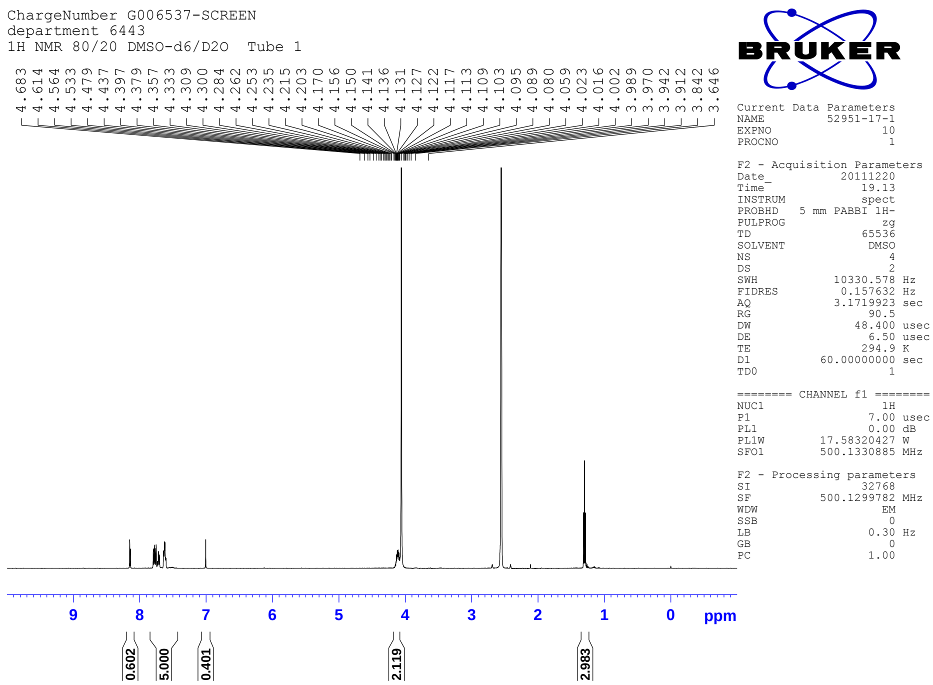

Figure B-49. ^{1}H NMR Tube 1: (10 mmol) EPP, (0 mmol) of 35

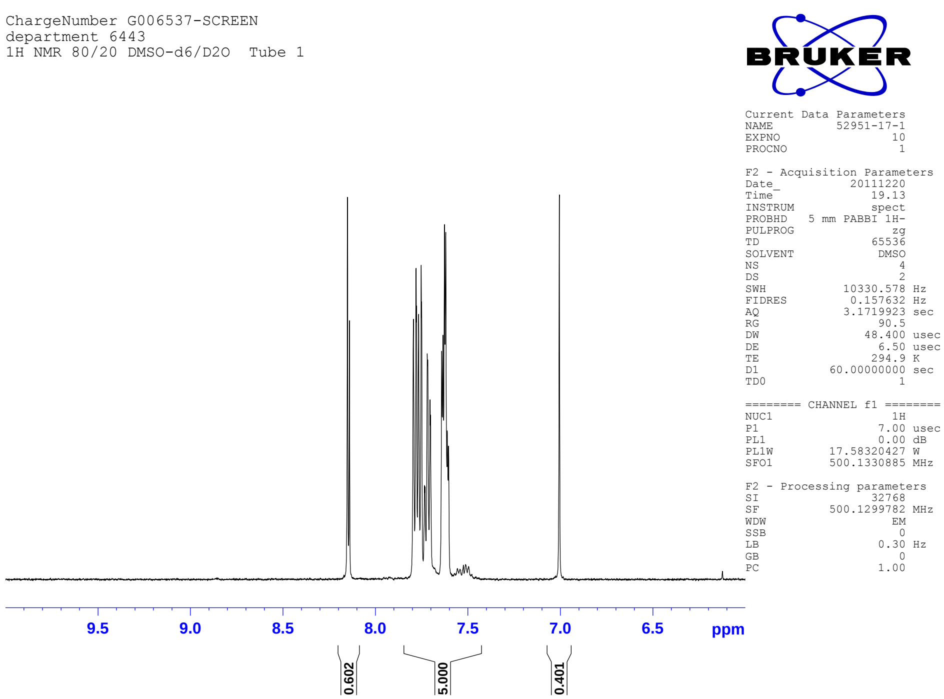

Figure B-50. Expanded View of ^{1}H NMR Tube 1: (10 mmol) EPP, (0 mmol) of 35

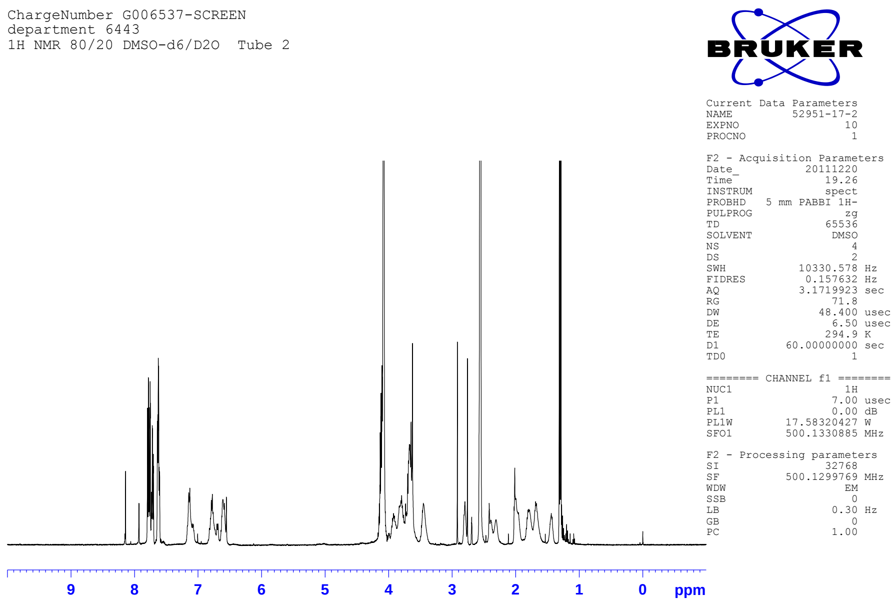

Figure B-51. ^{1}H NMR Tube 2: (10 mmol) EPP, (5 mmol) of 35

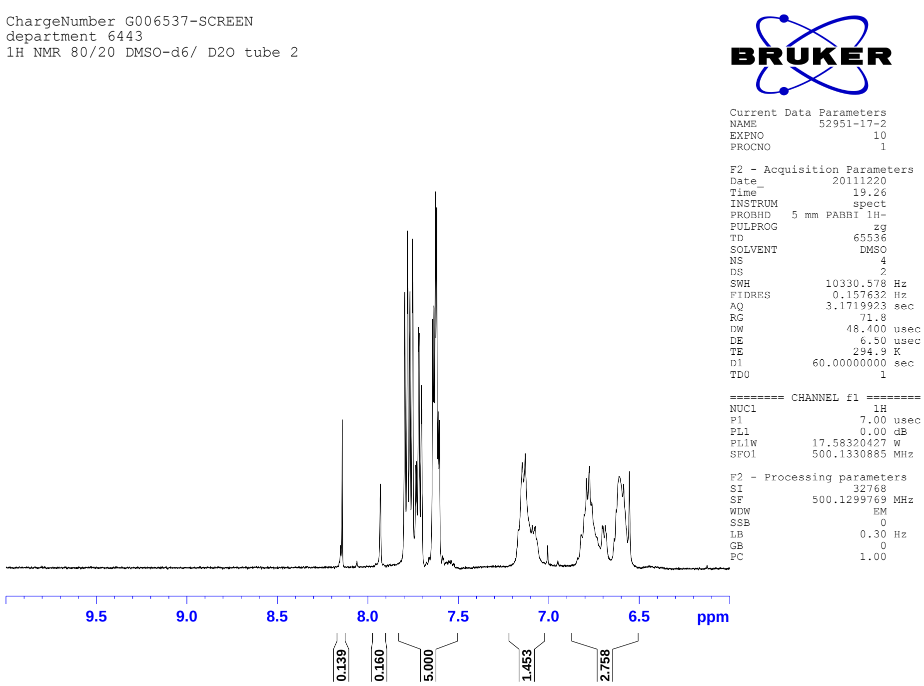

Figure B-52. Expanded View of ^{1}H NMR Tube 2: (10 mmol) EPP, (5 mmol) of 35

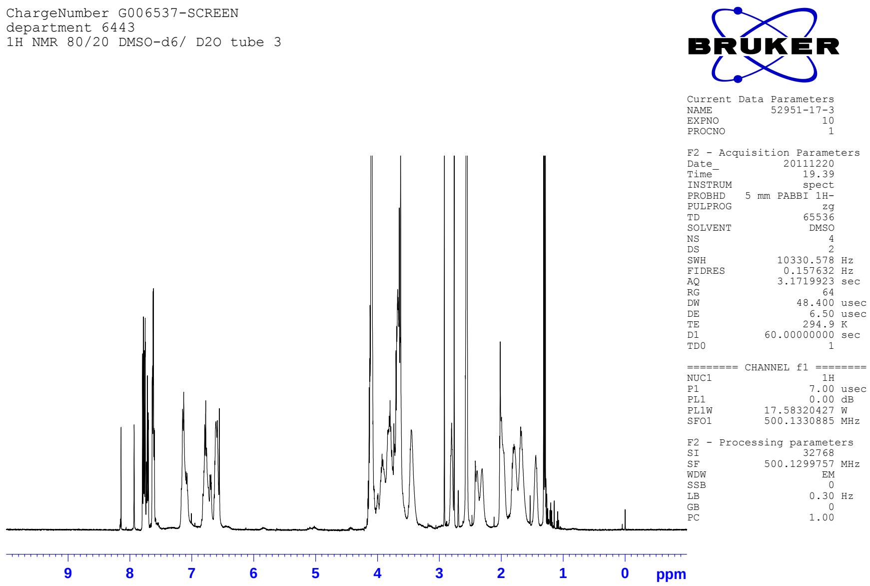

Figure B-53. ^{1}H NMR Tube 3: (10 mmol) EPP, (10 mmol) of 35

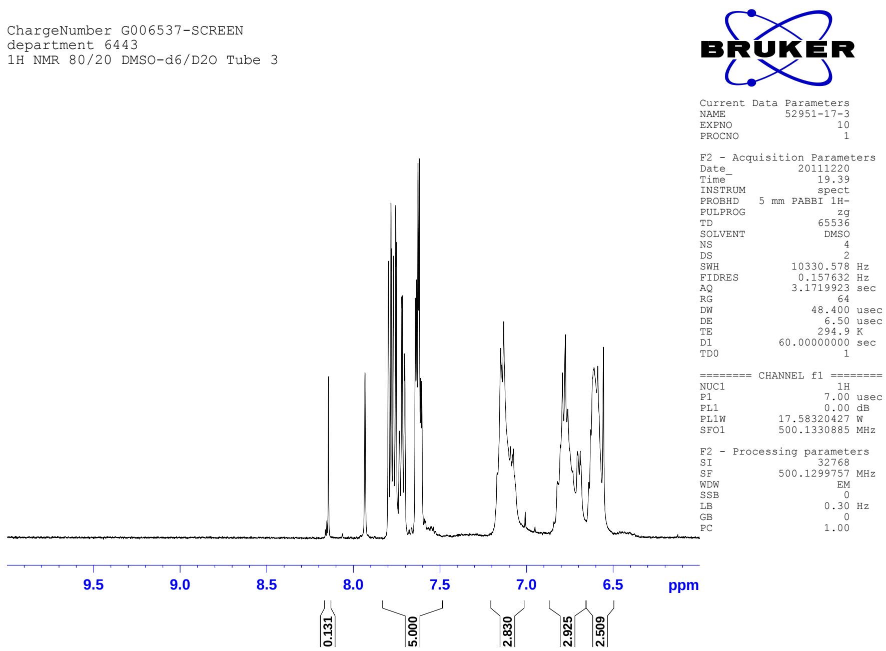

Figure B-54. Expanded View of ^{1}H NMR Tube 3: (10 mmol) EPP, (10 mmol) of 35

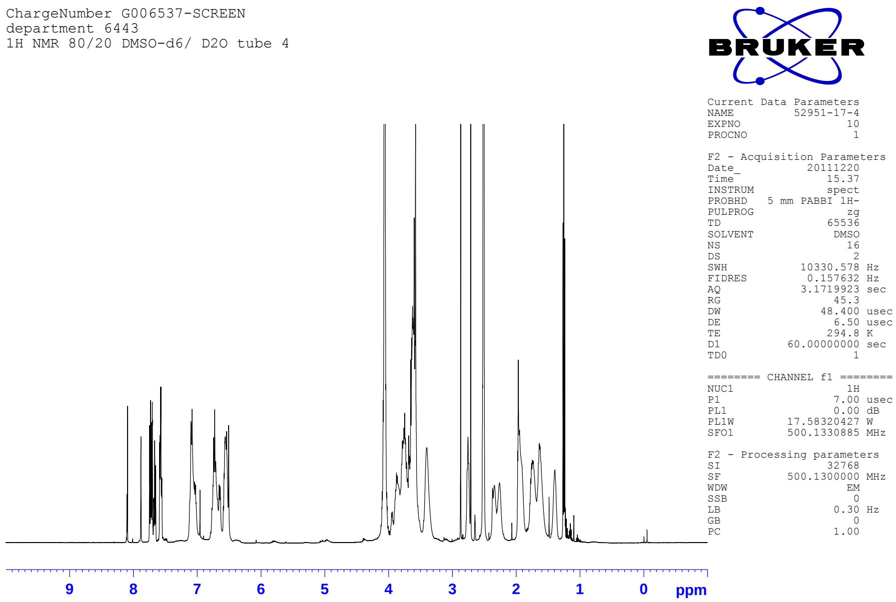

Figure B-55. ^{1}H NMR Tube 4: (10 mmol) EPP, (15 mmol) of 35

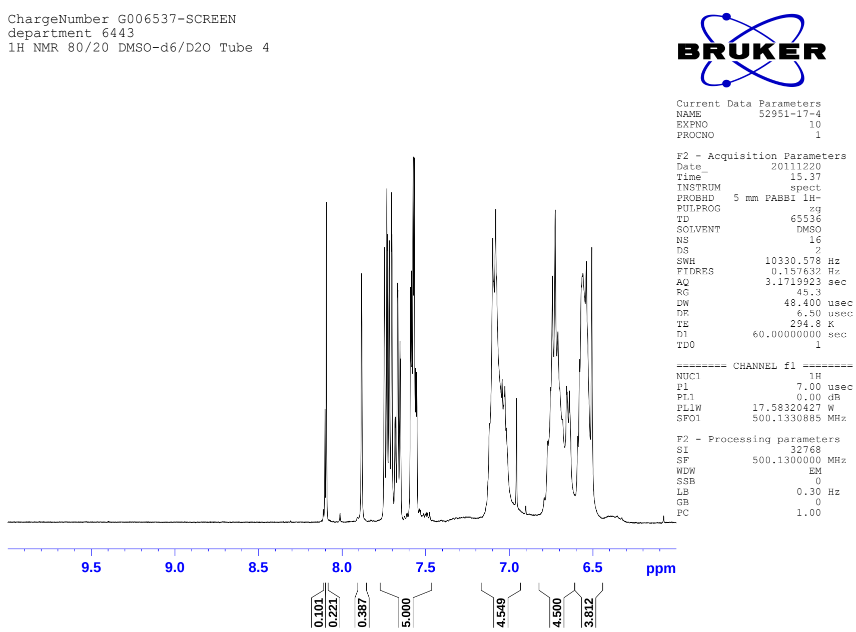

Figure B-56. Expanded View of ^{1}H NMR Tube 4: (10 mmol) EPP, (15 mmol) of 35

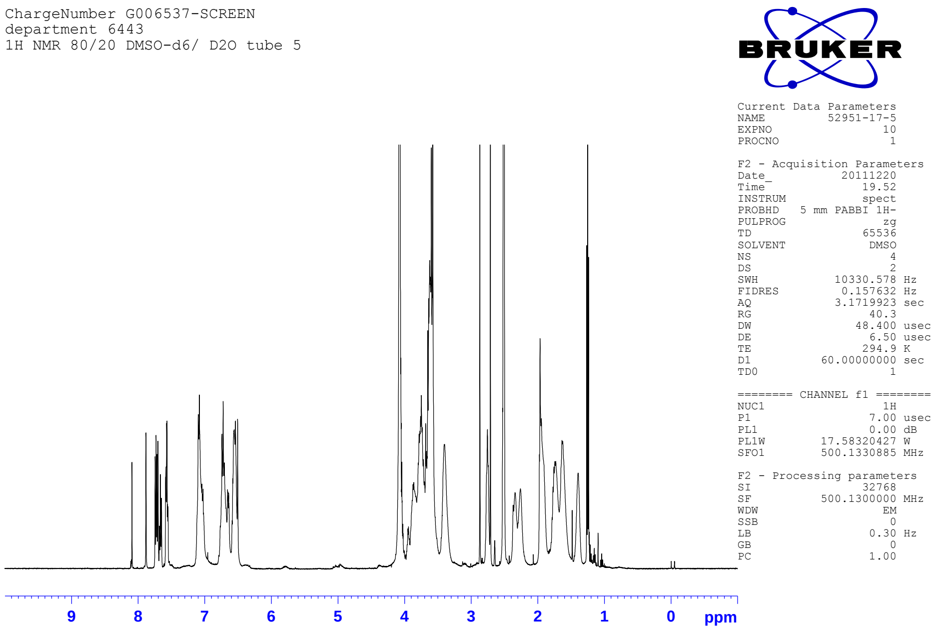

Figure B-57. ¹H NMR Tube 5: (10 mmol) EPP, (20 mmol) of 35

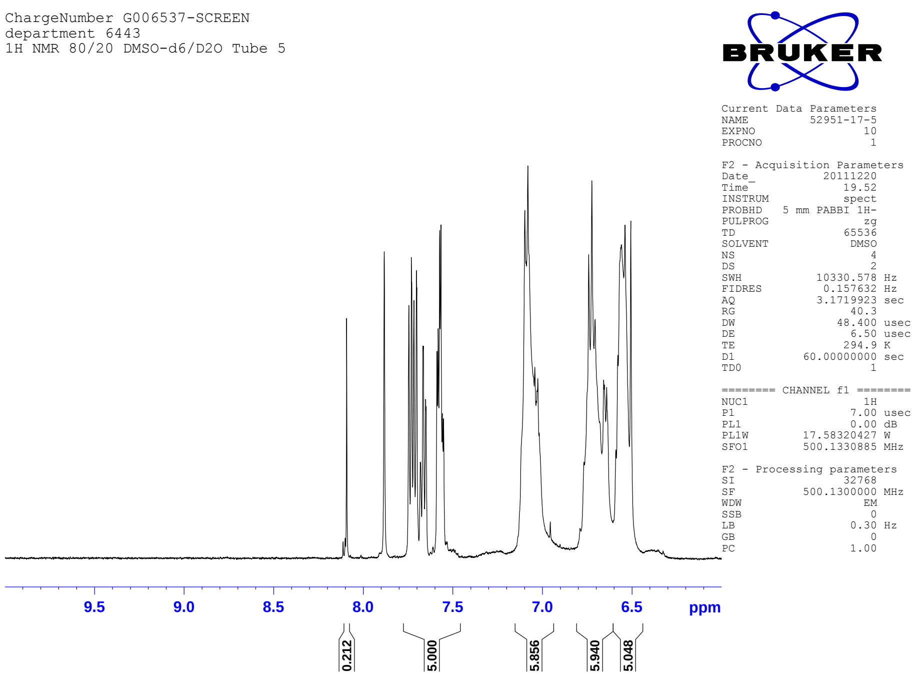

Figure B-58. Expanded View of ¹H NMR Tube 5: (10 mmol) EPP, (20 mmol) of 35

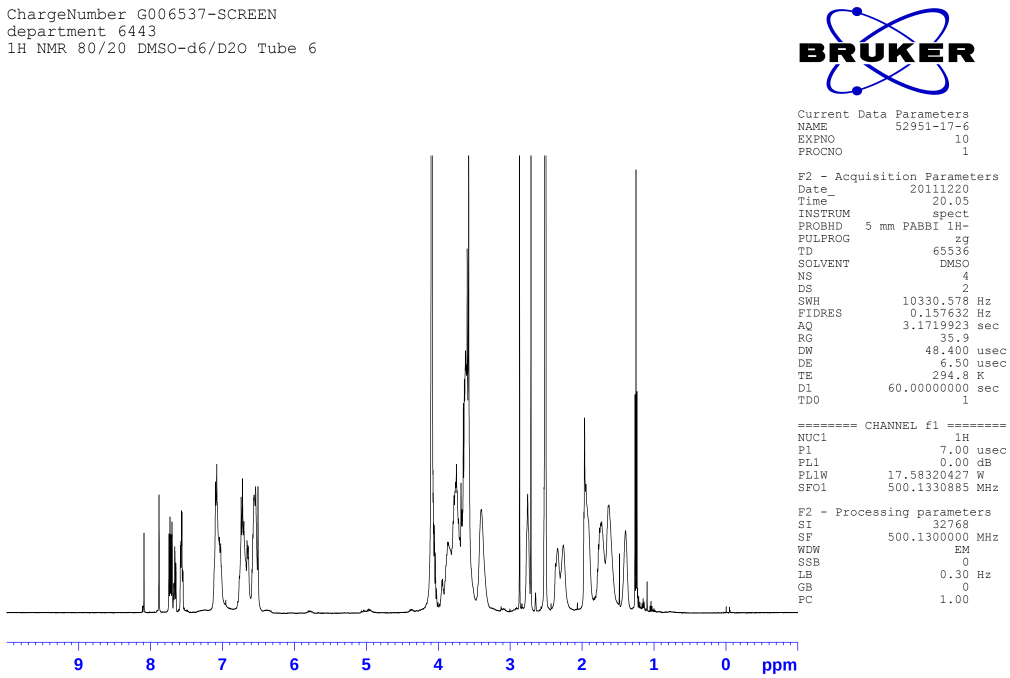

Figure B-59. ^{1}H NMR Tube 6: (10 mmol) EPP, (25 mmol) of 35

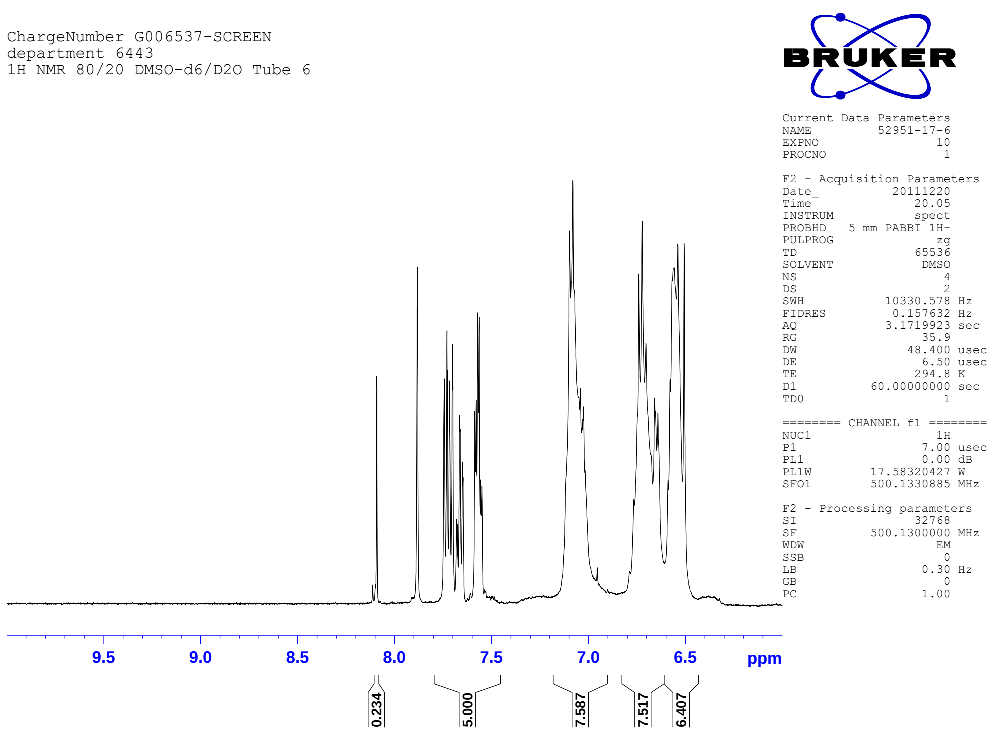

Figure B-60. Expanded View of ^{1}H NMR Tube 6: (10 mmol) EPP, (25 mmol) of 35

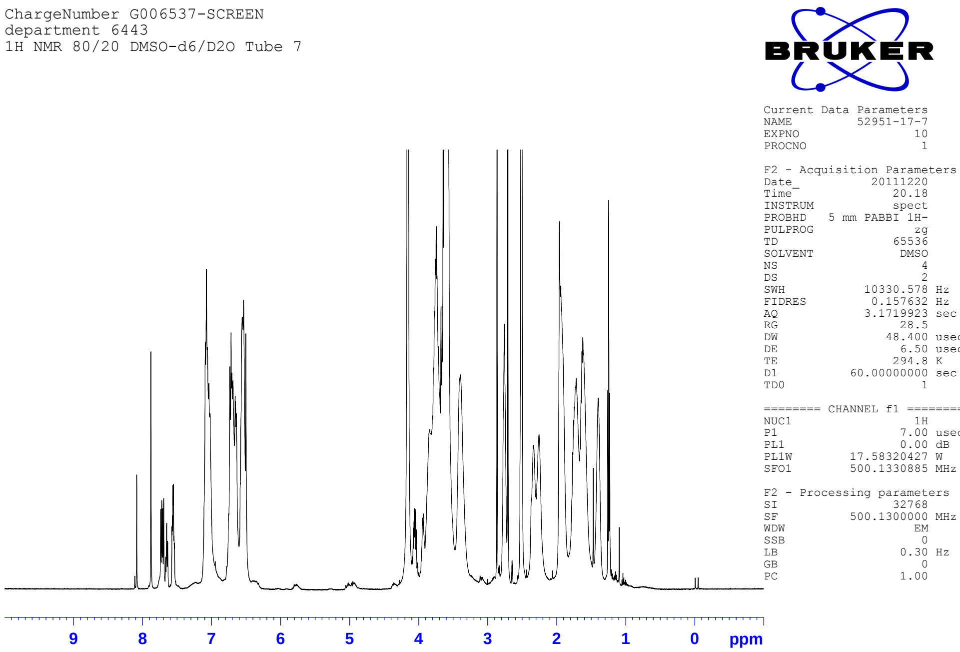

Figure B-61. ^{1}H NMR Tube 7: (10 mmol) EPP, (50 mmol) of 35

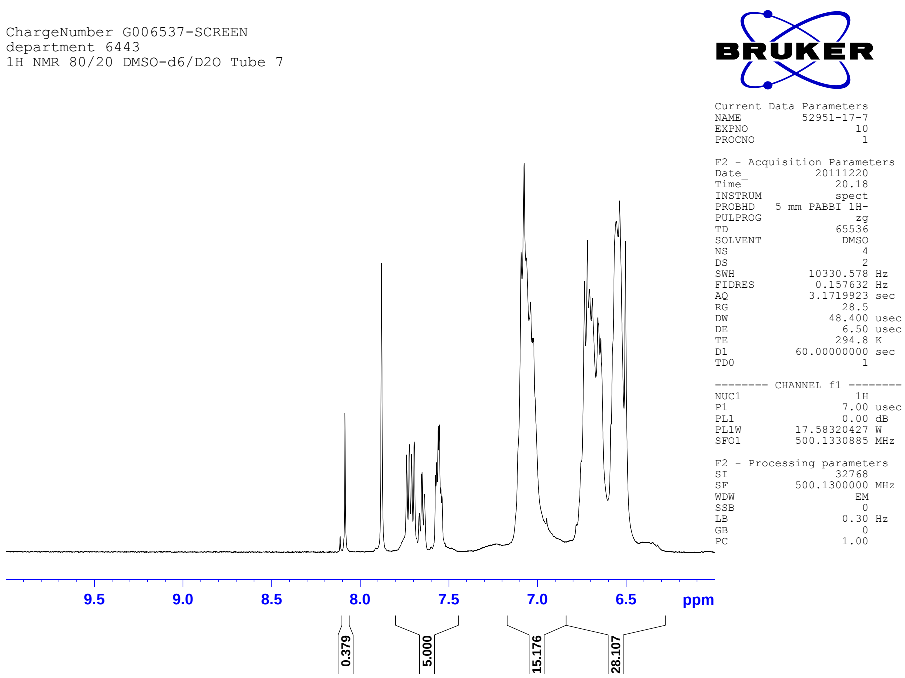

Figure B-62. Expanded View of ^{1}H NMR Tube 7: (10 mmol) EPP, (50 mmol) of 35

```
Nonlinear regression model
  model:  Y ~ P1 * P2 * X/(1 + P1 * X)
   data:  parent.frame()
     P1       P2
223.6086   0.4193
 residual sum-of-squares: 0.001997
Number of iterations to convergence: 7
Achieved convergence tolerance: 5.314e-06
```

*P1=K_a, P2= $(\Delta \text{ Area})_{Max}$, Y=(Δ Area), X=[Cyclophane 35]

Figure B-63. Non-Linear Least Squares Analysis

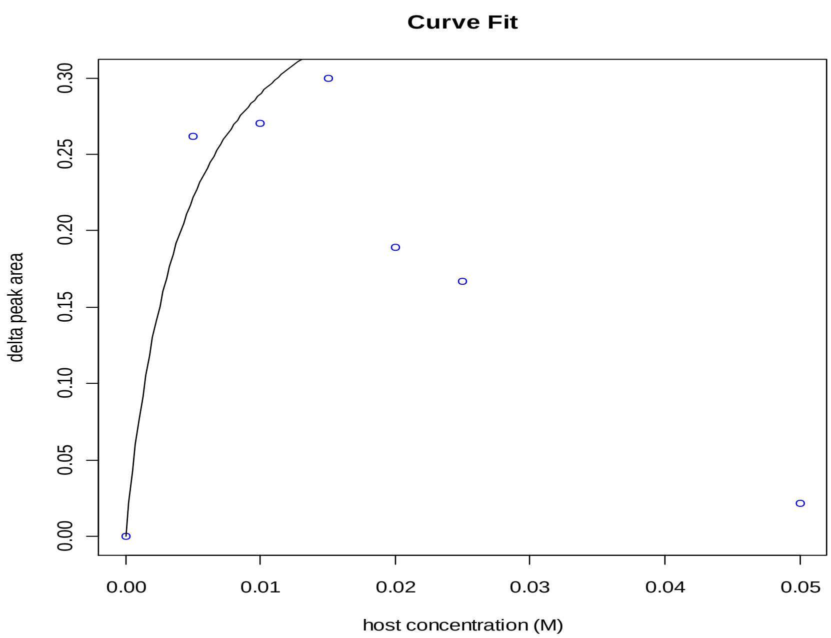

Figure B-64. Binding Curve for Cyclophane 35 and EPP at 80/20 DMSO-d_6 / D_2O

Appendix C: Alternative Synthetic Approach Outlines

May 6, 2010

Dr. Glenn E. Lawson

Science and Technology Manager
Hazard Mitigation DTRA-CBT
8725 John J. Kingman Rd
Fort Belvoir, VA 22060-6201

Dear Glenn:

Contract No. HDTRA1-10-C-0010
Alternative Syntheses for Rotaxane Reagent Tether

Enclosed is an alternative path for the fluorescent tether that we would like to pursue, instead of the one originally proposed. Don and his synthesis team have uncovered a preparation based in the literature which could provide us with a better source of starting material.

Please notify us of your concurrence of this alternative path. If you have any questions, please contact me at (614) 424-4113 or shawj@battelle.org .

Respectfully submitted,

John R. Shaw, Ph.D.
Project Manager
Battelle Memorial Institute

Enclosure

Alternative Syntheses for Rotaxane Reagent Tether
Donald W. Zehnder, II, Ph.D.; John R. Shaw, Ph.D
Battelle Memorial Institute

One of the items of concern in the synthetic route to a rotaxane chemical sensor for V- and G-agents is the availability and expense of the starting material, (5-bromomethyl)fluorescein required in Task 1: Synthesis of the Fluorescent Tether. The material may be purchased for \$976 for 50 mg (special order) as noted by Aldrich. There are no other suppliers that we have found. Another synthetic route has been identified, that could provide a better source of starting material. The following preparation is based in the literature and is amenable to scale up at significantly lower cost. This proposed route will be conducted within the existing budget.

The synthesis route in Figure A1 prepares a mixture of dibrominated fluorescein isomers (only 1 isomer shown). As stated during the post-award meeting, the use of isomerically pure fluorescein is not necessary. This may then be converted to the corresponding aldehyde derivative, as shown in step 3.

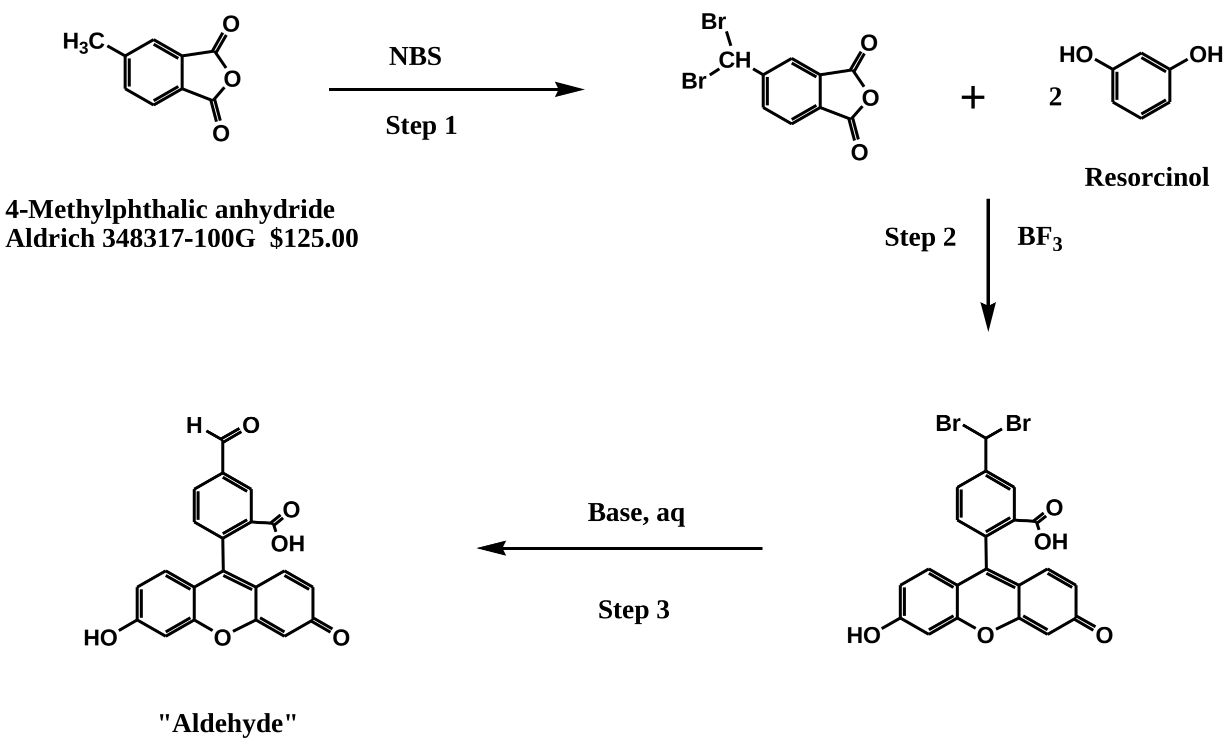

Figure A1. Proposed Route to Aldehydic Fluorescein.

The aldehyde will be used in the synthetic pathway shown in Figure A2. This path is preferable due to the reduced cost of obtaining the 6-Aminocaproic acid (\$59.40 for 100g, Aldrich) over

adipic aldehyde which is synthesized from 5- hexenoic acid ($138 for 5 g, Aldrich). This preparation decreases the number of overall steps by three over the original route proposed to make the fluorescent tether.

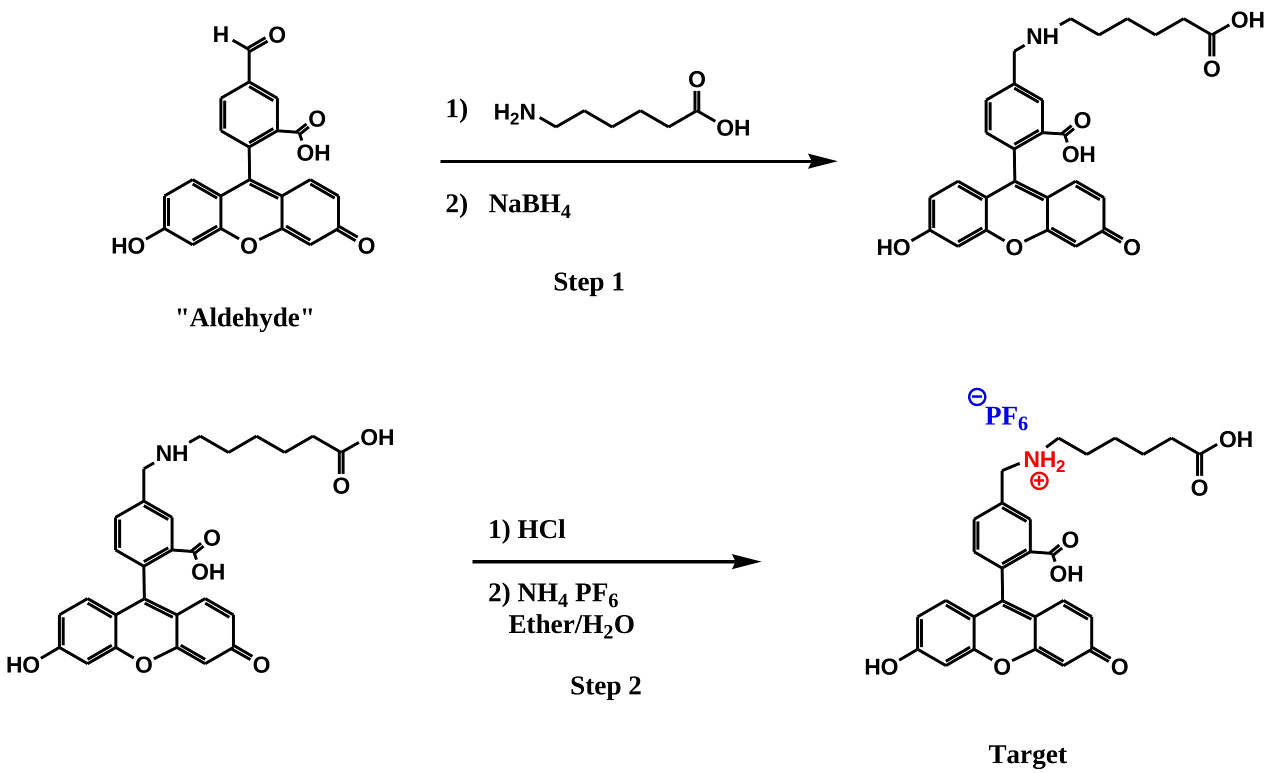

Figure A2. Proposed synthesis path to Fluorescent Tether using the Aldehyde Intermediate.

In summary, Battelle proposes following the synthetic steps outlined in this document to create the fluorescent tether molecule. This includes creating the aldehyde-containing fluorescein intermediate in route to completing the fluorescent tether. Performing these steps will not adversely impact the schedule or budget of this task.

References:

U.S. 3,711,473 (16 Jan. 1973) by Doebel et al.

McKenna, James F.; Sowa, Frank J. "Organic Reactions with Boron Fluoride. XVII." *J. Am. Chem. Soc.* **1938,** *60*, 124-125

Francis, John E.; et al." Pyridazino[3,4,5-de]phthalazines. I. Synthesis of the Heterocyclic System and Key Intermediates," *Can. J. Chem.* **1979**, *57*, 3320-3331.

Summary of Action Items from Battelle IPR: Mitigation Plan for Tether Synthesis.

9 August 2011
HDTRA1-10-C-0010

An interim project review (IPR) meeting was held on 8 August at Battelle to discuss technical progress on the synthesis work in HDTRA1-10-C-0010. A key milestone in the completion of the synthesis of the rotaxane receptor molecule is the successful synthesis of the "tether" linkage which provides the backbone of the rotaxane. The tether links the binding pocket to the indicator and provides a continuous path for rotaxane wheel to travel.

As discussed during the IPR, the current synthetic path (Scheme I) to the tether resulted in the desired product; however, the reaction sequence appears to be producing impurities that inhibit reaction efficiency. In order to address this issue, mitigation steps will be taken to prepare cleaner product for subsequent use in the rotaxane threading reaction. To assess the validity of the results, the first reaction will be repeated, but followed by a work-up in water to assist in removing the DMSO impurities that are formed as a result of the ozonolysis reaction of 5-hexenoic acid in the presence of dimethyl sulfide (DMS) to form compound **17** (Scheme I).

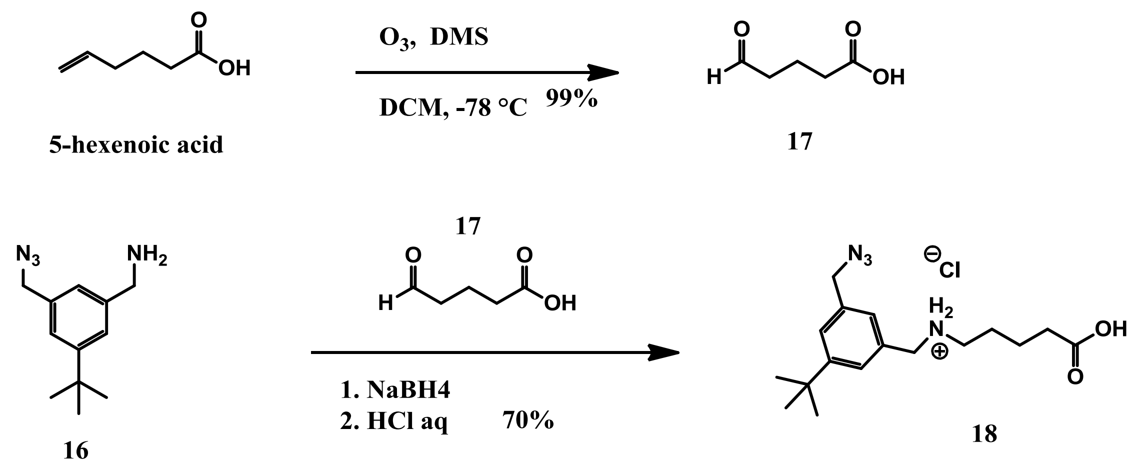

Scheme I. Proposed Reaction Scheme for Synthesizing the Tether (18) via Ozonolysis of 5-hexenoic acid.

Mitigation Plan B

The initial mitigation plan is to modify the ozonolysis reaction conditions using Pd/C and H_2, then H_2O work-up at room temperature, as described in the modified scheme below (Mayr,et al. 1994).

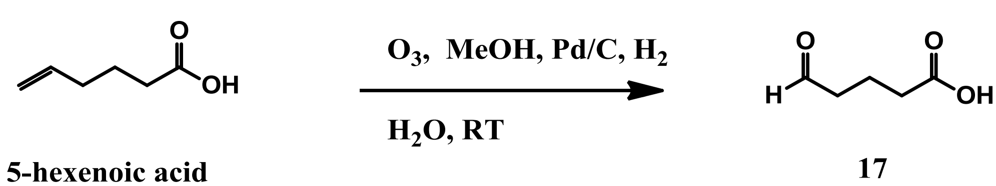

Scheme II. Modified Tether Reaction using Pd/C with Hydrogen in the Ozonolysis Step.

It is possible that this approach will produce mixtures of methyl esters rather than the desired acid aldehyde. If that is the case, another attempt will be made using metallic Zn as the catalyst in the presence of acetic acid to produce the acid aldehyde **17** (Mayr,et al. 1994). This approach has been used to specifically produce aldehydes from alkenes. Either route to producing compound **17** will avoid the presence of DMSO in the product, which may have been inhibiting subsequent reactions.

The product yield at the conclusion of the reaction sequence will indicate the effectiveness of the route. Further, a test rotaxane reaction using compound **18** will be performed and monitored using ^{1}H NMR to assess the effectiveness of the compound in the rotaxane threading reaction. The length of time to evaluate this approach is not expected to last beyond two weeks from the start of the synthesis. Further, the ending product of this tether approach could still be used to attach the indicator.

Mitigation Plan C

If the approaches in Plan B do not significantly improve the purity of the tether compound, then the alternative approach shown in Scheme III will taken. We will call this mitigation plan C. This reaction sequence has been published (Dvornikovs, et al, 2003) and has proven to be a useful tool in the construction of rotaxanes. The drawback with this approach is that the synthesis strategy incorporates the blocking group (3,5-tert-butylxylene) onto the tether. This precludes the ability to add the indicator as the terminal blocking group, so the use of this tether would require a different analytical approach (likely ^{1}H NMR) to determine the binding efficiency of the final Host[2]rotaxane with chemical agents. The length of time required to implement this synthetic approach would be approximately two weeks.

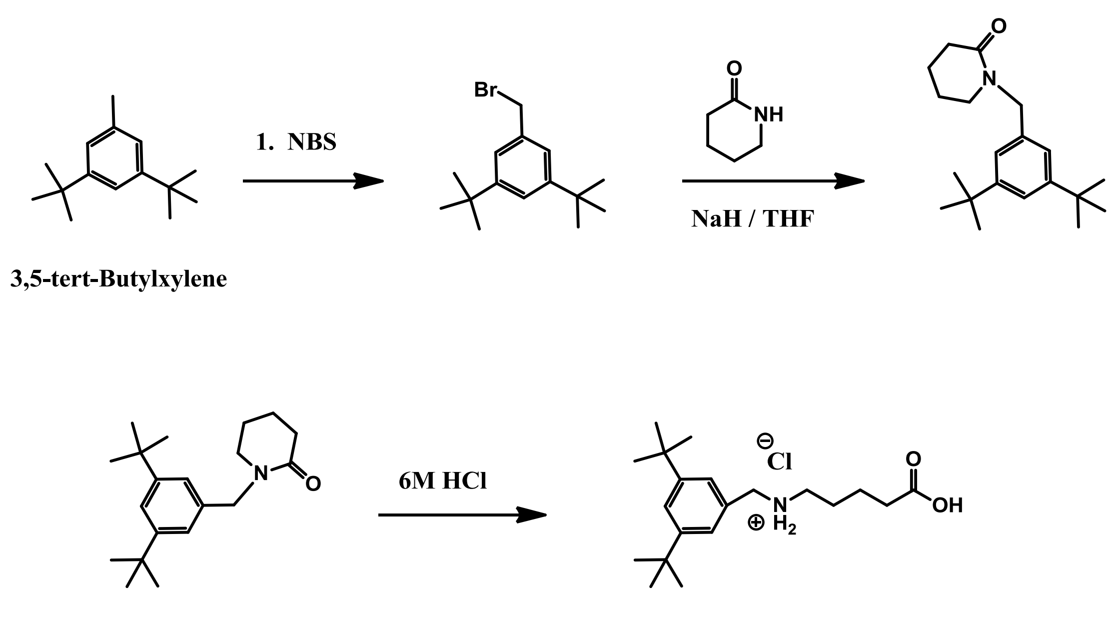

Scheme III. Synthesis of Tether Using Approach of Dvornikovs, et al (2003).

Mitigation Plan D

In the event that Mitigation Plan C does not provide a viable rotaxane product for further studies, a final plan to evaluate the binding efficiency of the binding pocket will be implemented. The synthesis of the binding pocket has been completed. The general approach will be to study the ability of the pocket (shown in Figure 1) to bind a G-agent simulant and selected G and/or V agents.

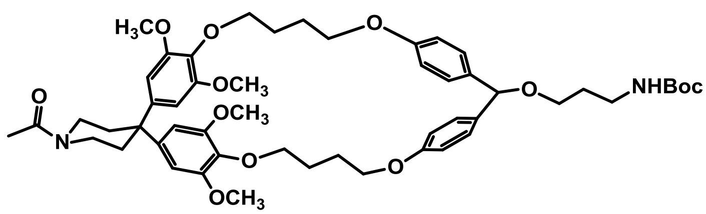

Figure 1. Chemical Structure of Binding Pocket

Studies will involve using simulant/agent at various levels of dilution to estimate the binding constant of the compound in solution. The binding studies will be performed using ^{1}H NMR.

References:

Dvornikovs, V., House, B., Kaetzel, M., Dedman, J., Smithrud, D., *J. Am. Chem. Soc.*, **2003**, 125 (27), 8290-8301.

Mayr, H., Baran, J., Will, E., Yamakoshi, H., Teshima, K., and Nojima, M., Journal of Organic Chemistry, **1994**, 59 (17), 5055-5058.

Appendix D: Experimental and Spectral Data for Task 1: Tether Development

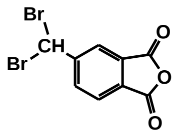

1

(1): 4-Methylphthalic anhydride (5 g, 30.8 mmol) was mixed with 2.05 eq. of N-bromosuccinimide (NBS) (11.25 g, 63.2 mmol) and benzoyl peroxide (373 mg. 1.54 mmol) in carbon tetrachloride (75 ml) under a nitrogen atmosphere. The solution and turned bright red as it was heated to reflux. After heating for 14 hours, the solution was cooled to ambient temperature. The white precipitates were removed by filtration through a medium porosity frit then the mixture was concentrated to dryness. ^{1}H NMR analysis showed a statistical mixture of mono, di, and tri-brominated material (Figure D1). TLC analysis showed the material was very difficult to separate on silica. As a result the reaction was repeated as describe above with 3 eq of NBS (16.46 g, 92.5 mmol). Purification by column chromatography (Hexane:EtoAc 75:25, silica gel) afforded 2 grams of material. ^{1}H NMR analysis show the material was approximately a 50/50 mixture of **1** and the tri-addition side product Figure D2. Further purification was not performed.

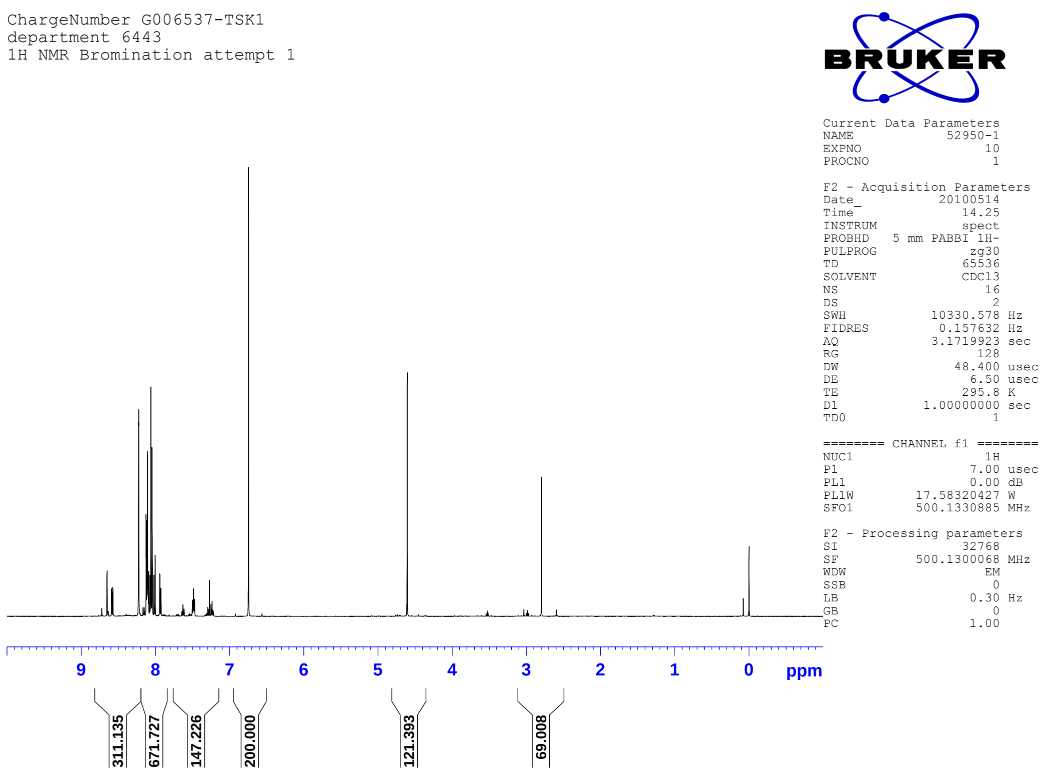

Figure D1. ^{1}H NMR in $CDCl_3$ of crude material from bromination attempt 1

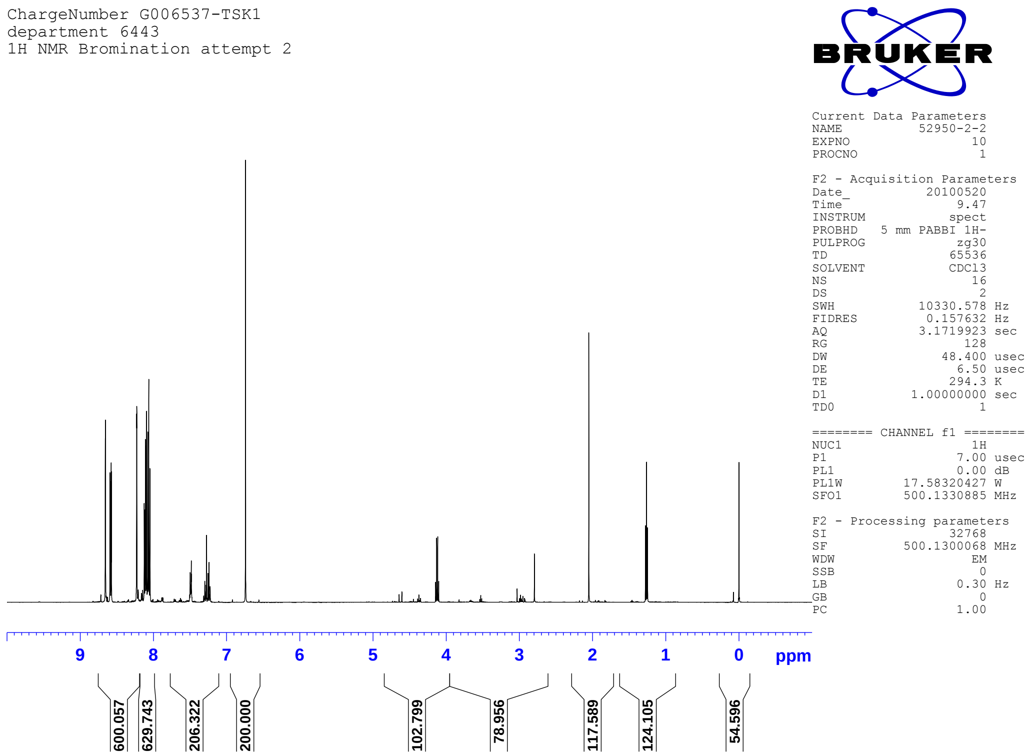

Figure D2. [1]H NMR in $CDCl_3$ of crude material from bromination attempt 2

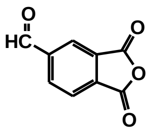

4

(4): The impure mixture of **1** (2 g, 6.25 mmol) was mixed with 5% aq. sodium carbonate (10 mL) then heated to 40 °C for 1 hour. The solution was acidified to pH 2 with aq. hydrochloric acid then extracted with $CHCl_3$ (2 X 25 mL). The combined extracts were dried with magnesium sulfate and concentrated to afford as white foam. [1]H NMR analysis showed conversion to the carboxylic acid derivative (Figure D3). There were no aldehyde signals in the 9-10.5 region.

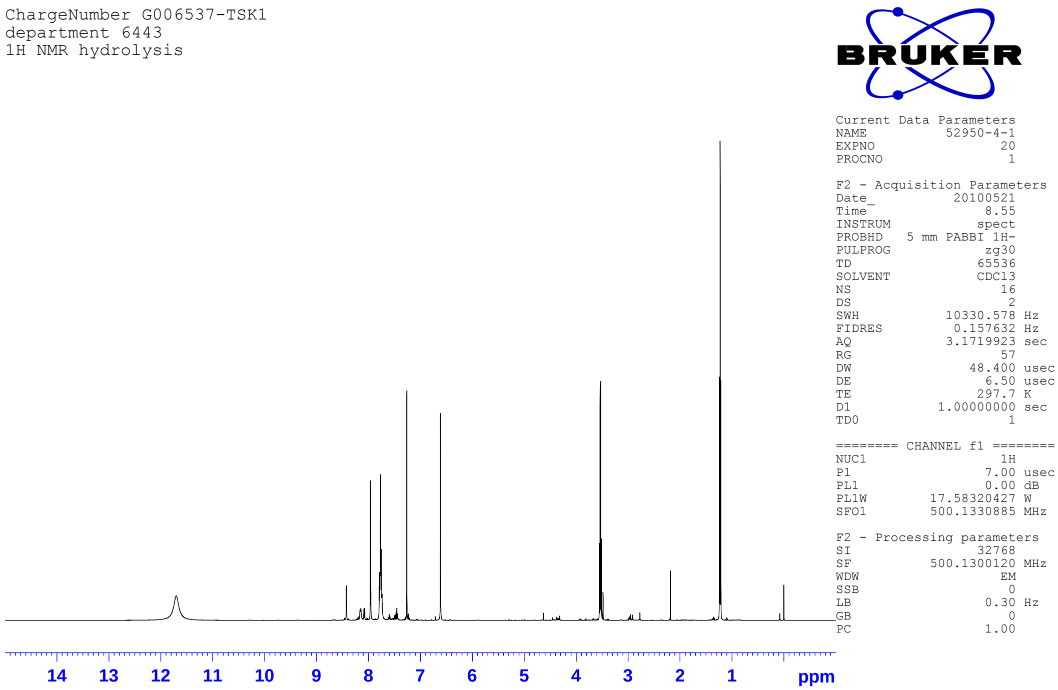

Figure D3. [1]H NMR in $CDCl_3$ of hydrolysis attempt *Note the lack of any aldehyde signal between 9 and 10.5

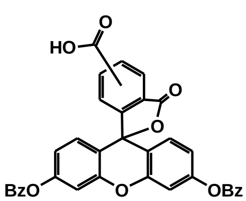

5

(5): A solution of 5,6-carboxyfluorescein (100 mg, 0.265 mmol) in anhydrous DMF was treated with sodium hydride (95% 19 mg, 0.795 mmol) and stirred under nitrogen for 10 minutes. Benzyl bromide (100 mg, 0.584 mmol, 2.2 eq.,) was added to the reaction then stirred at ambient temperature over night. TLC analysis showed one main product as well as staring material. Analysis by MS/ESI showed the product generated has an M/Z of 737 which is consistent with the addition of 4 benzyl groups (Figure D4). All attempts to repeat the protection reaction with weaker base triethylamine resulted in no reaction.

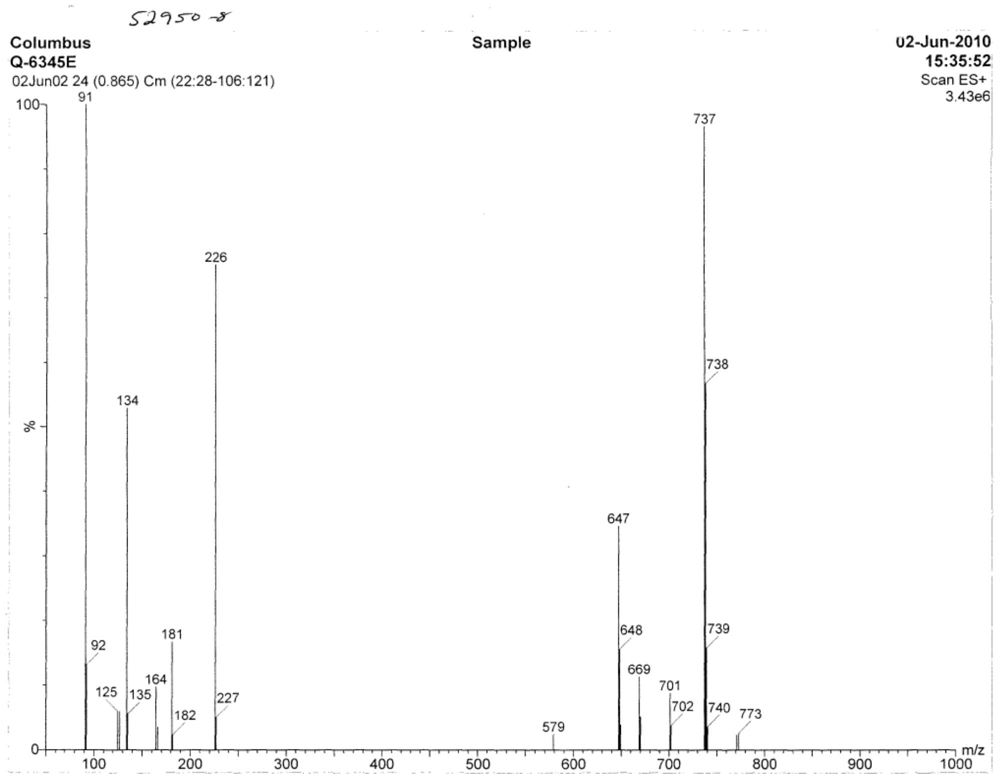

Figure D4. MS/ESI Spectrum of Compound **5**

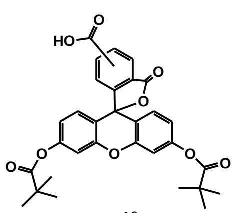

10

(10): A mixture of 5,6-carboxyfluorescein (14 g, 37.2 mmol), pivalic anhydride (14.5 g, 78.12 mmol) and diisopropylamine (19.23 g, 148.8 mmol) was stirred in anhydrous DMF for 72 hours at ambient temperature under a nitrogen atmosphere. Solvent was removed under reduced pressure to afford a light brown crude oil. The oil was dissolved in DCM (100 mL) then further diluted with ethyl acetate (400 ml). The organics were extracted with sodium phosphate buffer pH7 (400 mL) followed by a second extraction with sat sodium chloride. Organics were combined, dried with magnesium sulfate then concentrated to dryness. Purification by column chromatography ($CHCl_3$/CH_3OH 95:5, silica gel) afforded **10** (18.7 g, 90% yield) as a white foam. 1H NMR analysis is consistent with the desired product (Figure D5).

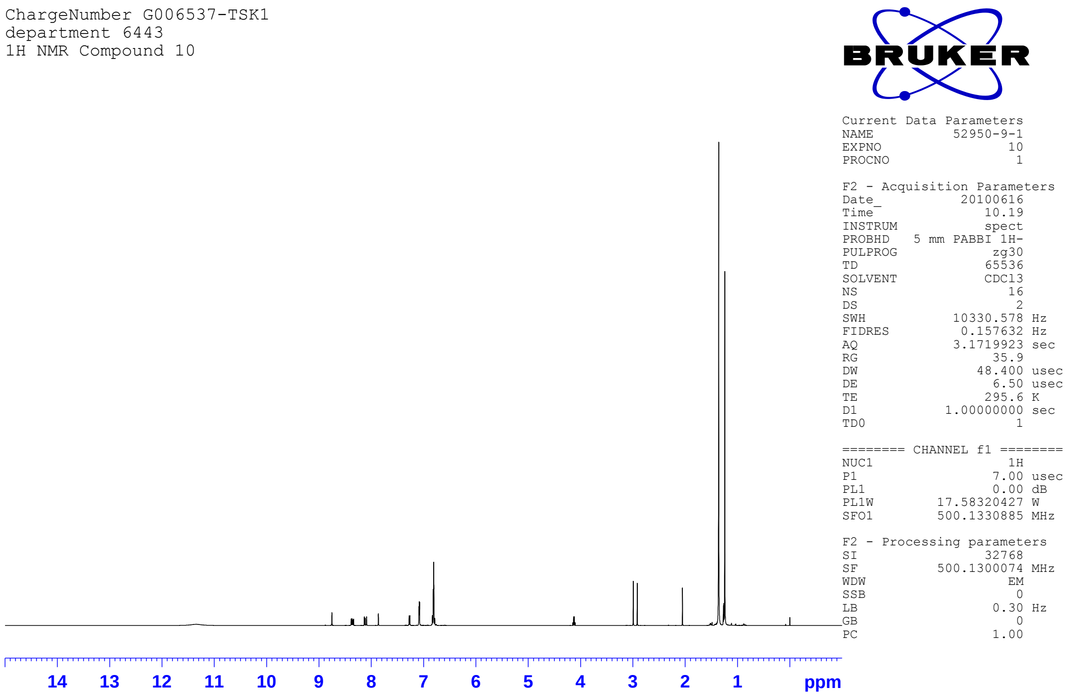

Figure D5. ^{1}H NMR in $CDCl_3$ of Compound 10

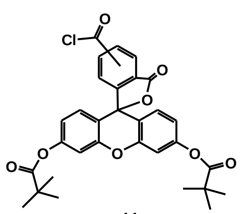

11

(11): Under a nitrogen atmosphere, oxalyl chloride was added over 15 minutes to a stirring solution of compound **10** (18.7 g, 33.5 mmol) in DCM (300 mL) cooled by an ice bath. Evolution of gas was observed and the solution had turned green. After stirring overnight in the melting ice bath, the mixture solution was concentrated to dryness to form **11** as a tan-colored foam. This material was used immediately in following step.

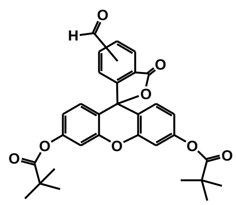

12

(12): Compound **11** (19.3 g, 33.5 mmol) in a DMF /THF 50: 50 solvent mix (200 mL) cooled by an ice bath was treated with sodium borohydride (1.26 g, 33.5 mmol) in DMF (50 mL) drop-wise over 30 minutes then stirred in the melting ice bath for 24 hours. In a separate flask, a suspension of PCC in DCM (100 ml) was cooled in an ice bath. The solution of borate adduct was added all at once to the suspension of PCC. A slight exotherm was observed. The mixture was stir continuously for 4 days. After diluting the mixture with diethyl ether (400 mL), the slurry was filtered through a florisil plug using a medium porosity frit. The organics were concentrated to dryness. Purification by column chromatography (80:20 DCM:Et_2O, silica gel) afforded **12** (10.8 g, 60% yield) as a mixture of isomers. The remaining mass was recovered as the alcohol derivatives. ^{1}H NMR analysis in Figure D6 indicates the material is consistent with compound **12**.

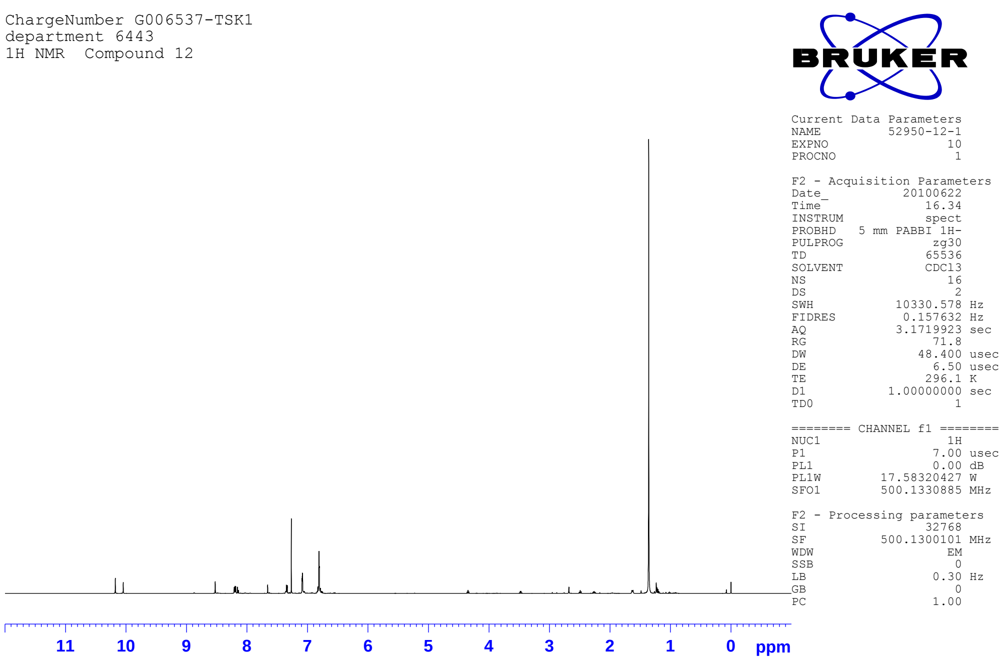

Figure D6. ^{1}H NMR in $CDCl_3$ of Compound 12

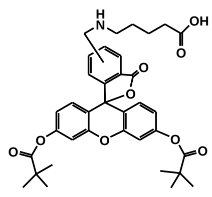

13

(13): Compound 12 (180 mg, 0.33 mmol) and 5-aminovaleric acid (39 mg, 0.33 mmol) were mixed together with 1 drop of acetic acid in DMF (5 mL) for 2 hours. Sodium triacetoxyborohydride (70 mg, 0.33 mmol) dissolved in DMF (3 mL) was added drop-wise. The solution was colorless indicating the protecting groups were still intact. The solvent was removed and replaced with chloroform. Immediately the solution fluoresced and orange solids precipitated. The protecting groups may have been lost by "walking" of the pivaldehyde group. As a result this route was no longer explored.

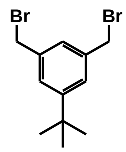

14

3,5-Bis(bromomethyl)-*tert*-butylbenzene (**14**): 5-*tert*-butyl-*m*-xylene (10 g, 61.6 mmol) solvated in carbon tetrachloride was mixed with benzolyl peroxide (1.5 g, 6.16 mmol) then heated to reflux for 12 hours. A Fredrick's condenser was used to maximize cooling efficiency. The resulting white precipitates were filtered with a medium porosity frit then the solution was concentrated to dryness. Purification by recrystalization with ethanol afforded 3,5-Bis(bromomethyl)-*tert*-butylbenzene (8.8 g, 42% yield) as colorless needles. Yields and ^{1}H NMR, Figure D7, are consistent with literature reported values.

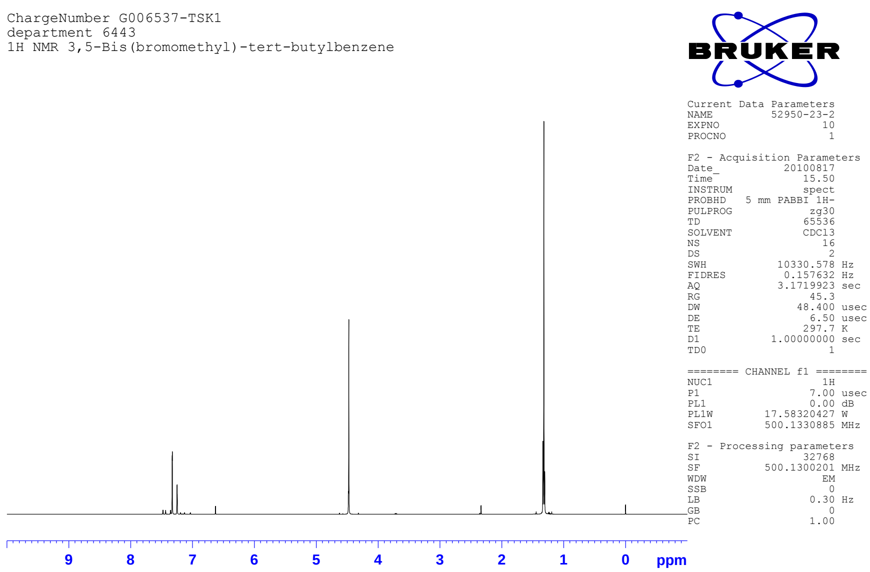

Figure D7. ^{1}H NMR in $CDCl_3$ of 3,5-Bis(bromomethyl)-*tert*-butylbenzene

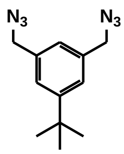

15

(15): 3,5-Bis(bromomethyl)-*tert*-butylbenzene (13.35 g, 39.26 mmol) in ethanol was mixed with sodium azide (5.36 g, 82.44 mmol) then heated to reflux for 12 hours. After removing the solvent, the material was extracted 3X (water 100 ml / $CHCl_3$ 50 ml). The combined organics were dried with magnesium sulfate, filtered then concentrated. Compound **15** was generated in a quantitative yield and used without further purification. ^{1}H NMR is consistent with literature reported values (Figure D8).

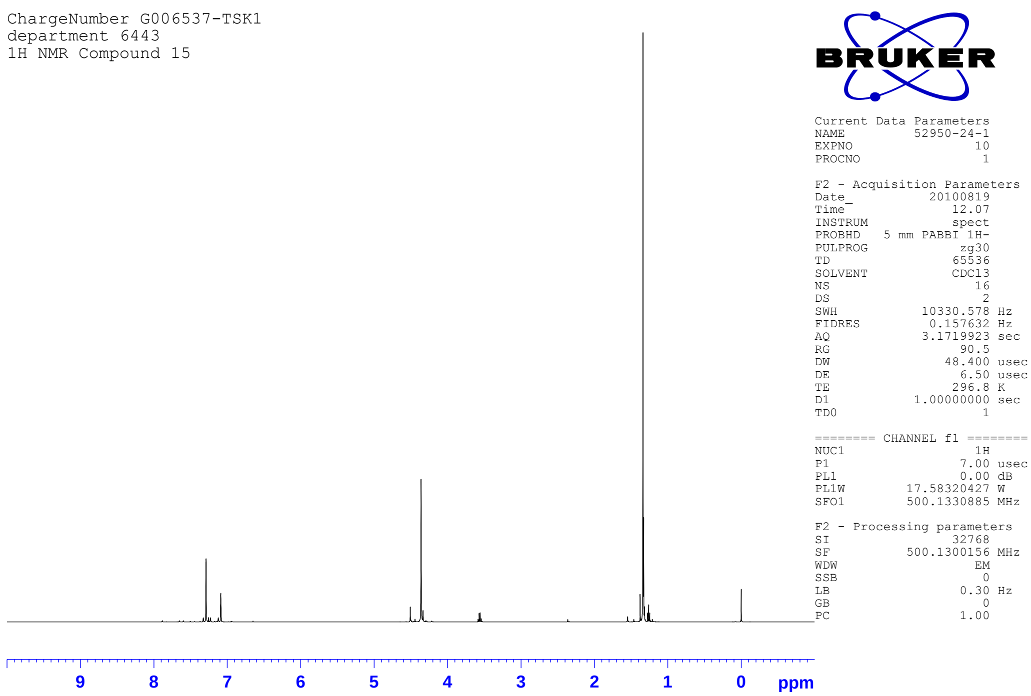

Figure D8. ^{1}H NMR in $CDCl_3$ of Compound 15

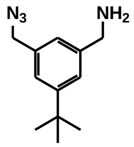

16

(16): Compound **15** (9.59 g, 39.3 mmol) was vigorously mixed with phosphoric acid (0.65M, 200 mL). Triphenylphosphine (10.3 g, 39.3 mmol) dissolved in diethyl ether (200 mL) was added drop-wise over 2 hours. During the addition the solution became opaque; however, no precipitates formed. Stirring was continued for 12 hours, then the mixture was treated with potassium hydroxide pellets (65 g, 1.15 mol). The bi-phasic mixture was rotary evaporated to remove the diethyl ether, and then extracted with chloroform (3 X 75 mL). The combined organics were dried with magnesium sulfate, filtered and concentrated. Purification by column chromatography ($CHCl_3$/CH_3OH 95:5) in a continuous solvent gradient separated the material affording **16** (5.0 g, 58% yield). ^{1}H NMR analysis in Figure D9 is consistent with literature reported values.

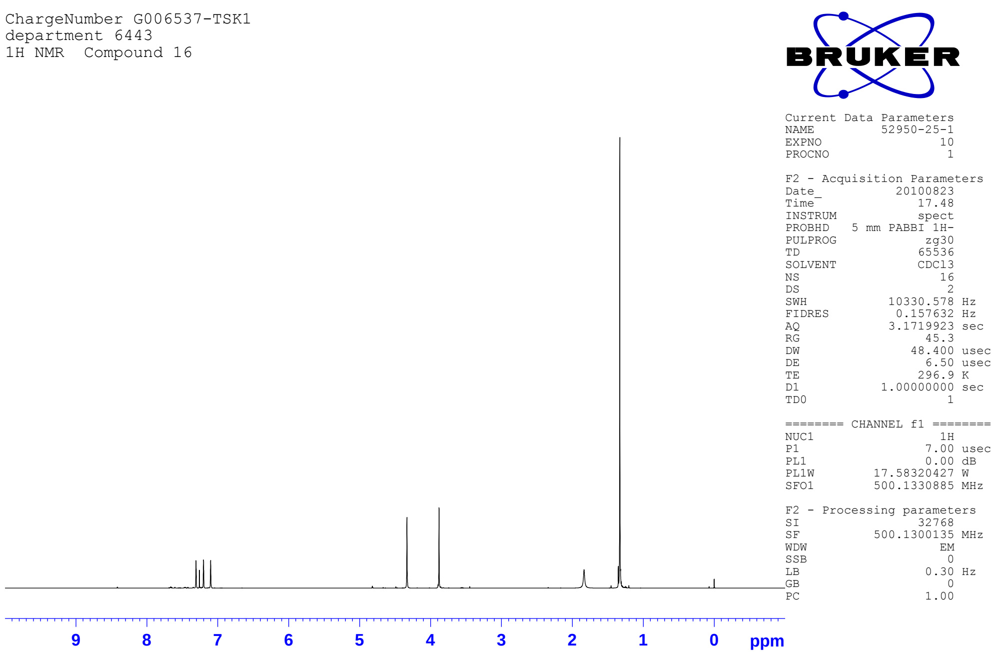

Figure D9. ^{1}H NMR in $CDCl_3$ of Compound 16

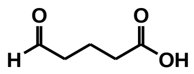

17

(17): 5-Hexenoic acid (1 g, 8.8 mmol) dissolved in anhydrous DMC (50 mL) was cooled to -78 °C by a dry-ice acetone bath. Ozone was bubbled into the solution with stirring until the solution reached a brilliant blue color. Nitrogen was then bubbled in to remove excess ozone then dimethylsulfide (DMS) (2 mL) was added all at once. The reaction was sealed and stirred at ambient temperature for 2 days. The solvents were removed affording **17** in a quantative yield. The material was use as is. ^{1}H NMR analysis, Figure D10, is consistent with literature reported values.

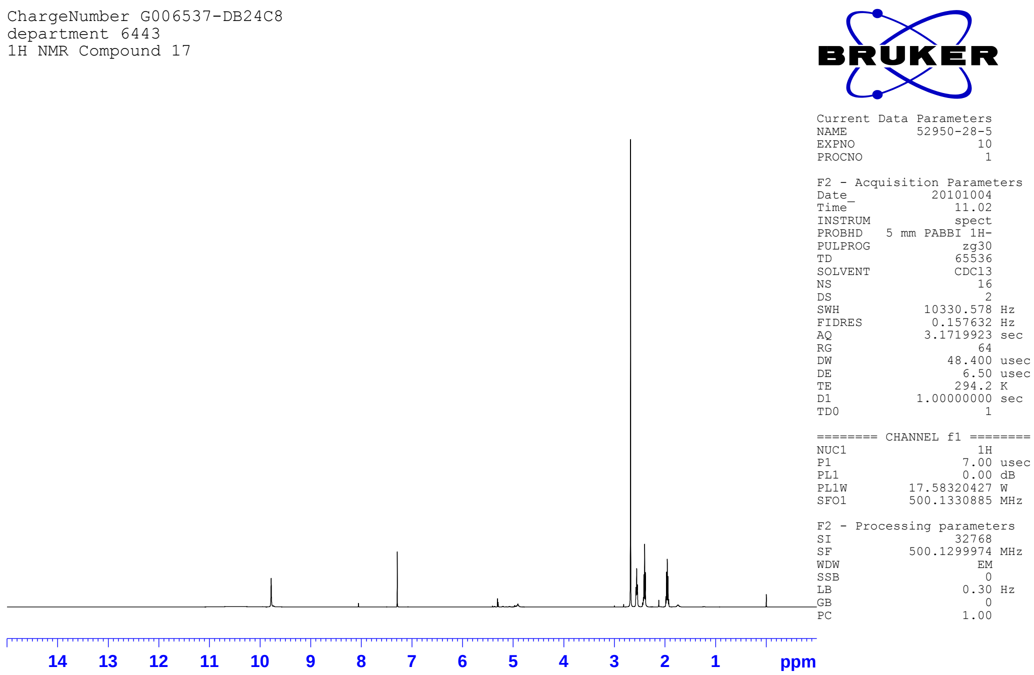

Figure D10. ^{1}H NMR in $CDCl_3$ of Compound 17

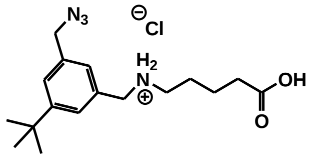

18

(18): Compound **16** (1.31 g, 6.0 mmol) was mixed with the triethylamine salt of **17** (1.30 g, 6.0 mmol) in mixed solvent system ($CHCl_3$:CH_3OH 50:50) (30 mL) for 15 minutes. Sodium cyanoborohydride (377 mg, 6.0 mmol) was added to the solution and stirred at ambient temperature for 12 hours. The mixture was treated with 5% aq HCl (100 mL), additional chloroform (100 mL) then stirred for 2 hours. The organics were separated, dried with magnesium sulfate and concentrated to afford **18** (1.5 g, 70% yield) as a tan foam. ^{1}H NMR indicates retention of borate species (Figure D11). This is causing challenges in material's purification. Reaction was repeated to generate more material.

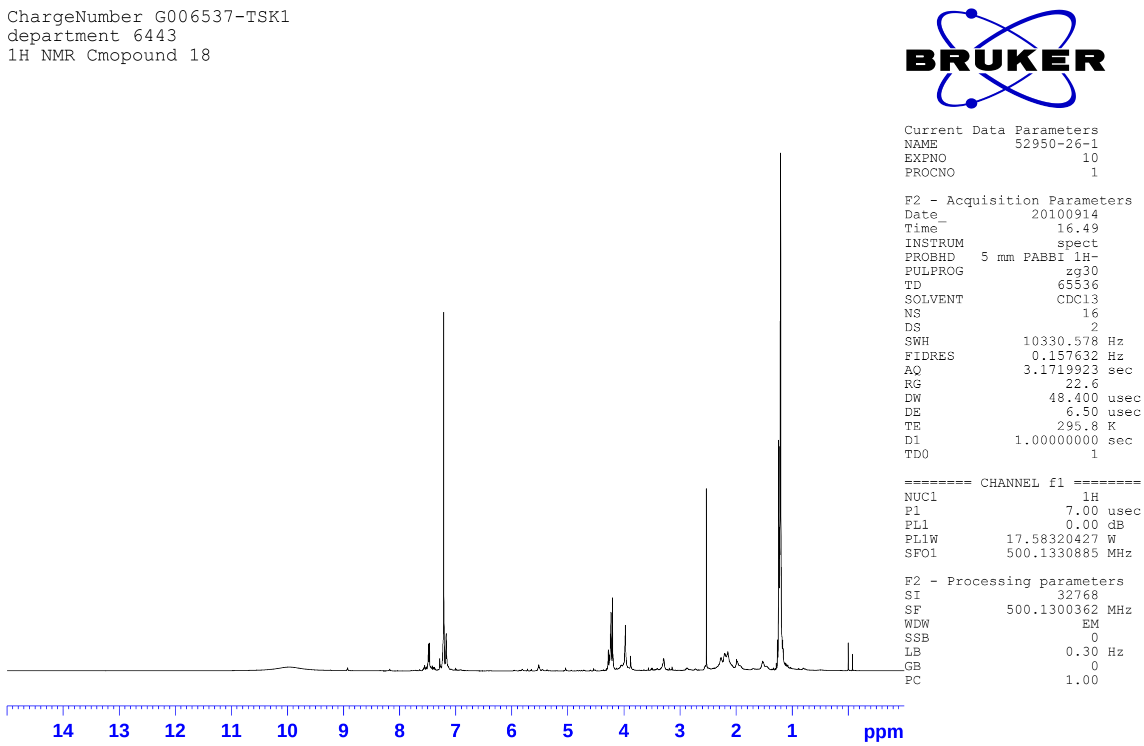

Figure D11. ^{1}H NMR in $CDCl_3$ of Compound 18

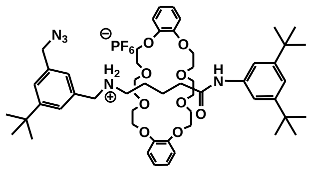

28

(28): Tether compound **18** was extracted between 5% aq HCl (20 mL) containing ammoniumhexafluoroposphate 3 eq. and diethyl ether (20 mL) for 30 minutes. The organics were separated, dried with magnesium sulfate and concentrated affording 2 g of material. Chloroform (25mL) was added to **18** followed by DB24C8 (1.93 g, 4.3 mmol). After mixing for 20 minutes, DCC (887 mg, 4.3 mmol) was added and stirred for an additional 20 minutes. 3,5 di-*tert*-butylaniline was stirred into the solution for 12 hours. Analysis of crude reaction mixture by MS/ESI indicates the reaction produced rotaxane. Purification by column chromatography afforded **28** (50 mg, 10%). The MS/ESI spectrum shown in Figure D12 indicates the material with M/Z of 955. The hexafluorophosphate anion is not observed.

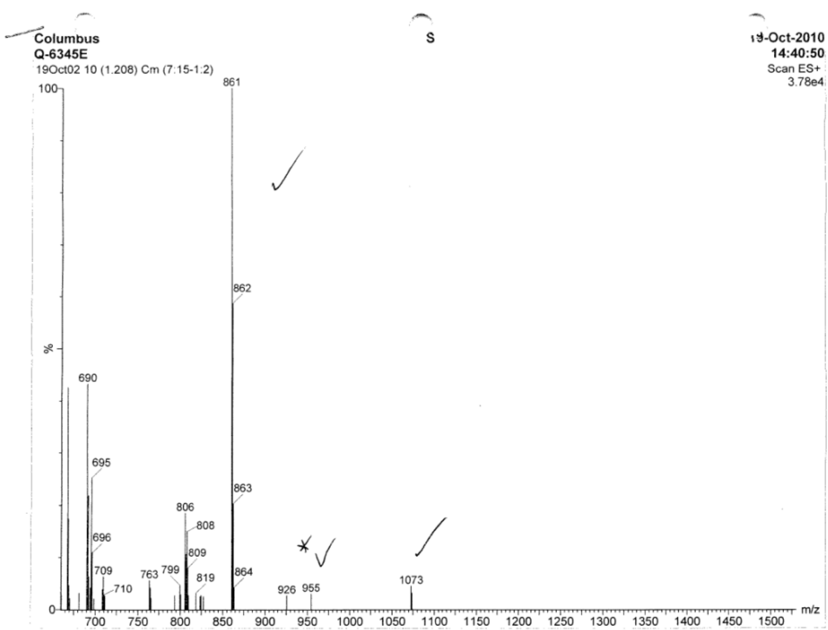

Figure D12. MS/ESI of material generated in the attempt to form Compound 28

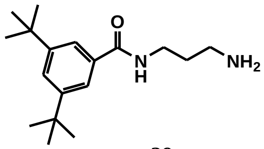

29

(29): 3,5 di-tert-butylbenzoic acid (5 g, 21.3 mmol) in chloroform (100 mL) was treated with DCC (4.39 g, 21.3 mmol) then stirred for 20 minutes under at ambient temperature. This mixture was added drop-wise to a stirring solution of 1.3 diaminopropane (15.7 g, 213 mmol) over 30 minutes. After stirring for 2 hours at ambient temperature, the solvent was removed and the crude product was purified by column chromatography (silica gel, $CHCl_3$:CH_3OH gradient 90:10). The reaction produced 3.43 g 56% yield. The remaining material recovered was di-addition. ^{1}H NMR analysis is consistent with compound **29** (Figure D13).

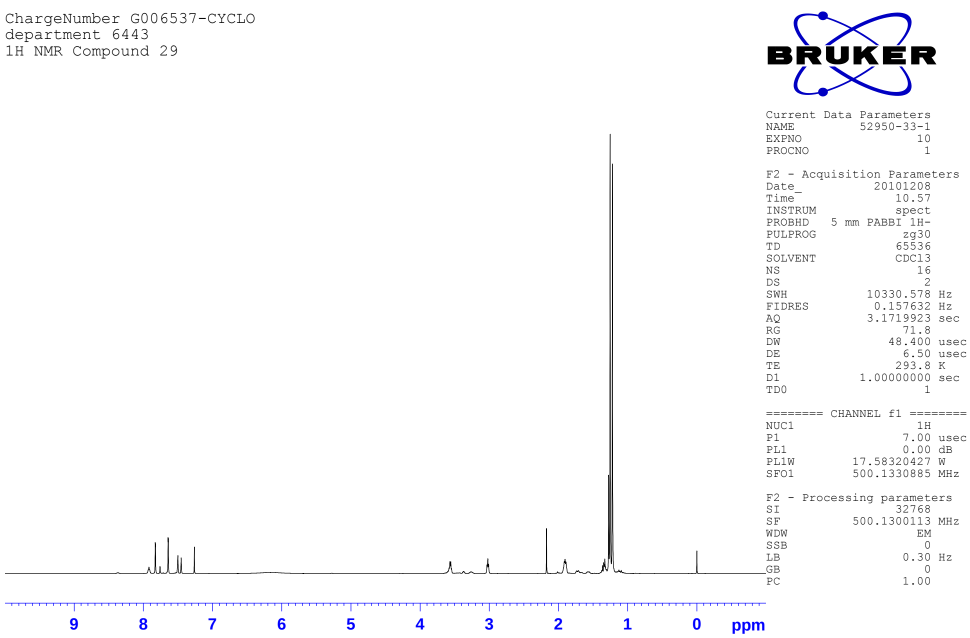

Figure D13. ^{1}H NMR in $CDCl_3$ of Compound 29